

LiDAR Remote Sensing Data Collection:

Department of Geology & Mineral Industries

Oregon Department of Forestry

Puget Sound LiDAR Consortium

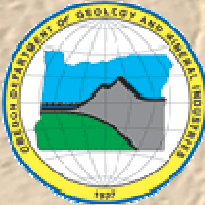
Submitted to:



**Puget Sound Regional Council
1011 Western Avenue, Suite 500
Seattle, Washington 98104-1035**



**Phyllis A. Mann
Kitsap County
911 Carver Street
Bremerton, Washington 98312**



**Ian Madin, Chief Scientist
Oregon Department of Geology &
Mineral Industries
800 NE Oregon St. Suite 965
Portland OR 97232
(971) 673-1542**



**Emmor Nile, GISP
GIS Coordinator
Oregon Department of Forestry
2600 State Street, Building E
Salem, Oregon 97310
(503) 945-7418**

Submitted by:



**Watershed Sciences
529 SW Third Ave, Suite 300
Portland, Oregon 97204
(971) 223-5152**

June 19, 2009

LIDAR REMOTE SENSING DATA COLLECTION: DOGAMI, ODF STUDY AREAS

TABLE OF CONTENTS

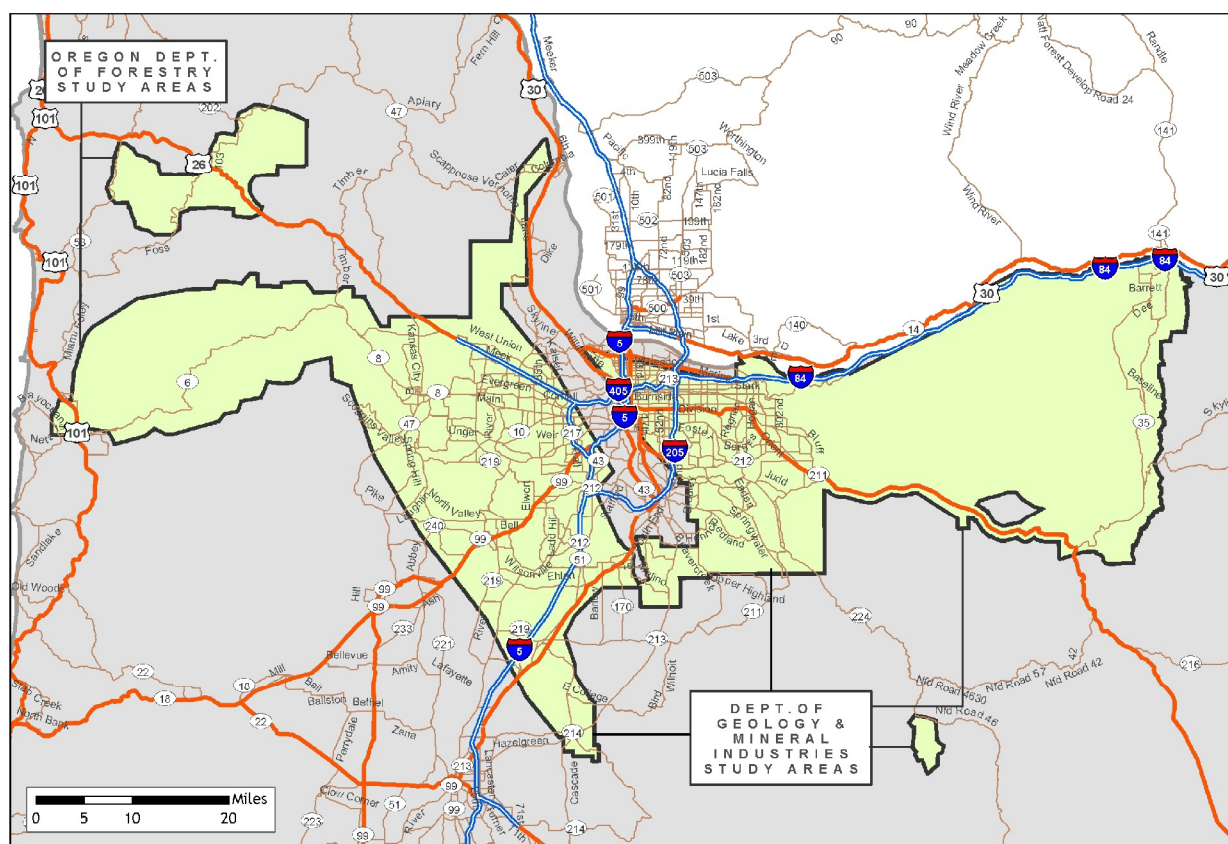
| | |
|--|------------|
| 1. Overview..... | 1 |
| 1.1 DOGAMI and ODF Study Areas..... | 1 |
| 1.2 Areas Delivered..... | 2 |
| 1.3 Accuracy and Resolution..... | 4 |
| 1.4 Data Format, Projection, and Units..... | 4 |
| 2. Acquisition..... | 5 |
| 2.1 Airborne Survey –Instrumentation and Methods..... | 5 |
| 2.1.1 Acquisition Specifics per Delivery Area | 7 |
| 2.2 Ground Survey –Instrumentation and Methods | 10 |
| 3. LiDAR Data Processing..... | 38 |
| 3.1 Applications and Work Flow Overview..... | 38 |
| 3.2 Aircraft Kinematic GPS and IMU Data..... | 38 |
| 3.3 Laser Point Processing | 39 |
| 4. LiDAR Accuracy and Resolution | 40 |
| 4.1 Laser Point Accuracy | 40 |
| 4.1.1 Relative Accuracy..... | 40 |
| 4.1.2 Absolute Accuracy | 44 |
| 4.2 Data Density/Resolution | 46 |
| 4.2.1 First Return Laser Pulses per Square Foot | 47 |
| 4.2.2 Classified Ground Points per Square Foot | 50 |
| 4.3 Data Density/Resolution per AOI | 53 |
| 4.3.1 Portland AOI | 53 |
| 4.3.2 ODF AOI..... | 55 |
| 4.3.3 Upper Sandy / Bull Run AOIs | 55 |
| 4.3.4 Collawash AOI | 56 |
| 4.3.5 Lower Sandy AOI | 57 |
| 4.3.6 Mount Hood AOI | 58 |
| 4.3.7 Columbia River Gorge AOI | 59 |
| 5. Mt. Hood / Columbia River Gorge Acquisition Discussion | 60 |
| 6. Deliverables | 64 |
| 6.1 Point Data (per 0.75' USGS Quad)..... | 65 |
| 6.2 Vector Data | 65 |
| 6.3 Raster Data | 65 |
| 6.4 Data Report | 65 |
| 6.5 Datum and Projection | 65 |
| 7. Selected Images | 65 |
| 7.1 Three Dimensional Oblique View Data Pairs..... | 65 |
| 8. Glossary | 126 |
| 9. Citations..... | 127 |

1. Overview

1.1 DOGAMI and ODF Study Areas

Watershed Sciences, Inc. (WS) collected Light Detection and Ranging (LiDAR) data for the Department of Geology and Mineral Industries (DOGAMI) and the Oregon Department of Forestry (ODF). The Areas of Interest (AOIs) cover portions of eight counties in northwest Oregon. The extent of requested LiDAR area totals ~1,549,015 acres; the map below shows the extent of the LiDAR area delivered, covering ~1,586,385 acres. The delivered acreage for the study area is greater than the original amount due to buffering of the original AOIs for flight planning optimization. This is the final, comprehensive data report for all areas in the LiDAR survey.

Figure 1.1. Extent of Department of Geology and Mineral Industries (DOGAMI) and Oregon Department of Forestry (ODF) Study Areas.



1.2 Areas Delivered

The total delivered acreage is detailed below.

| ODF Area | | |
|-----------------------------|------------------|------------------|
| Delivery Date | AOI Acres | TAF Acres |
| September to December, 2007 | 305,930 | 314,950 |
| Portland Area | | |
| Delivery Date | AOI Acres | TAF Acres |
| October 15, 2007 | 207,046 | 210,945 |
| November 1, 2007 | 115,136 | 118,909 |
| November 12, 2007 | 164,418 | 167,193 |
| January 29, 2008 | 80,397 | 83,576 |
| February 19, 2008 | 115,092 | 116,652 |
| March 4, 2008 | 23,829 | 23,829 |
| April 4, 2008 | 74,035 | 77,753 |
| April 11, 2008 | 73,856 | 74,582 |
| December 4, 2008 | 29,565 | 32,659 |
| January 23, 2009 | 41,859 | 42,288 |
| February 13, 2009 | 65,318 | 65,429 |
| February 27, 2009 | 34,345 | 35,035 |
| March 11, 2009 | 22,019 | 22,424 |
| April 10, 2009 | 15,035 | 15,715 |
| April 17, 2009 | 23,163 | 23,937 |
| May 7, 2009 | 47,087 | 48,325 |
| May 27, 2009 | 110,883 | 112,184 |
| Total | 1,549,015 | 1,586,385 |

Figure 1.2. DOGAMI and ODF study areas, illustrating the delivered portion of the areas.

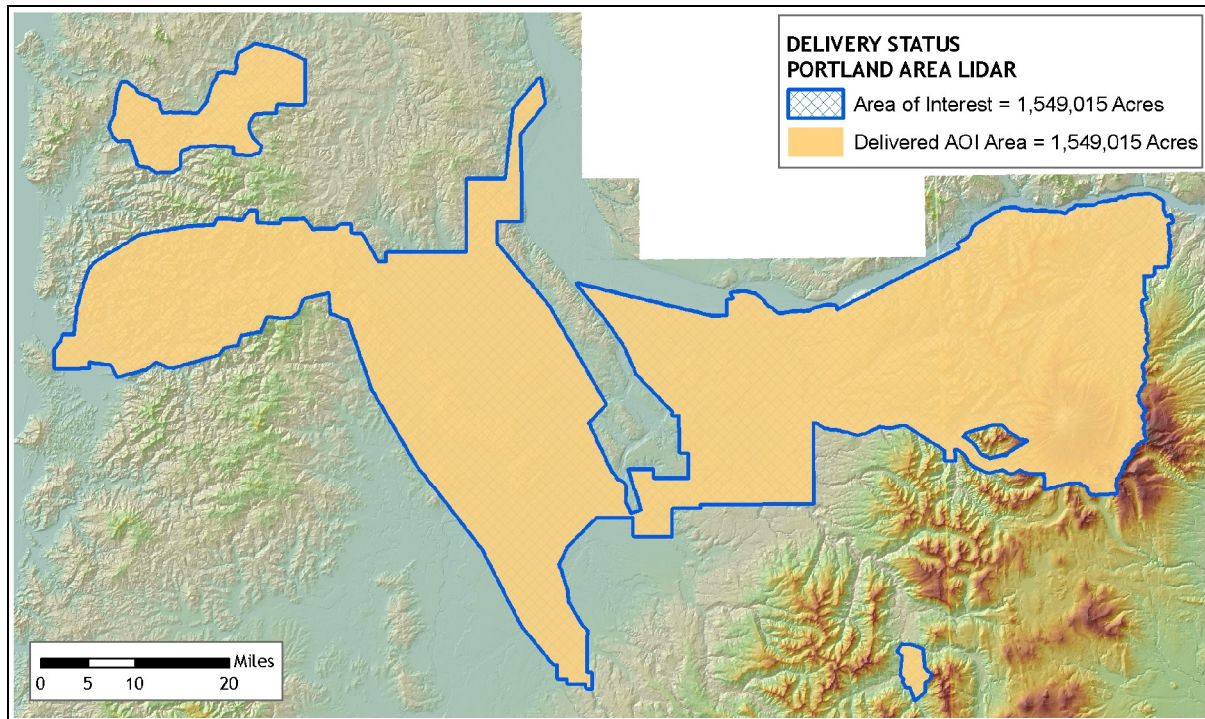
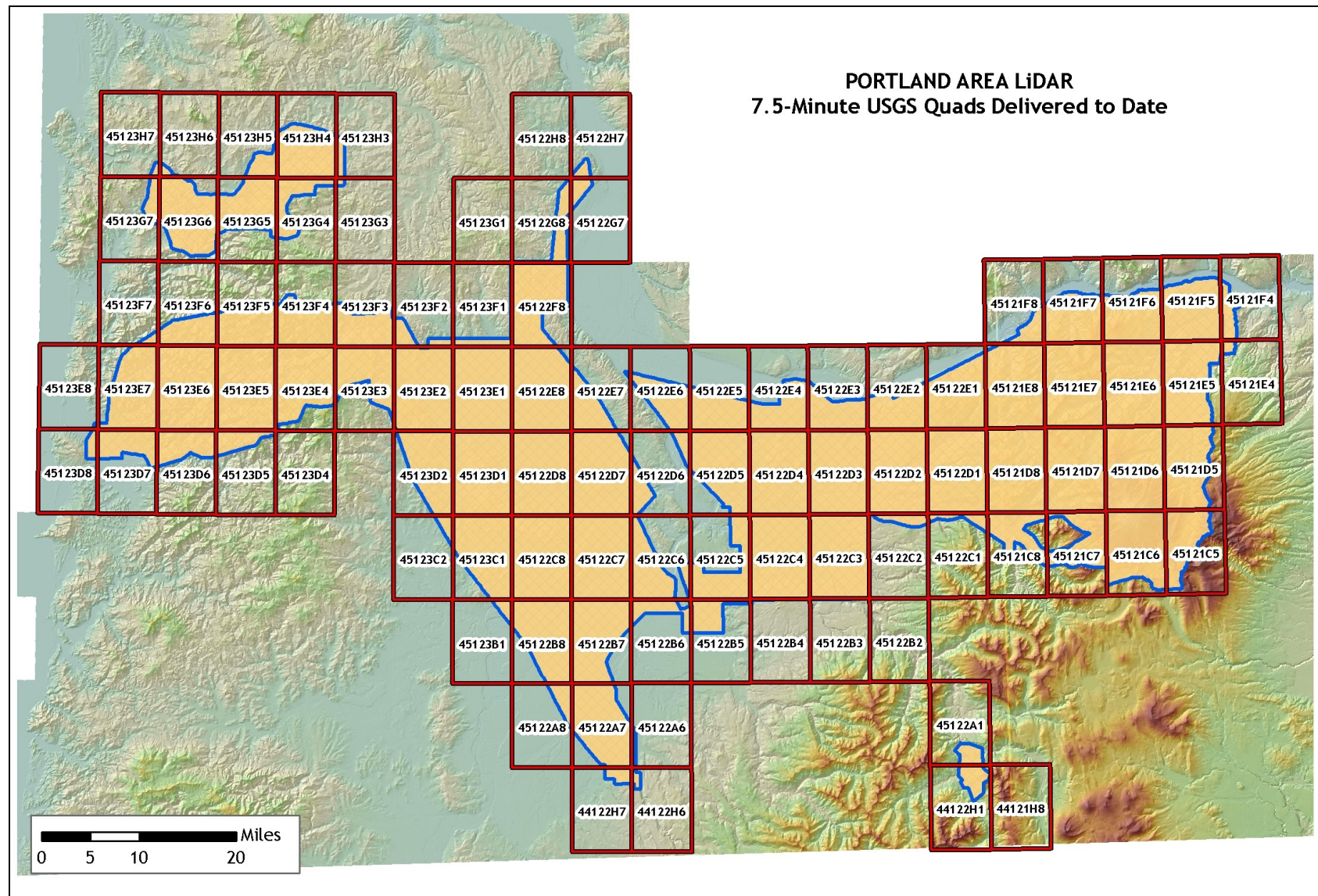


Figure 1.3. DOGAMI and ODF study areas, illustrating the delivered 7.5-minute USGS quads.



1.3 Accuracy and Resolution

Real-time kinematic (RTK) surveys were conducted in multiple locations throughout the study area for quality assurance purposes. The accuracy of the LiDAR data is described as standard deviations of divergence ($\sigma \sim \sigma$) from RTK ground survey points and root mean square error (RMSE) which considers bias (upward or downward). These statistics are calculated cumulatively for each acquisition year. For the DOGAMI / ODF study areas, the data have the following accuracy statistics:

| | RMSE | 1-sigma absolute deviation | 2-sigma absolute deviation |
|---|-----------|----------------------------|----------------------------|
| 2007 ODF and DoGAMI Data Acquisitions Processing Complete | 0.11 feet | 0.11 feet | 0.23 feet |
| 2008 DoGAMI Data Acquisition Processing Complete | 0.13 feet | 0.11 feet | 0.27 feet |

Data resolution specifications are for ≥ 8 pts per m^2 . Section 4.2 demonstrates that total pulse density for the Portland AOI delivered to date have the following statistics:

| | Total Pulse Density | Ground Pulse Density |
|--|---|---|
| 2007 ODF Data Acquisition Processing Complete | 7.71 points per square meter 0.72 points per square foot | 0.71 points per square meter 0.07 points per square foot |
| 2007 DoGAMI Data Acquisition Processing Complete | 6.90 points per square meter 0.64 points per square foot | 1.28 points per square meter 0.12 points per square foot |
| 2008 DoGAMI Data Acquisition Processing Complete | 7.75 points per square meter 0.72 points per square foot | 0.76 points per square meter 0.07 points per square foot |

1.4 Data Format, Projection, and Units

Deliverables include point data in *.las v 1.1 and ascii format, 3-foot resolution bare ground model ESRI GRID, 3-foot resolution above ground surface ESRI GRID, 1.5-foot resolution intensity images in GeoTIFF format, Smoothed Best Estimate of Trajectory (5Hz frequency) information in ascii text format, and data report.

- ODF AOIs are delivered in Oregon Lambert, EPSG 2992, with horizontal units in International Feet and vertical units in US Survey Feet, in the NAD83/NAVD88 datum (Geoid 03).
- All other AOIs are delivered in Oregon State Plane North, with horizontal units in International Feet and vertical units in US Survey Feet, in the NAD83 HARN/NAVD88 datum (Geoid 03).

2. Acquisition

2.1 Airborne Survey –Instrumentation and Methods

The LiDAR survey utilized a Leica ALS50 Phase II mounted in Cessna Caravan 208B and an Optech 3100 laser system mounted in a Cessna Caravan 208. The Leica ALS50 Phase II system was set to acquire =105,000 laser pulses per second (i.e. 105 kHz pulse rate) and flown at 900 meters above ground level (AGL), capturing a scan angle of $\pm 14^\circ$ from nadir¹. The Optech 3100 system was set to acquire 71,000 laser pulses per second (i.e. 71 kHz pulse rate) and flown at 900 meters above ground level (AGL) capturing a scan angle of $\pm 14^\circ$ from nadir. These settings are developed to yield points with an average native density of ≥ 8 points per square meter over terrestrial surfaces. The native pulse density is the number of pulses emitted by the LiDAR system. Some types of surfaces (i.e., dense vegetation or water) may return fewer pulses than the laser originally emitted. Therefore, the delivered density can be less than the native density and lightly variable according to distributions of terrain, land cover and water bodies.



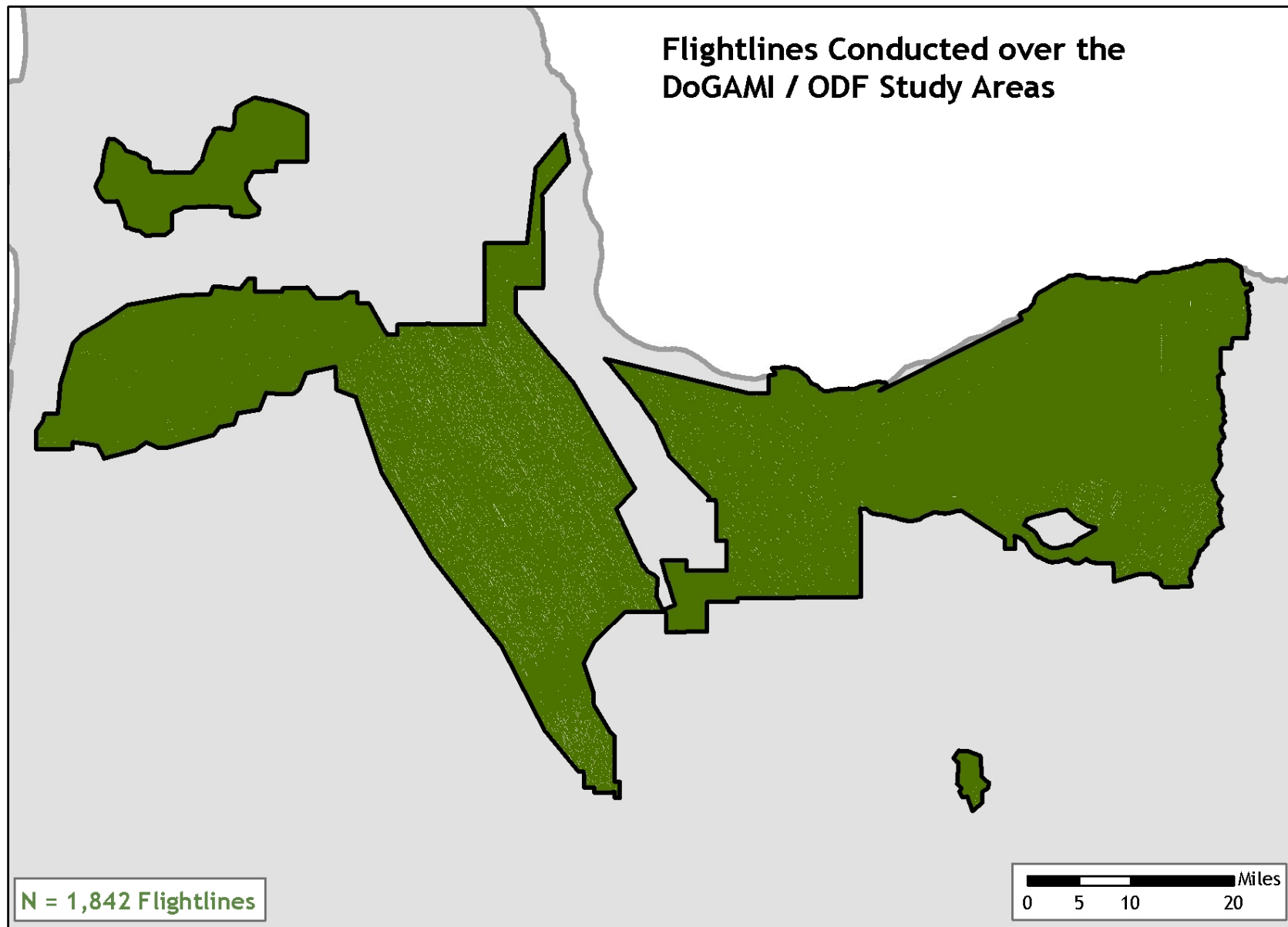
The Cessna Caravan is a powerful, stable platform, which is ideal for the often remote and mountainous terrain found in the Pacific Northwest. The Leica ALS50 sensor head installed in the Caravan is shown on the right.

The completed areas were surveyed with opposing flight line side-lap of =50% (=100% overlap) to reduce laser shadowing and increase surface laser painting. The system allows up to four range measurements per pulse, and all discernable laser returns were processed for the output dataset.

To solve for laser point position, it is vital to have an accurate description of aircraft position and attitude. Aircraft position is described as x, y and z and measured twice per second (2 Hz) by an onboard differential GPS unit. Aircraft attitude is measured 200 times per second (200 Hz) as pitch, roll and yaw (heading) from an onboard inertial measurement unit (IMU). **Figure 2.1** illustrates the location, swath width and overlap of the actual flight lines for the DOGAMI/ODF study areas.

¹ Nadir refers to the perpendicular vector to the ground directly below the aircraft. Nadir is commonly used to measure the angle from the vector and is referred to a “degrees from nadir”.

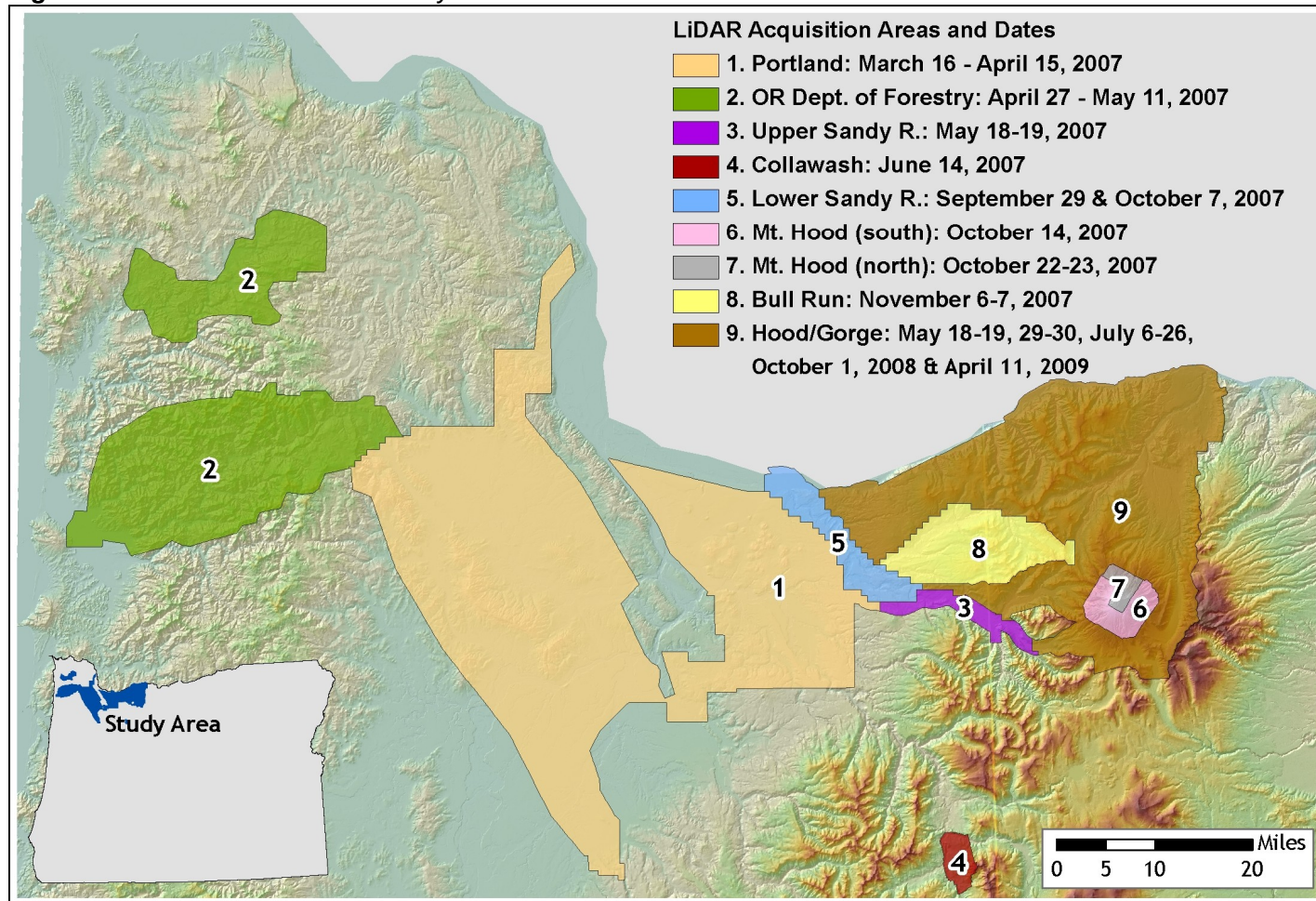
Figure 2.1. Actual flightlines in ODF and DOGAMI study areas.



2.1.1 Acquisition Specifics per Delivery Area

The DOGAMI and ODF study areas delivered to date are composed of nine unique study areas (**Figure 2.2**). Each area was flown during a unique time period and there is no overlap of LiDAR points between study areas. The LiDAR points that fall within each acquisition area represent the unique ground and vegetation conditions for the time period it was flown. Specifics for each area are discussed below.

Figure 2.2. DOGAMI and ODF Delivery Areas to Date.

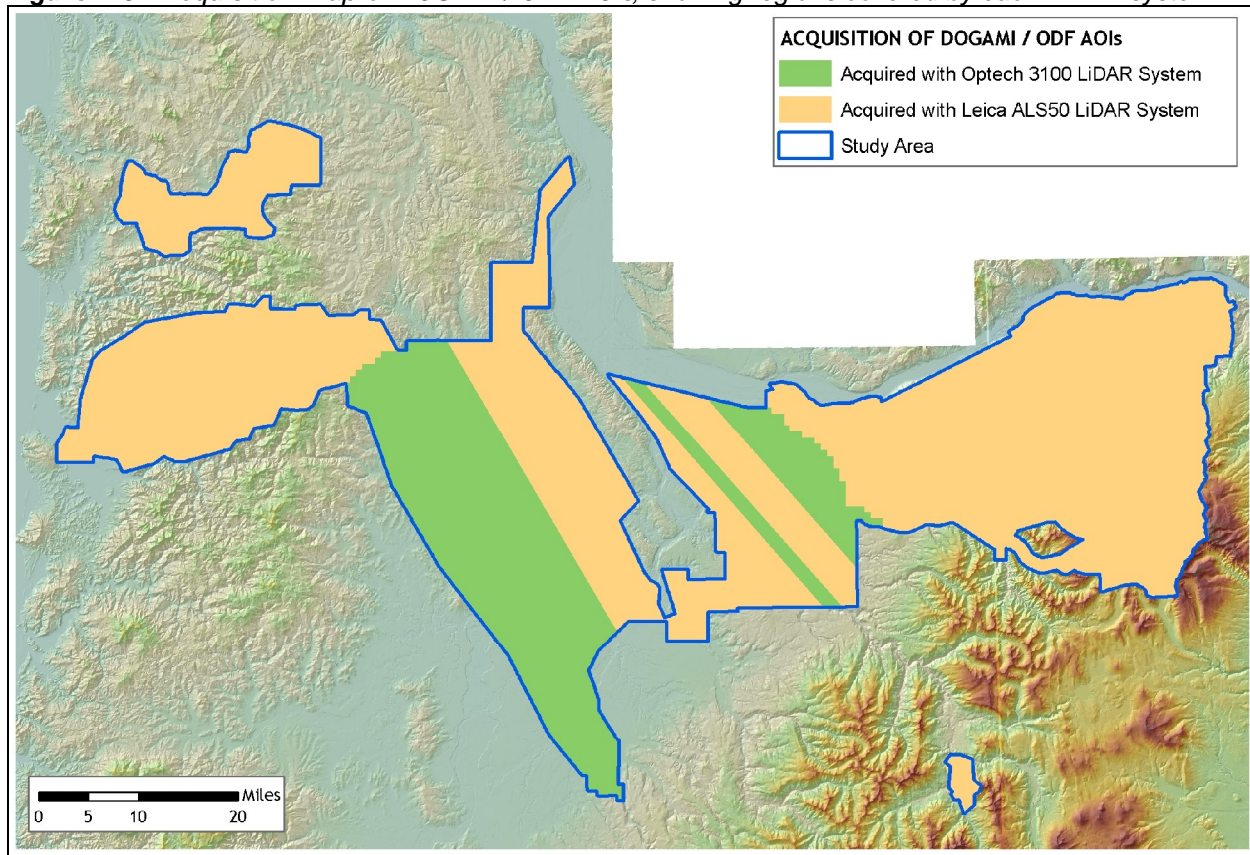


The data for the DOGAMI and ODF study areas were collected with two different LiDAR systems.

Table 2.1 LiDAR Survey Specifications

| AOI | ODF, Upper Sandy, Collawash, Lower Sandy, Bull Run, portions of Portland, and Hood/Gorge. | Portions of Portland AOI | Mount Hood (Extreme Relief Areas) |
|-----------------------|---|--------------------------|-----------------------------------|
| Sensor | Leica ALS50 Phase II | Optech 3100 | Leica ALS50 Phase II |
| Survey Altitude (AGL) | 900 m | 900 m | 1800 m |
| Pulse Rate | >105 kHz | >71 kHz | >50 kHz |
| Pulse Mode | Single | Single | Single |
| Mirror Scan Rate | 52 Hz | 45 Hz | 21 Hz |
| Field of View | 28° (±14° from nadir) | 28° (±14° from nadir) | 28° (±14° from nadir) |
| Roll Compensated | Up to 15° | None | Up to 15° |
| Overlap | 100% (50% Side-lap) | 100% (50% Side-lap) | 100% (50% Side-lap) |

Figure 2.3. Acquisition map of DOGAMI / ODF AOIs, showing regions covered by each LiDAR system.



Delivery Area 1 - Portland: These data were collected between March 16 –April 15, 2007, with both the Leica ALS50 and the Optech 3100 LiDAR systems, as shown in Figure 2.4.

Delivery Area 2 –ODF: These data were collected between April 27 –May 11, 2007 with the Leica ALS50 LiDAR System.

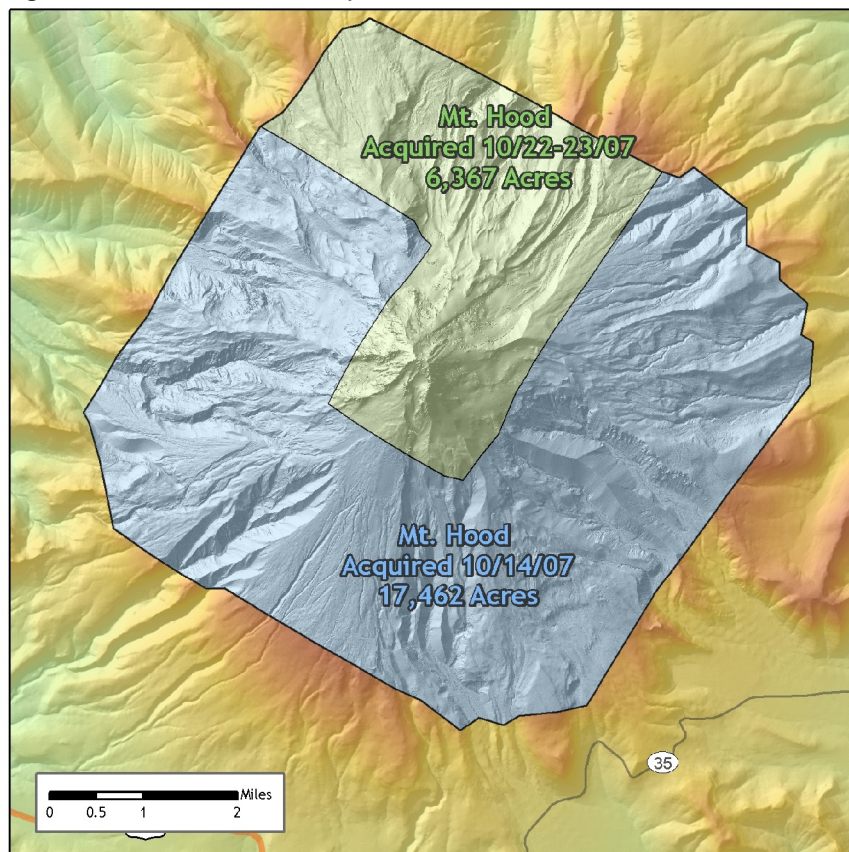
Delivery Area 3 –Upper Sandy River: These data were collected between May 18-19, 2007 with the Leica ALS50 LiDAR System.

Delivery Area 4 –Collawash: These data were collected on June 14, 2007 with the Leica ALS50 LiDAR System.

Delivery Area 5 –Lower Sandy River: These data were collected September 29 –October 7, 2007 with the Leica ALS50 LiDAR System.

Delivery Areas 6 & 7 –Mount Hood: These data were collected on October 14 and October 22-23, 2007 with the Leica ALS50 LiDAR System (in the Mount Hood high relief settings, see **Table 2.1**). Due to adverse weather, the area was acquired in two portions, one week apart. **Figure 2.4** below shows the extent of the Mount Hood area collected, visually divided into the two different acquisition windows. As a result, the two areas reflect two different snow levels, both accurate for the acquisition date in which they were acquired.

Figure 2.4. Mount Hood acquisition areas and dates.



Delivery Area 8 –Bull Run: These data were collected on November 6-7, 2007 with the Leica ALS50 LiDAR System.

Delivery Area 9 –Hood / Gorge: These data were collected on May 18-19, 29-30, July 6-26, October 1, 2008 & April 11, 2009 with the Leica ALS50 LiDAR System.

2.2 Ground Survey –Instrumentation and Methods

During the LiDAR survey of the study area, a static (1 Hz recording frequency) ground survey was conducted over monuments with known coordinates. Coordinates are provided in **Table 2.2** and shown in **Figure 2.5**. After the airborne survey, the static GPS data are processed using triangulation with CORS stations and checked against the Online Positioning User Service (OPUS²) to quantify daily variance. Multiple sessions are processed over the same monument to confirm antenna height measurements and reported position accuracy.

Table 2.2. Base Station Surveyed Coordinates, (NAD83/NAVD88, OPUS corrected) used for kinematic post-processing of the aircraft GPS data for the DOGAMI and ODF AOIs.

| Study Area | Base Station ID | Datum NAD83(HARN) | | GRS80 |
|------------|-----------------|-------------------|------------------|----------------------|
| | | Latitude (North) | Longitude (West) | Ellipsoid Height (m) |
| DOGAMI | ORMI_1 | 45 07 38.77347 | 122 47 50.69501 | 29.077 |
| DOGAMI | SCJR_1 | 45 01 16.71080 | 122 44 37.15483 | 77.597 |
| DOGAMI | ORMI_2 | 45 30 30.86516 | 123 05 27.70581 | 26.630 |
| DOGAMI | ORMI_3 | 45 24 08.24317 | 122 54 59.88436 | 32.208 |
| DOGAMI | ORMI_4 | 45 14 34.58806 | 122 46 02.63126 | 37.028 |
| DOGAMI | SCJR3 | 44 54 08.93624 | 122 42 08.33058 | 325.829 |
| DOGAMI | ORJR_1 | 45 19 53.37805 | 122 20 55.26176 | 95.011 |
| DOGAMI | ORJR_2 | 45 27 24.86103 | 122 33 33.65264 | 181.756 |
| DOGAMI | ORJM2 | 45 27 24.86103 | 122 33 33.65264 | 181.756 |
| DOGAMI | ORJR5 | 45 46 22.21129 | 122 53 01.10672 | 3.562 |
| DOGAMI | ORJR6 | 45 53 43.01413 | 122 48 48.08575 | 6.210 |
| DOGAMI | ORSP14 | 45 52 23.25109 | 123 33 38.28134 | 108.139 |
| DOGAMI | ORSP15 | 45 39 02.12095 | 123 16 33.08583 | 136.147 |
| DOGAMI | ORSP16 | 45 39 02.12095 | 123 16 33.08583 | 136.147 |
| DOGAMI | ORJR21 | 45 18 23.10077 | 121 49 49.67527 | 808.484 |
| DOGAMI | ORSP20 | 45 23 19.99348 | 122 09 23.35649 | 359.167 |
| DOGAMI | ORSP22 | 45 33 29.27716 | 122 38 34.17056 | 47.016 |
| DOGAMI | RD4237 | 45 28 29.30798 | 122 23 46.92313 | 118.878 |
| DOGAMI | MHJR1 | 45 19 52.00870 | 121 42 29.96298 | 1779.251 |
| DOGAMI | MHJR2 | 45 19 52.09620 | 121 42 29.82020 | 1779.331 |
| DOGAMI | MHJR3 | 45 19 49.38051 | 121 42 27.45942 | 1766.825 |
| DOGAMI | BRCD1 | 45 26 38.51568 | 121 47 36.77702 | 844.046 |
| DOGAMI | BRCD2 | 45 22 38.24522 | 121 13 33.71829 | 348.435 |
| DOGAMI | ORSP28 | 45 07 30.53044 | 122 29 42.45664 | 248.593 |
| DOGAMI | ORSP29 | 45 02 57.81336 | 121 58 55.33389 | 1261.986 |
| DOGAMI | ORSP27 | 45 02 57.45546 | 121 58 55.35578 | 1261.736 |
| DOGAMI | CDSD1 | 45 27 11.90589 | 122 17 20.60722 | 201.565 |
| DOGAMI | CDSD2 | 45 33 3.80949 | 122 23 42.14002 | -11.974 |

² Online Positioning User Service (OPUS) is run by the National Geodetic Survey to process corrected monument positions.

Table 2.2 (cont). Base Station Surveyed Coordinates, (NAD83/NAVD88, OPUS corrected) used for kinematic post-processing of the aircraft GPS data for the DOGAMI and ODF AOIs.

| | | Datum NAD83(HARN) | | GRS80 |
|------------|-----------------|-------------------|------------------|----------------------|
| Study Area | Base Station ID | Latitude (North) | Longitude (West) | Ellipsoid Height (m) |
| DOGAMI | CDAP1 | 45 33 4.03516 | 122 23 41.80716 | -12.027 |
| DOGAMI | CDAP2 | 45 27 11.90589 | 122 17 20.60722 | 201.565 |
| DOGAMI | HOODR01 | 45 34 7.17772 | 121 32 3.01136 | 615.155 |
| DOGAMI | HOODR02 | 45 34 7.53745 | 121 32 2.45680 | 615.154 |
| DOGAMI | HR3 | 45 50 19.31931 | 121 32 15.13764 | 169.179 |
| DOGAMI | CLCF1 | 45 41 7.84953 | 121 51 18.81158 | 16.812 |
| DOGAMI | CLCF2 | 45 41 0.16753 | 121 51 22.83026 | 17.309 |
| DOGAMI | HCF1 | 45 36 9.25198 | 122 2 37.45339 | 0.146 |
| DOGAMI | HCF2 | 45 32 43.93173 | 121 42 33.87275 | 422.973 |
| DOGAMI | FLJ1 | 45 31 33.01482 | 122 8 20.68793 | 648.857 |
| DOGAMI | FLJ2 | 45 31 7.77908 | 122 17 48.68460 | 197.157 |
| DOGAMI | CLJ1 | 45 27 41.34656 | 121 46 36.49291 | 726.274 |
| DOGAMI | CLJ2 | 45 27 41.38403 | 121 46 36.35757 | 726.334 |
| DOGAMI | HLJ1 | 45 25 19.67182 | 121 49 5.41887 | 927.163 |
| DOGAMI | HDCF1 | 45 23 49.10281 | 121 51 40.19938 | 756.402 |
| DOGAMI | TMCF1 | 45 18 21.84889 | 121 42 8.43103 | 1431.959 |
| DOGAMI | TMCF2 | 45 18 22.21004 | 121 42 7.46317 | 1433.992 |
| DOGAMI | MHMC1 | 45 18 40.62153 | 121 38 40.56026 | 1408.434 |
| DOGAMI | PWHAP2 | 45 33 3.93810 | 122 23 44.21777 | -12.395 |
| DOGAMI | PWHSD1 | 45 27 11.69280 | 122 17 20.83247 | 201.685 |
| DOGAMI | RC1674 | 45 42 39.37193 | 121 32 59.76037 | 81.122 |
| DOGAMI | GKHD1 | 45 41 56.21874 | 121 40 05.15627 | 10.851 |
| ODF | ORSP10 | 45 51 45.02398 | 123 35 01.16219 | 139.9685 |
| ODF | ORSP11 | 45 51 16.03468 | 123 32 26.33048 | 187.864 |
| ODF | ORSP12 | 45 37 08.06456 | 123 23 50.39774 | 402.8955 |
| ODF | ORSP13 | 45 29 59.43934 | 123 38 32.06929 | 280.969 |
| ODF | ORSP14 | 45 52 23.25109 | 123 33 38.28134 | 108.139 |

Multiple DGPS units are used for the ground real-time kinematic (RTK) portion of the survey. To collect accurate ground surveyed points, a GPS base unit is set up over monuments to broadcast a kinematic correction to a roving GPS unit. The ground crew uses a roving unit to receive radio-relayed kinematic corrected positions from the base unit. This method is referred to as real-time kinematic (RTK) surveying and allows precise location measurement ($\sigma = 1.5 \text{ cm} \sim 0.6 \text{ in}$). For the DOGAMI and ODF study areas, 17,162 RTK points were collected. These were compared to LiDAR data for accuracy assessment. **Figure 2.5** shows base station locations and **Figures 2.6-2.29** show detailed views of RTK point locations.



Figure 2.5. Base station locations in the ODF and DOGAMI study areas.

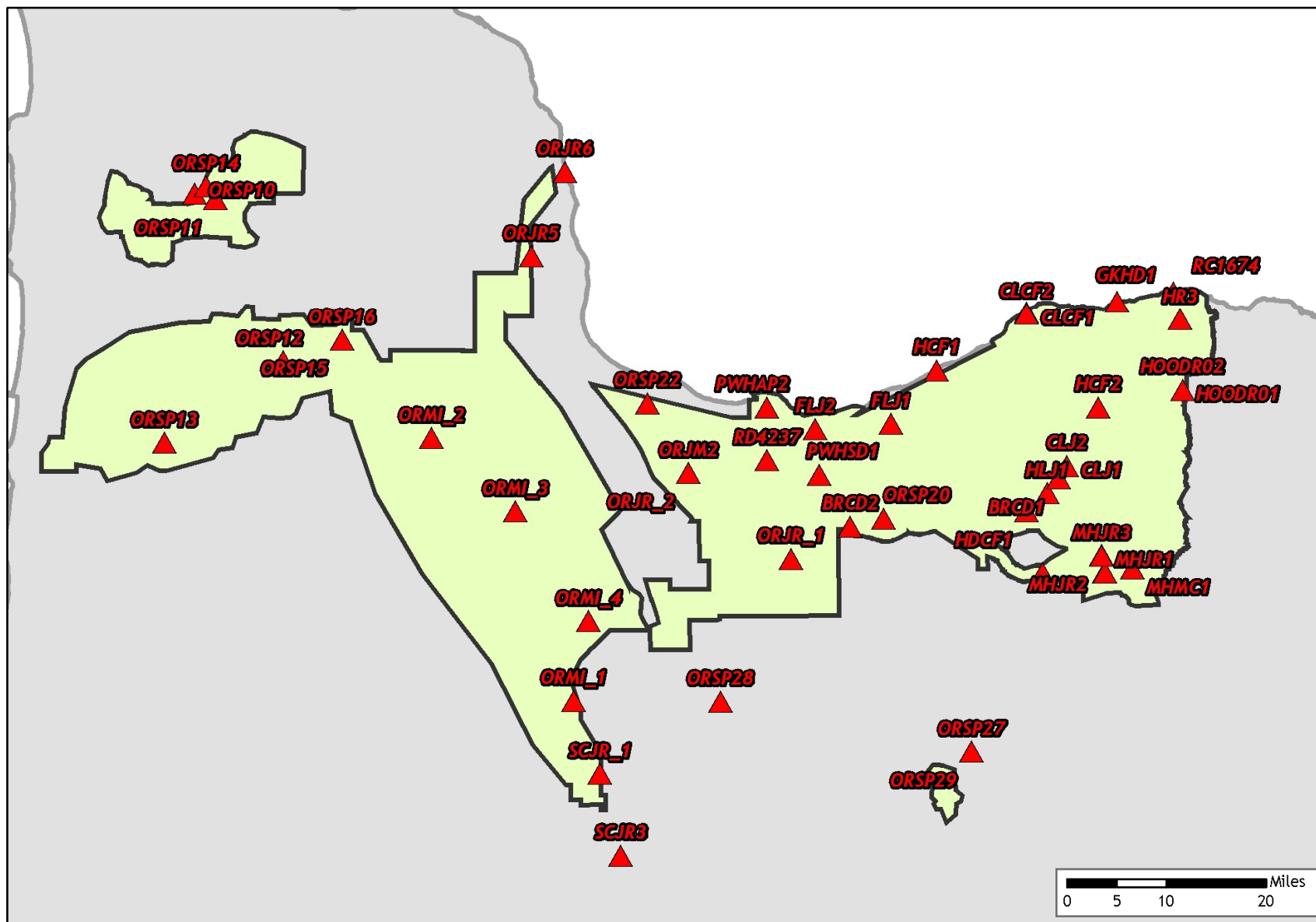


Figure 2.6. RTK point locations in the ODF study areas; color images are NAIP Orthoimages, black and white image is 1.5-foot resolution intensity image derived from LiDAR data.

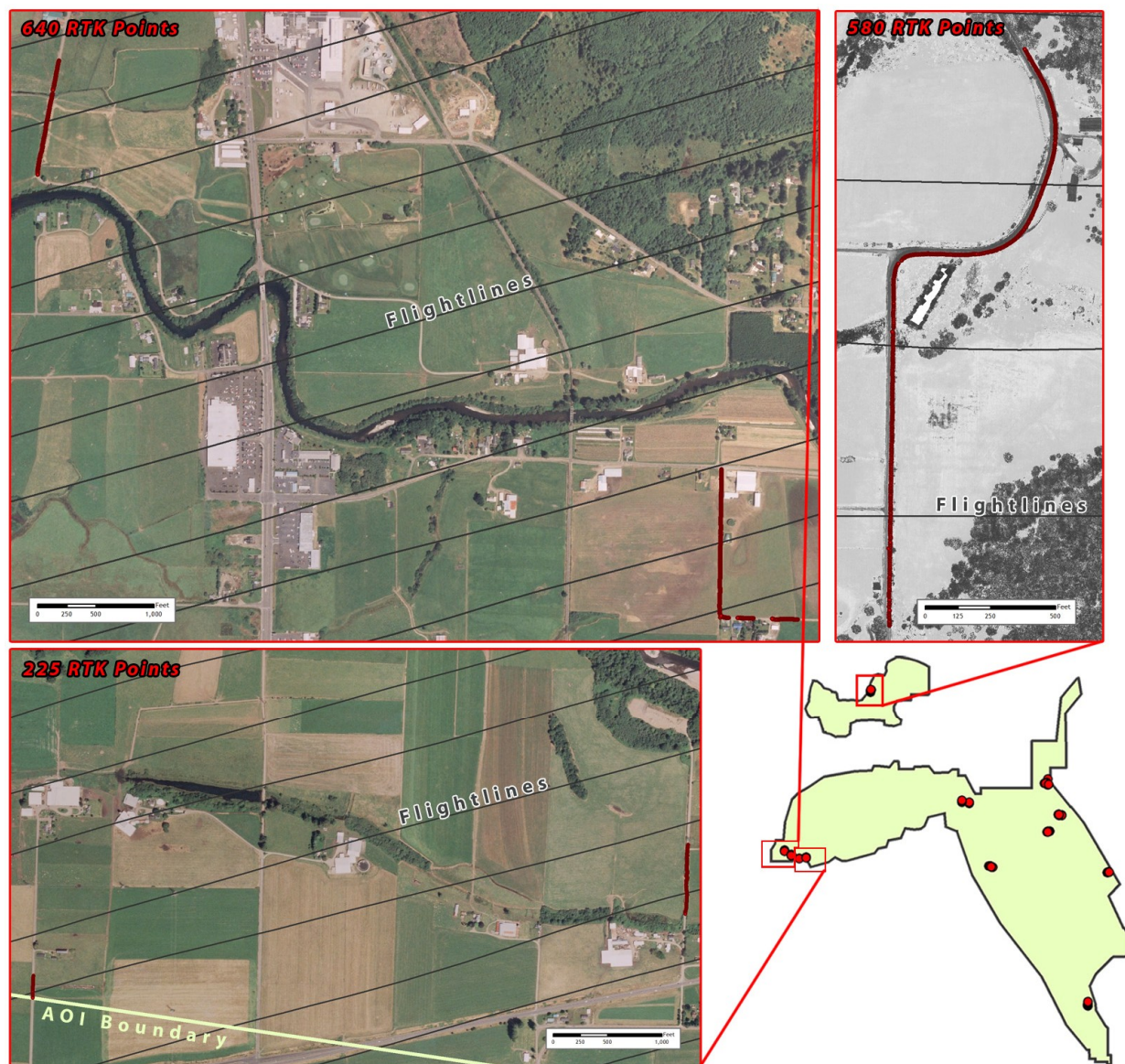


Figure 2.7. RTK point locations in the DOGAMI study areas; color images are NAIP Orthoimages.



Figure 2.8. RTK point locations in the DOGAMI study areas; color images are NAIP Orthoimages.

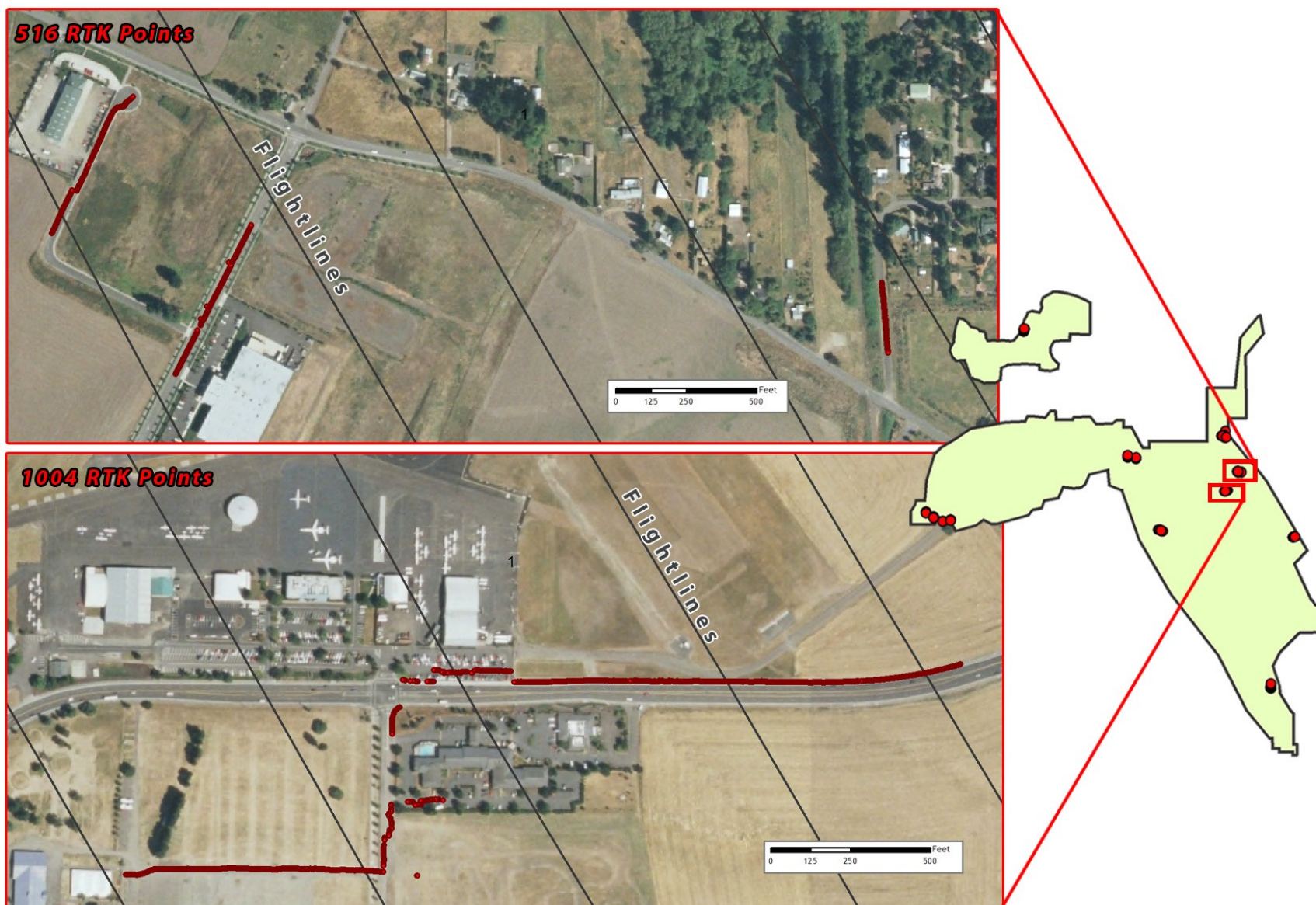


Figure 2.9. RTK point locations in the DOGAMI study areas; color images are NAIP Orthoimages.

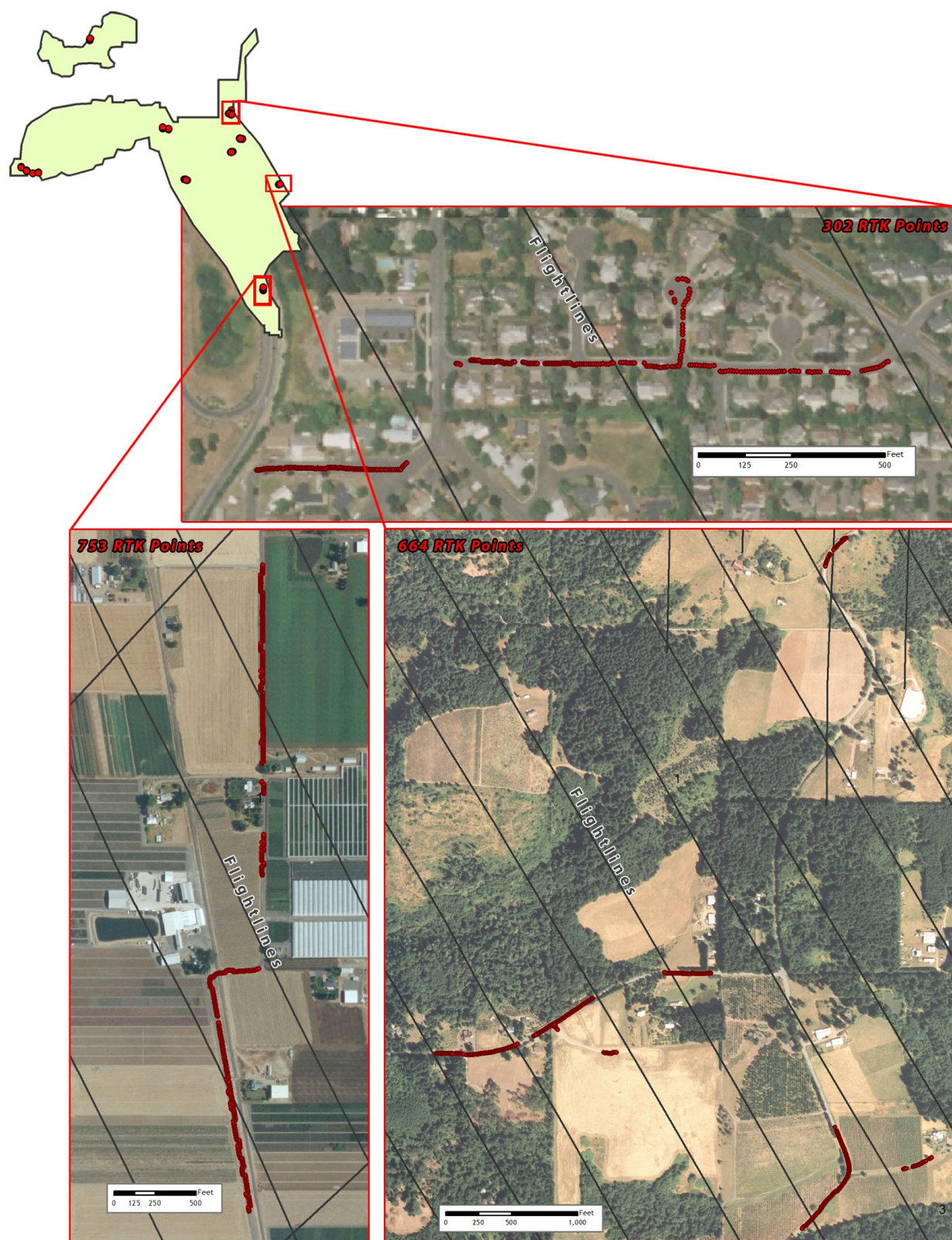


Figure 2.10. RTK point locations in the DOGAMI study areas; color images are NAIP Orthoimages.

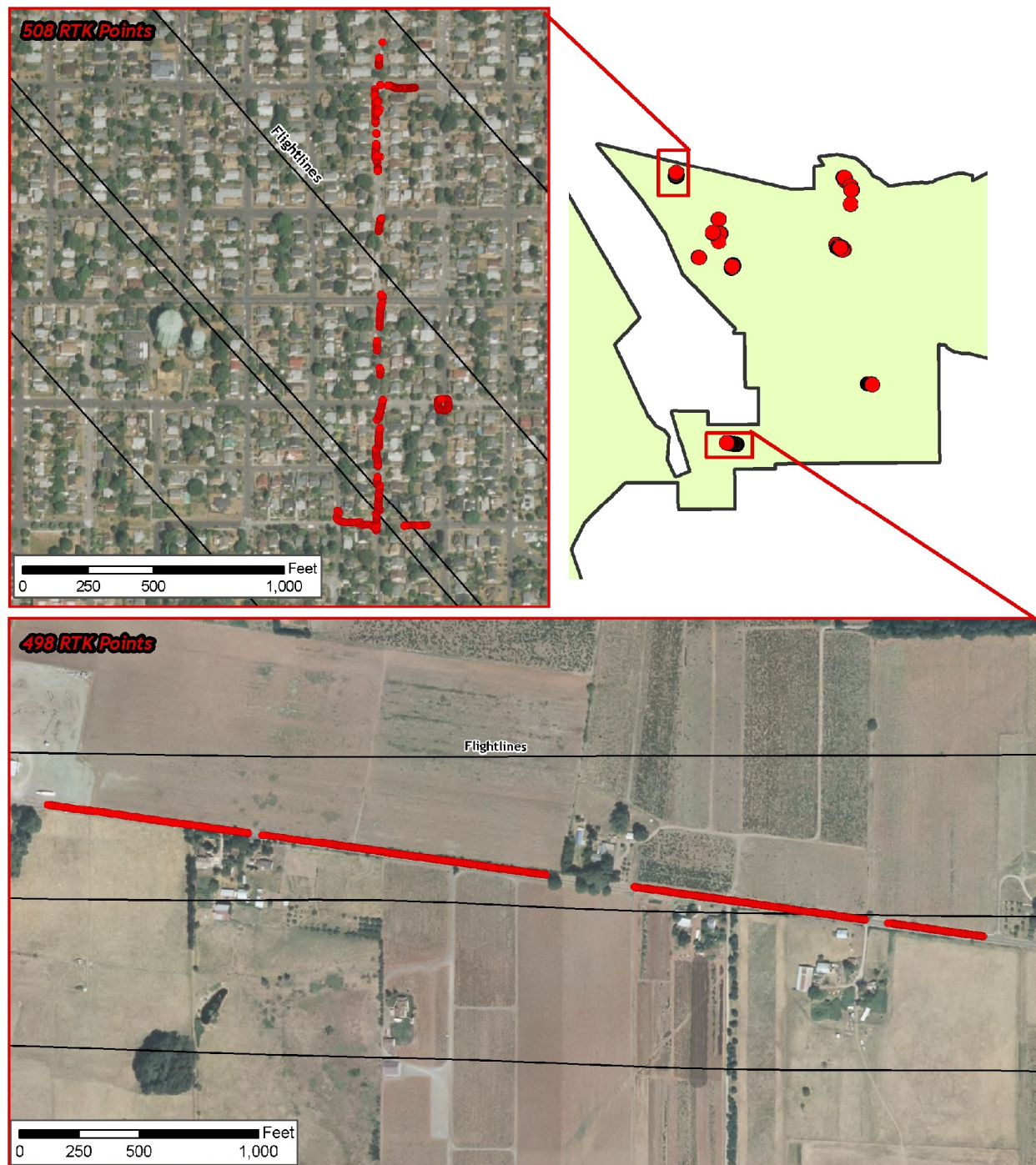


Figure 2.11. RTK point locations in the DOGAMI study areas; color images are NAIP Orthoimages.

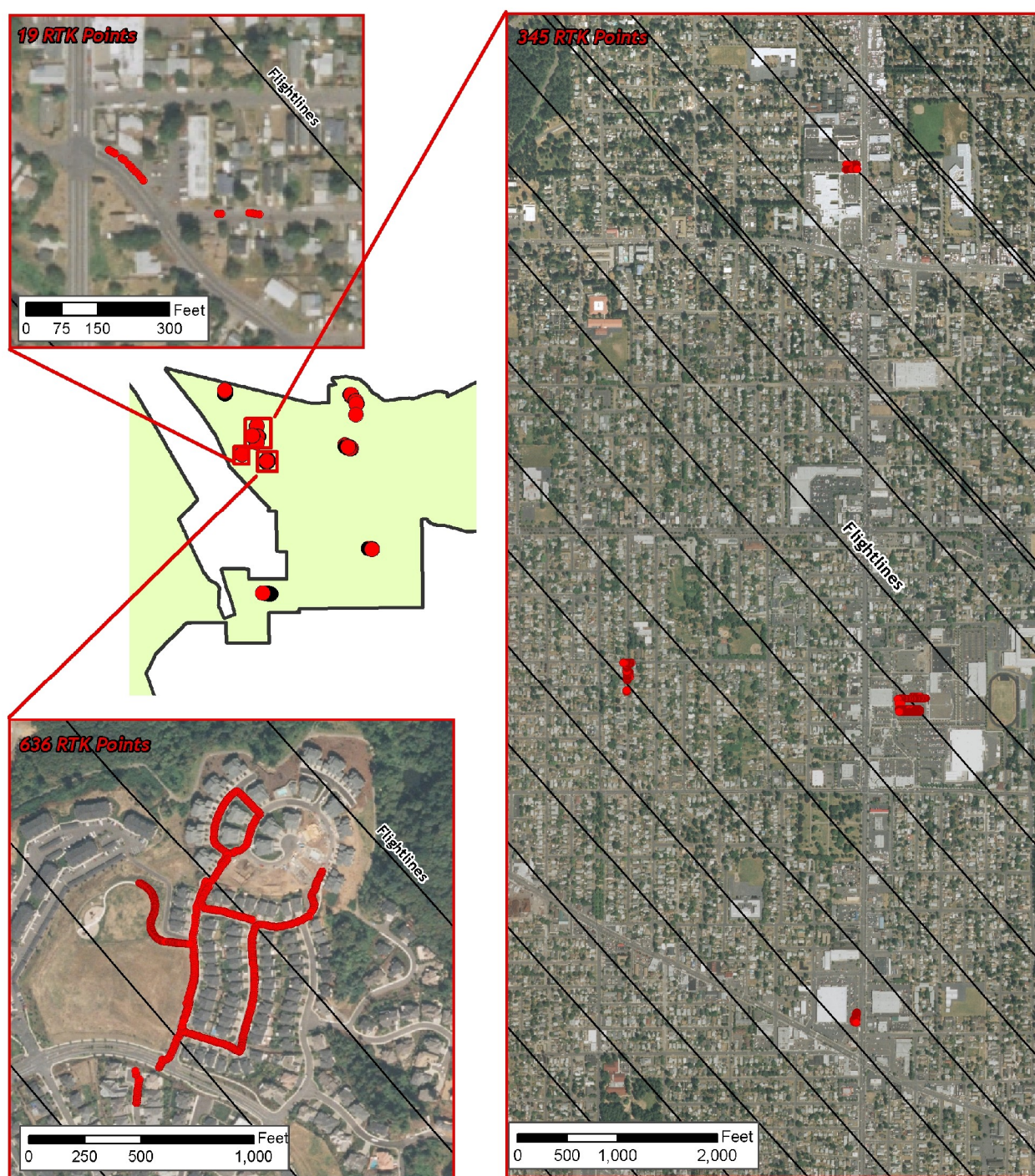


Figure 2.12. RTK point locations in the DOGAMI study areas; color images are NAIP Orthoimages.



Figure 2.13. RTK point locations in the DOGAMI study areas; color images are NAIP Orthoimages.

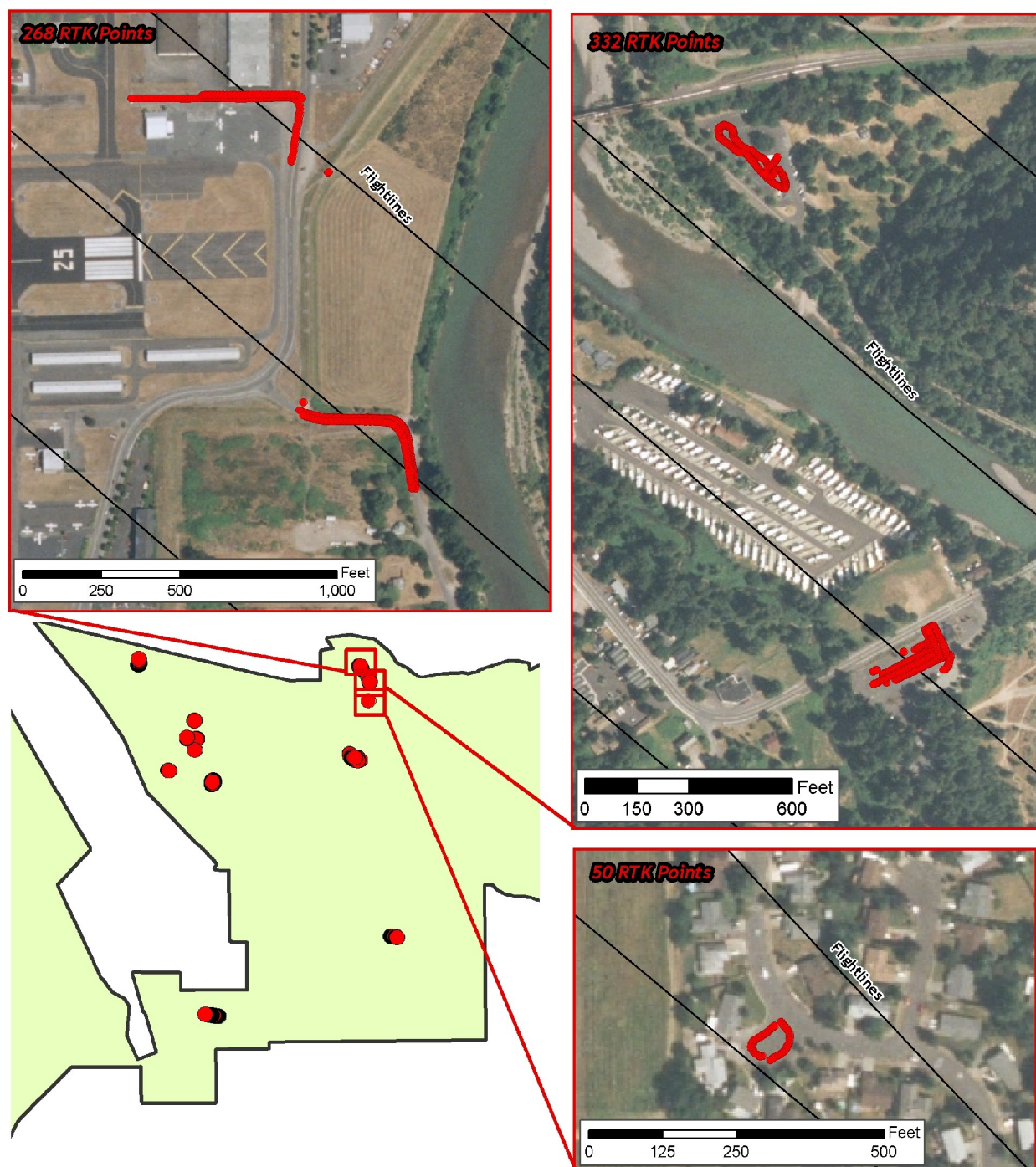


Figure 2.14. RTK point locations in the DOGAMI study areas; color images are NAIP Orthoimages; RTK points shown over bare-earth surface created from LiDAR data.

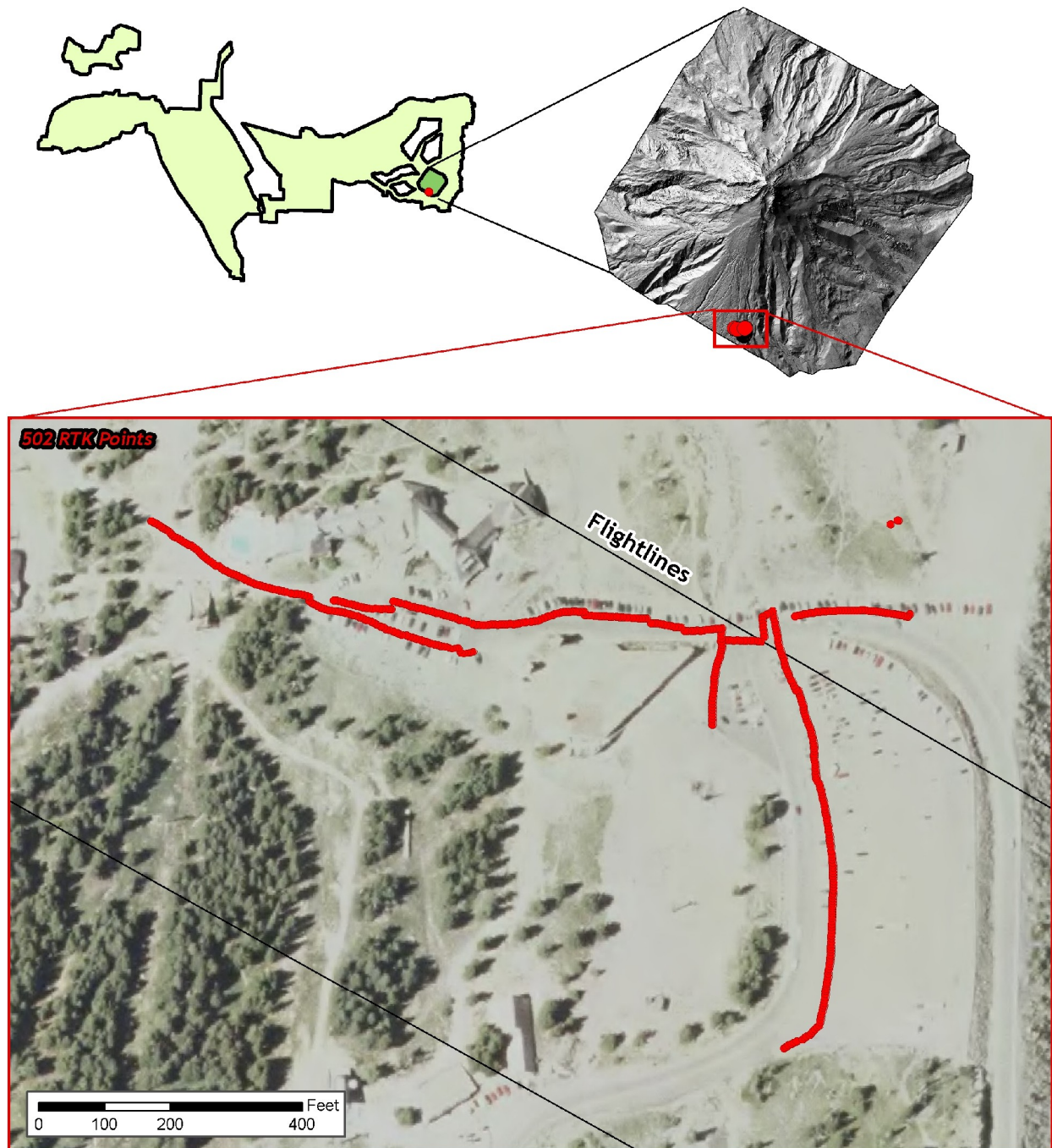


Figure 2.15. RTK point locations in the DOGAMI study areas; color images are NAIP Orthoimages.

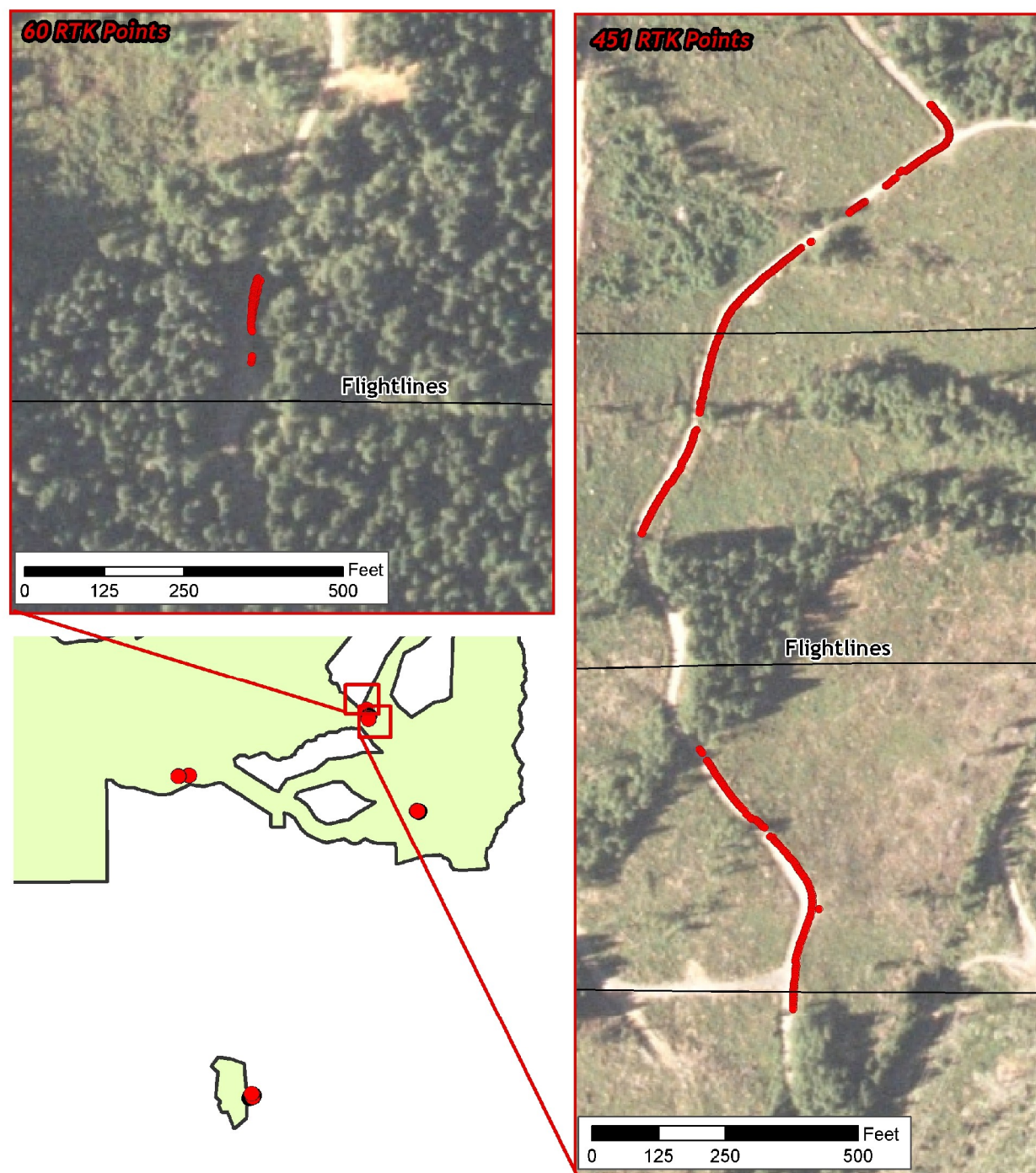


Figure 2.16. RTK point locations in the DOGAMI study areas; color images are NAIP Orthoimages.

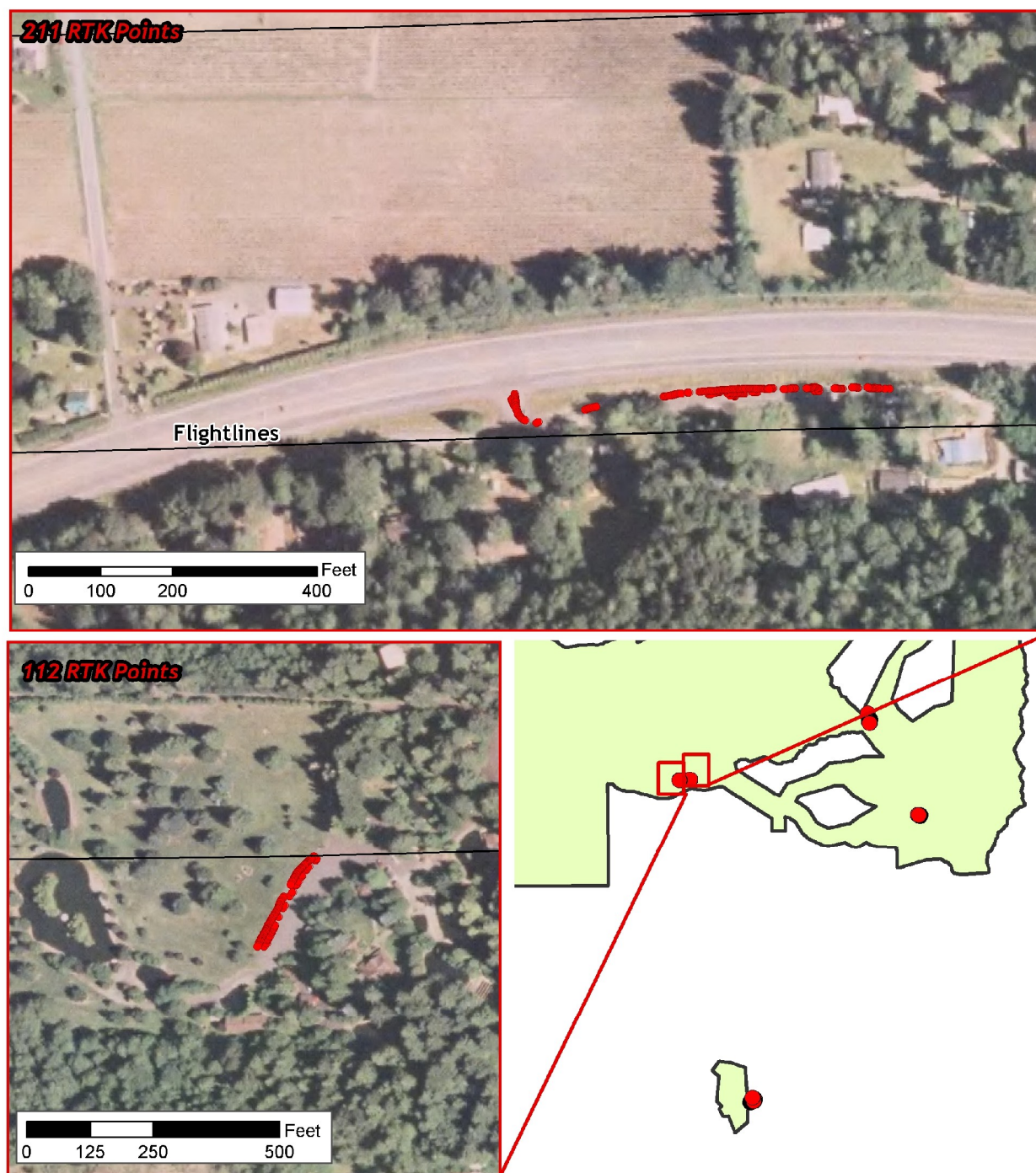


Figure 2.17. RTK point locations in the DOGAMI study areas; color images are NAIP Orthoimages.

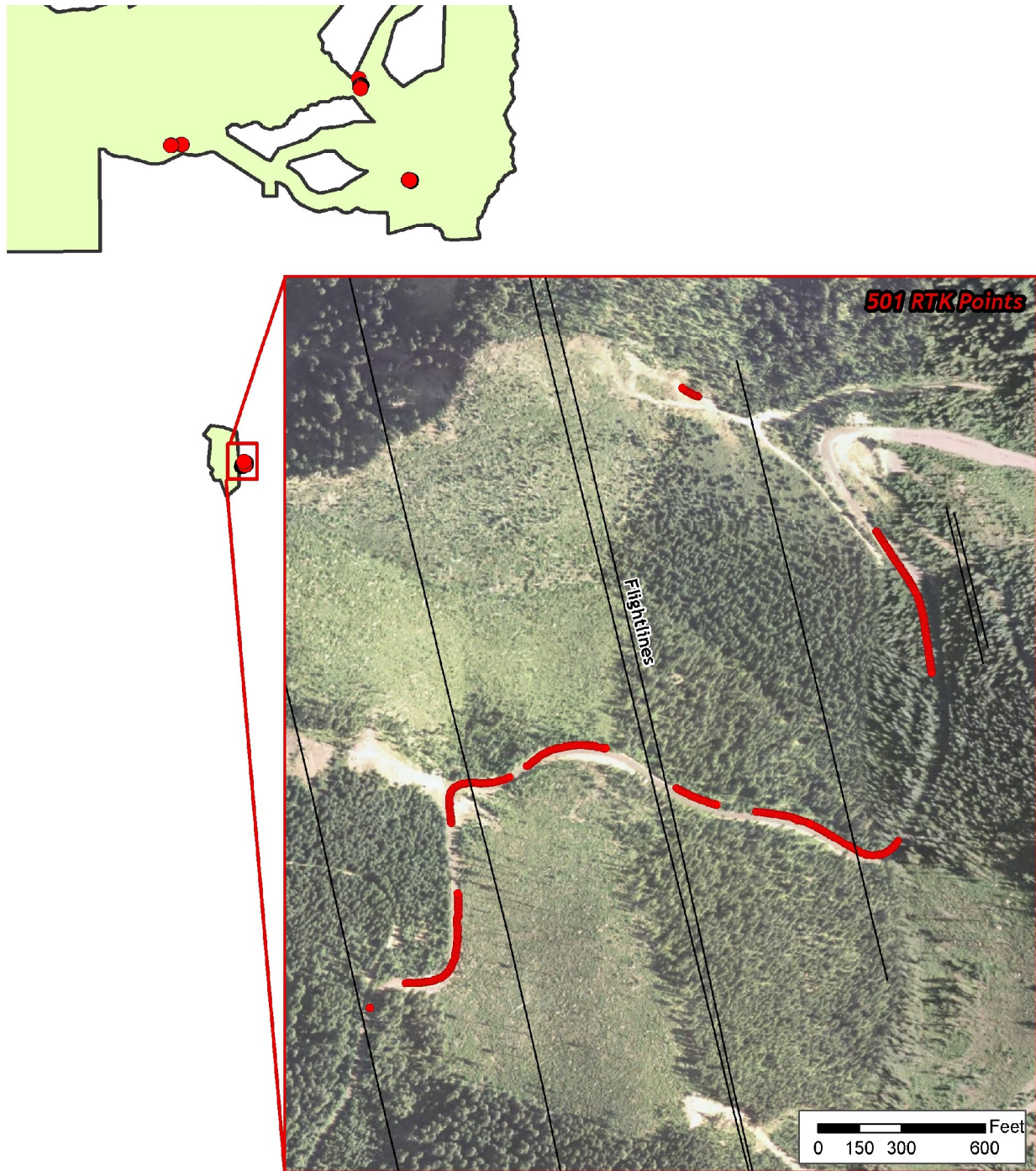


Figure 2.18. RTK point locations in the DOGAMI study area; color images are NAIP Orthoimages.

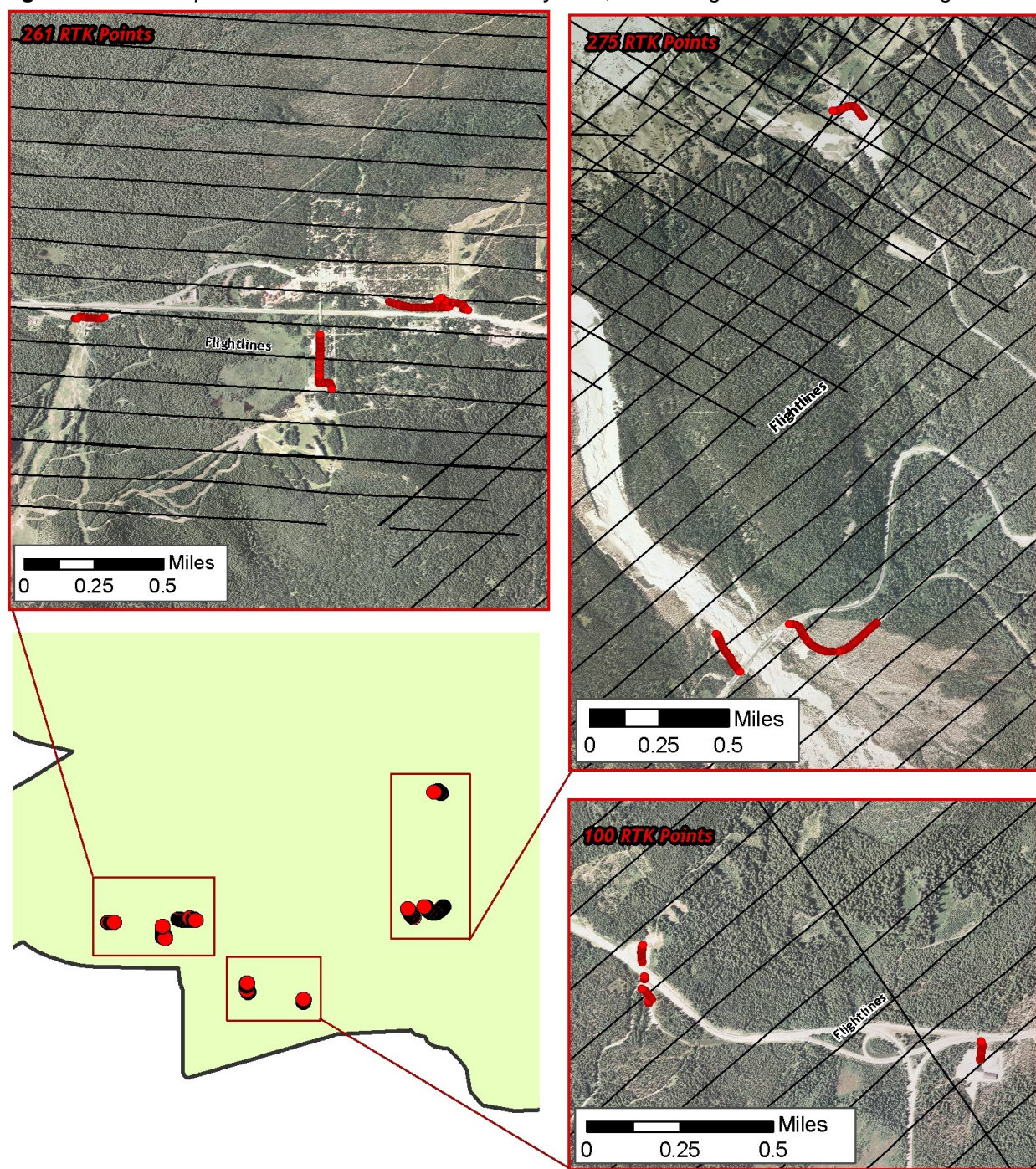


Figure 2.19. RTK point locations in the DOGAMI study area; color images are NAIP Orthoimages.

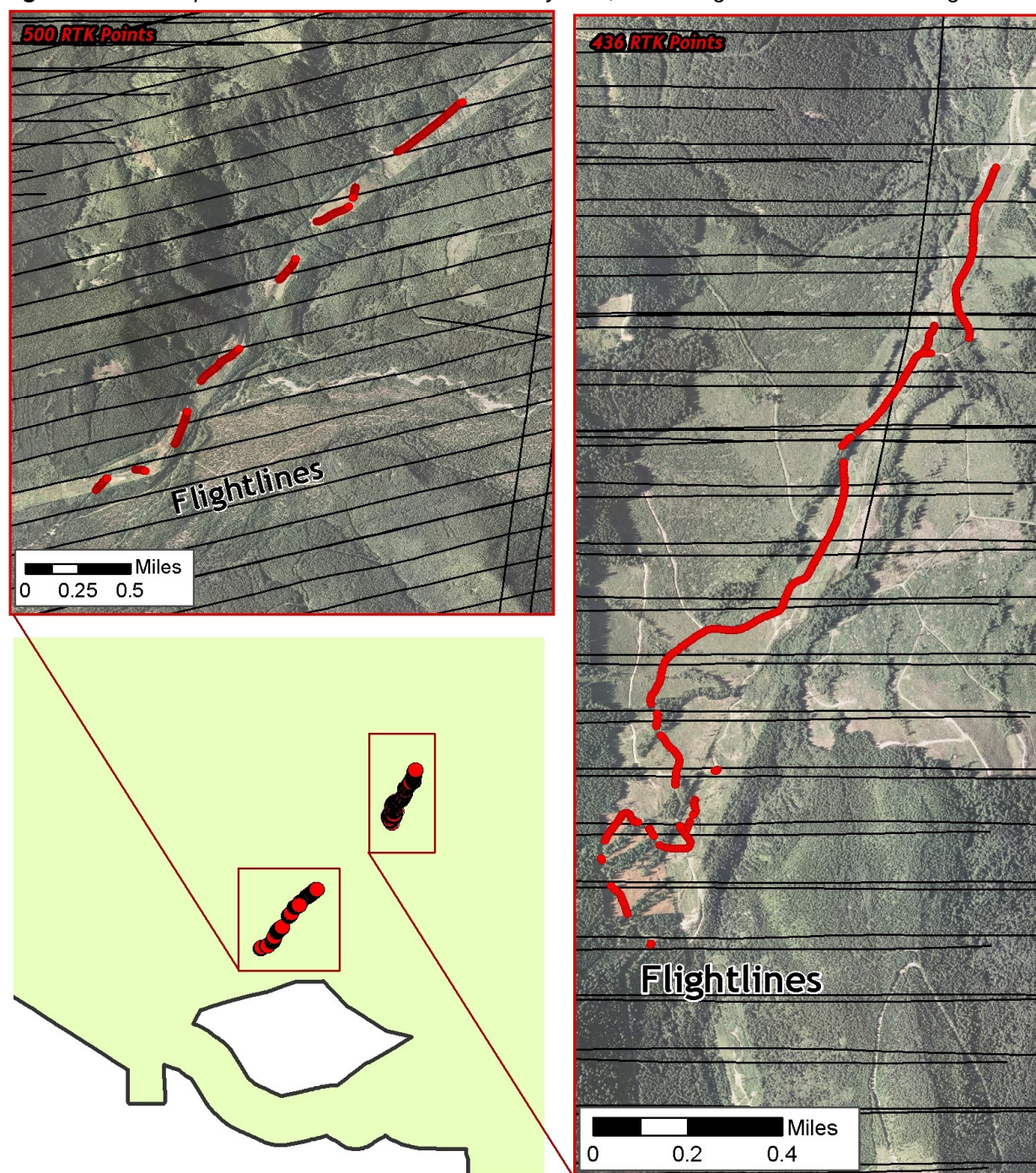


Figure 2.20. RTK point locations in the DOGAMI study area; color images are NAIP Orthoimages.

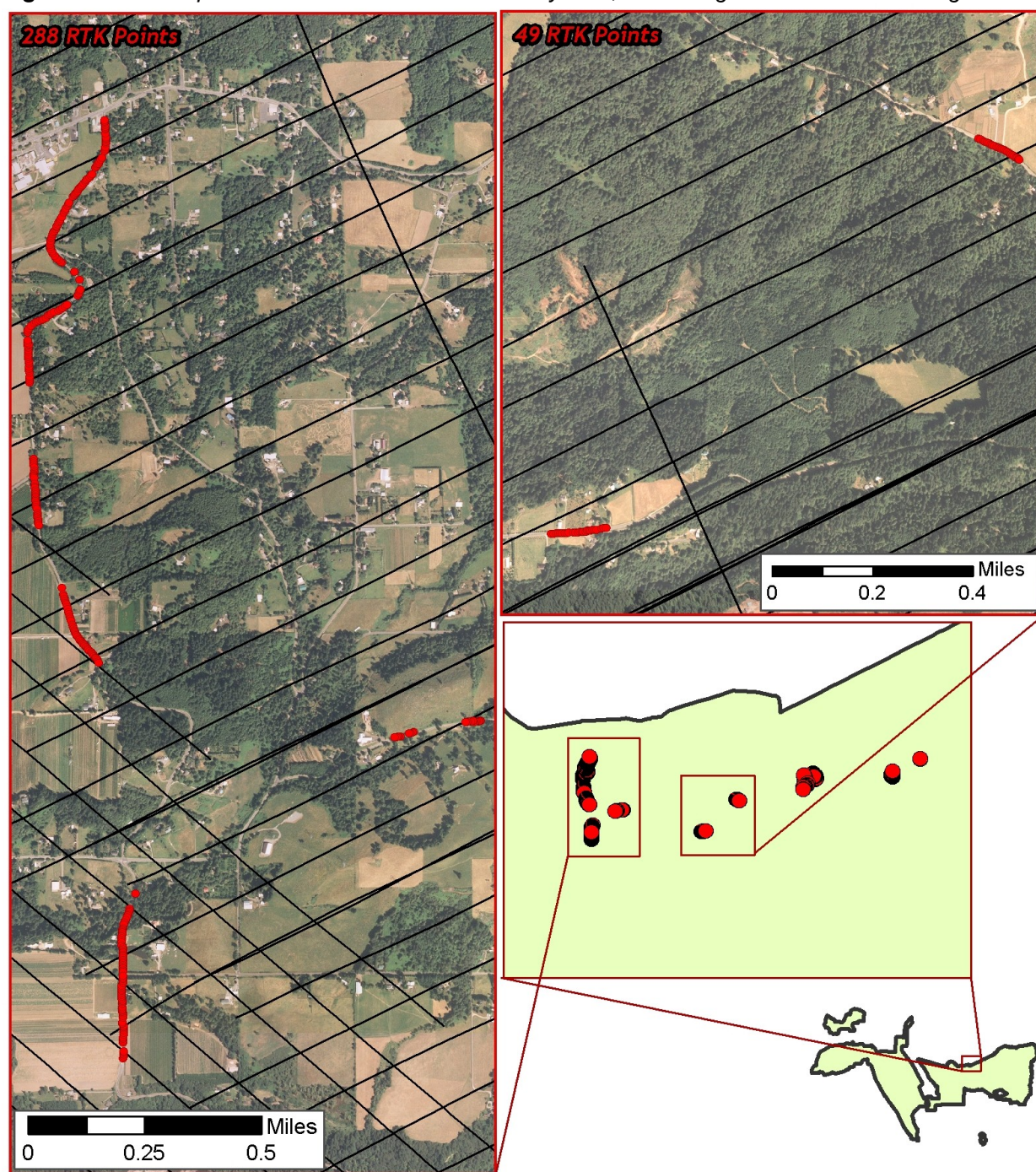


Figure 2.21. RTK point locations in the DOGAMI study area; color images are NAIP Orthoimages.

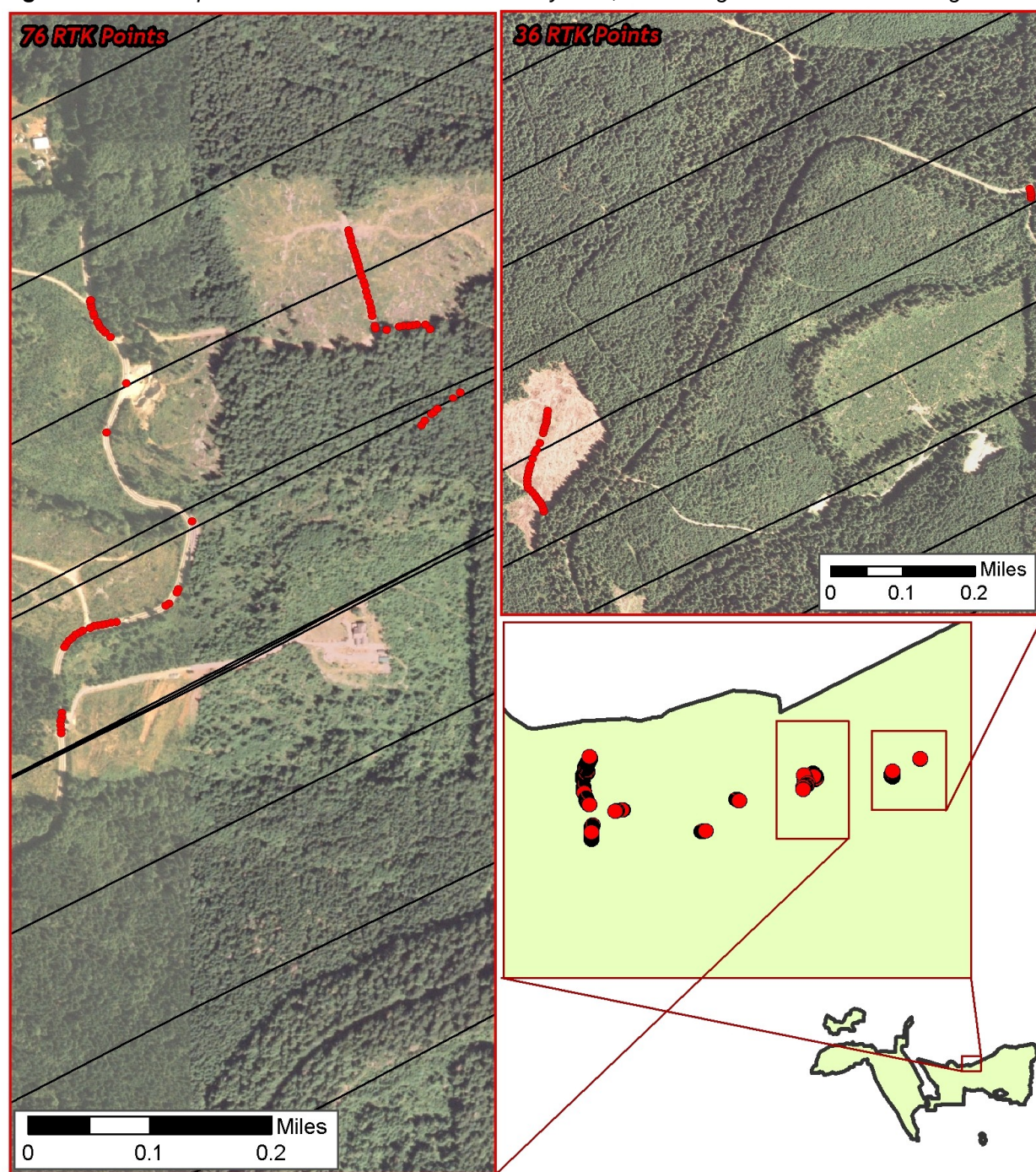


Figure 2.22. RTK point locations in the DOGAMI study area; color images are NAIP Orthoimages.

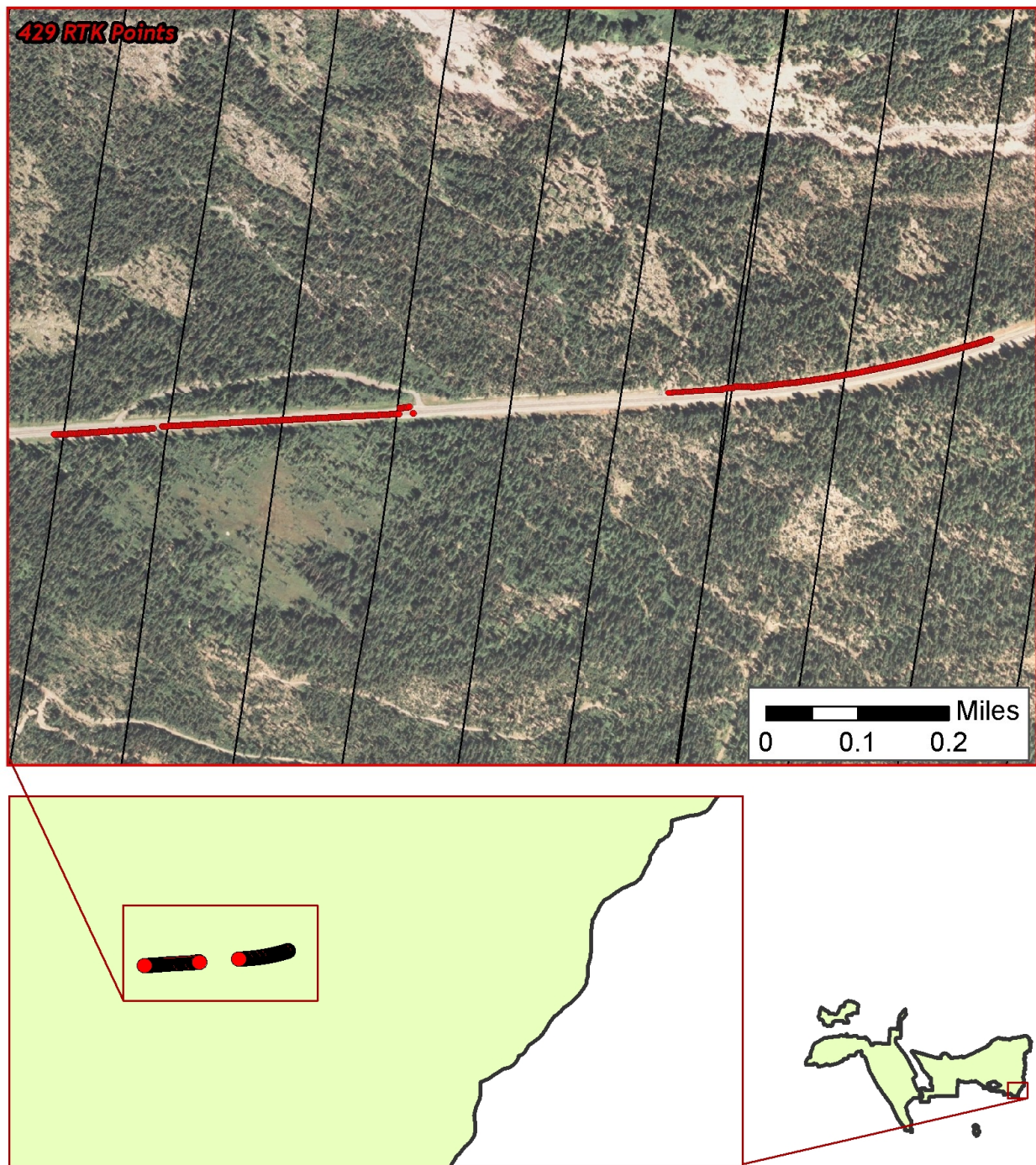


Figure 2.23. RTK point locations in the DOGAMI study area; color images are NAIP Orthoimages.

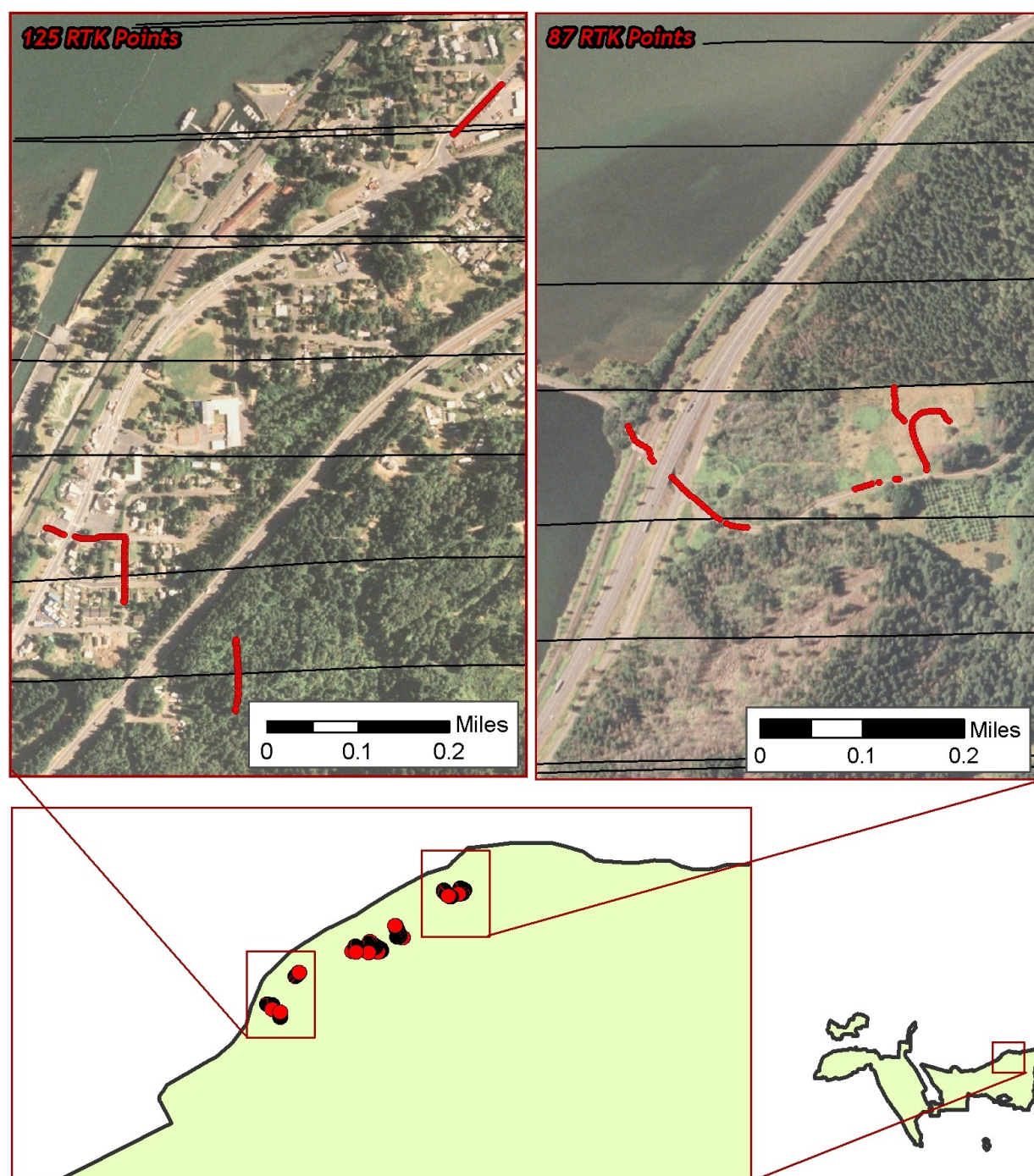


Figure 2.24. RTK point locations in the DOGAMI study area; color images are NAIP Orthoimages.

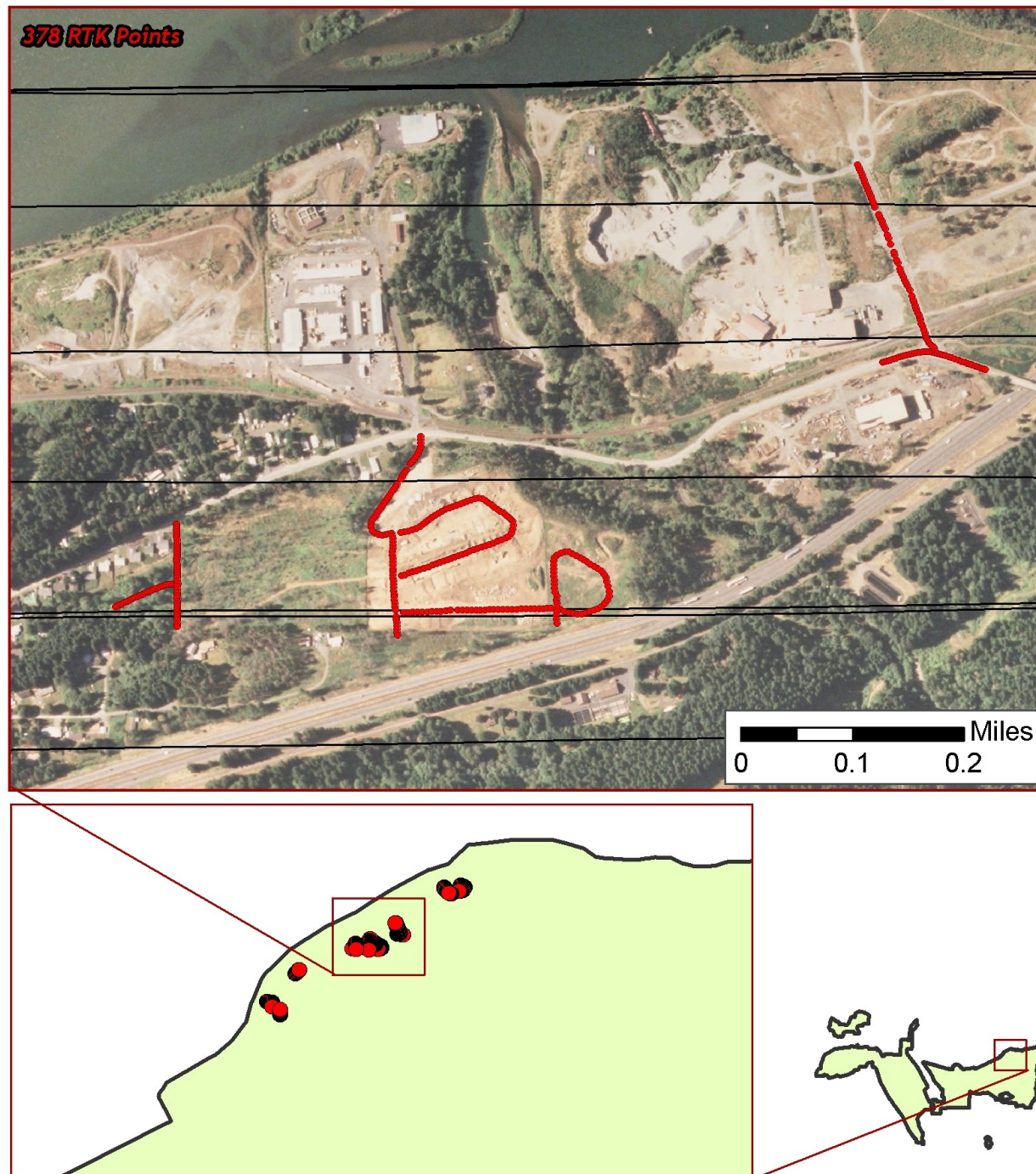


Figure 2.25. RTK point locations in the DOGAMI study area; color images are NAIP Orthoimages.

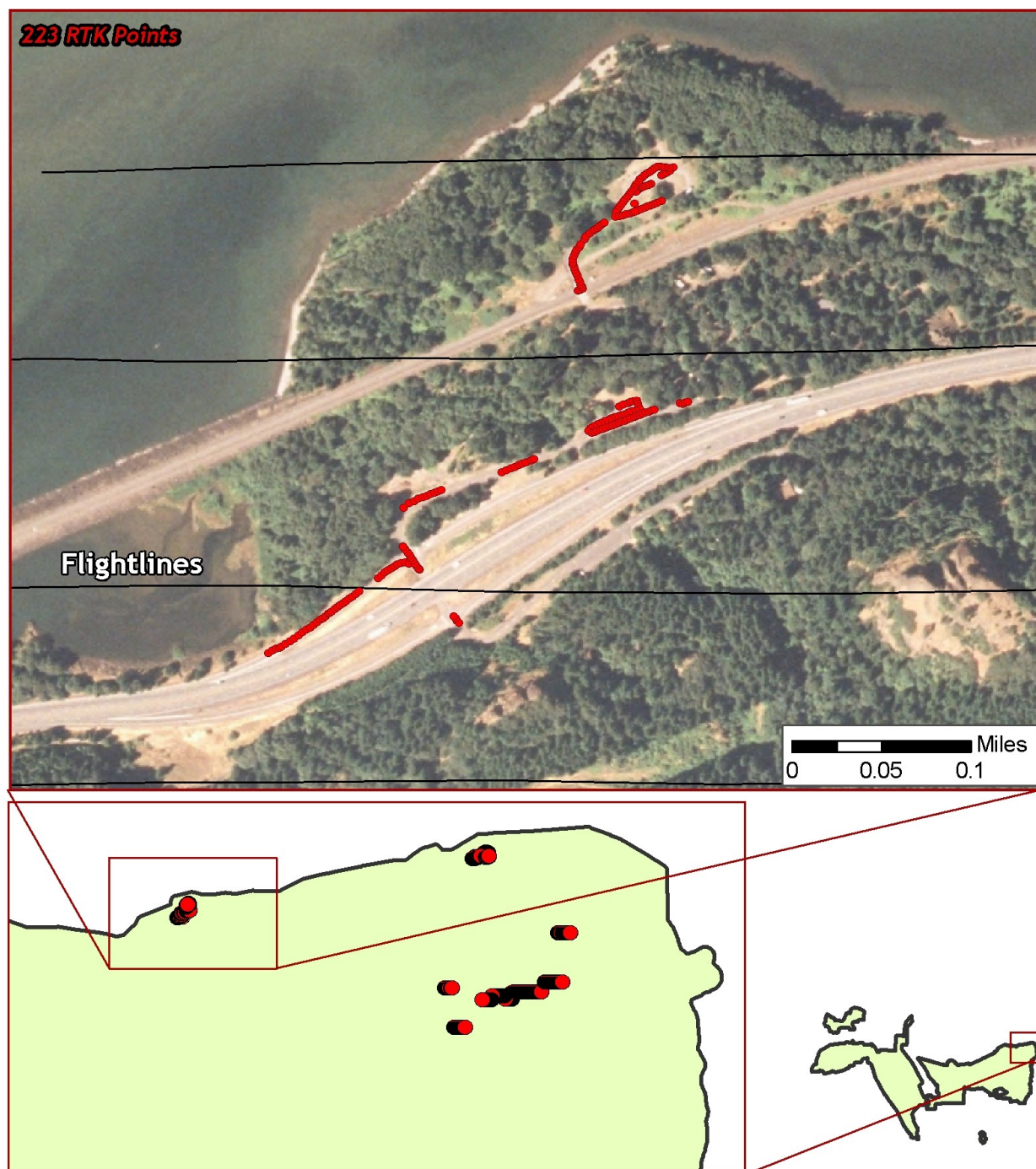


Figure 2.26. RTK point locations in the DOGAMI study area; color images are NAIP Orthoimages.

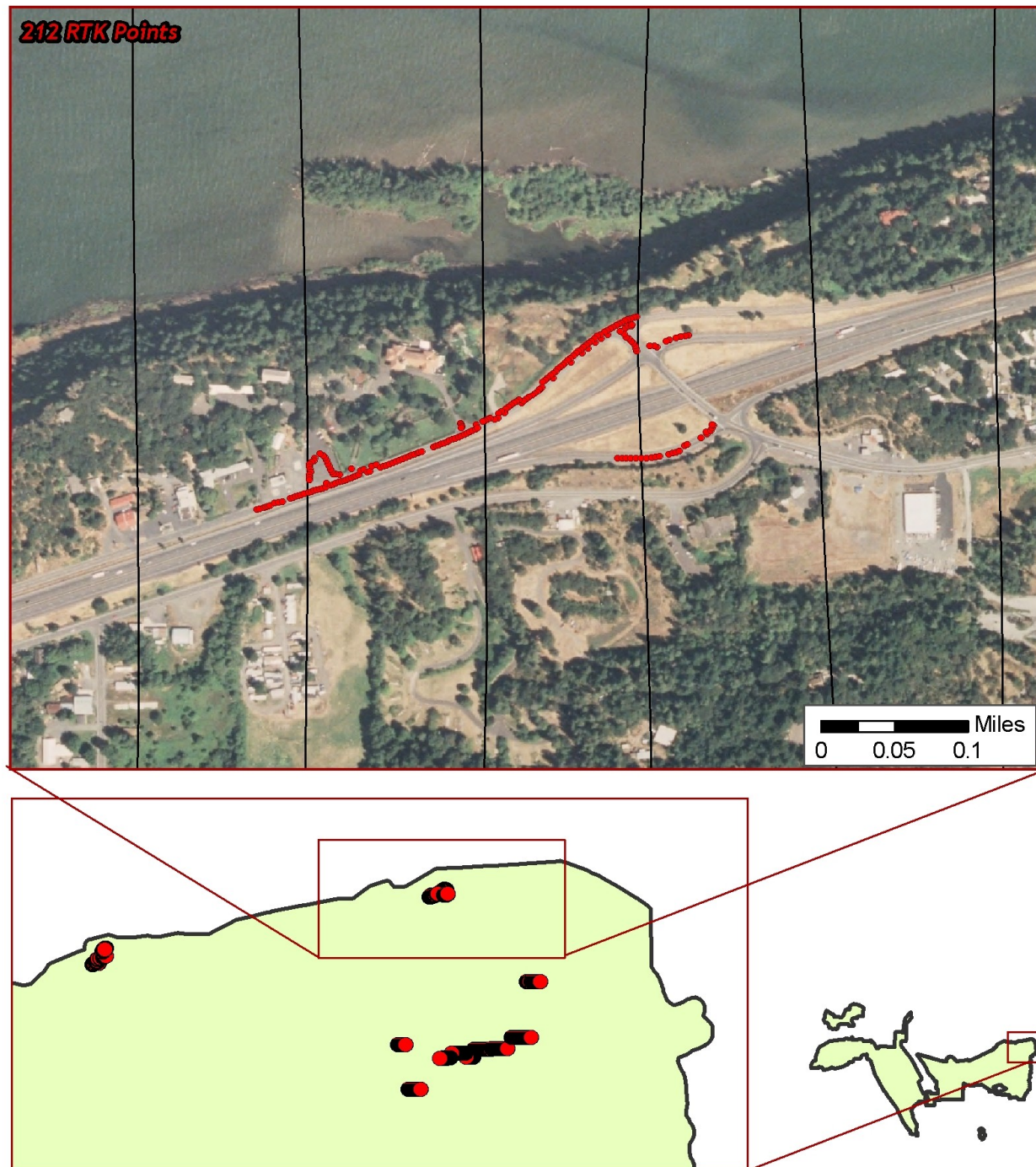


Figure 2.27. RTK point locations in the DOGAMI study area; color images are NAIP Orthoimages.

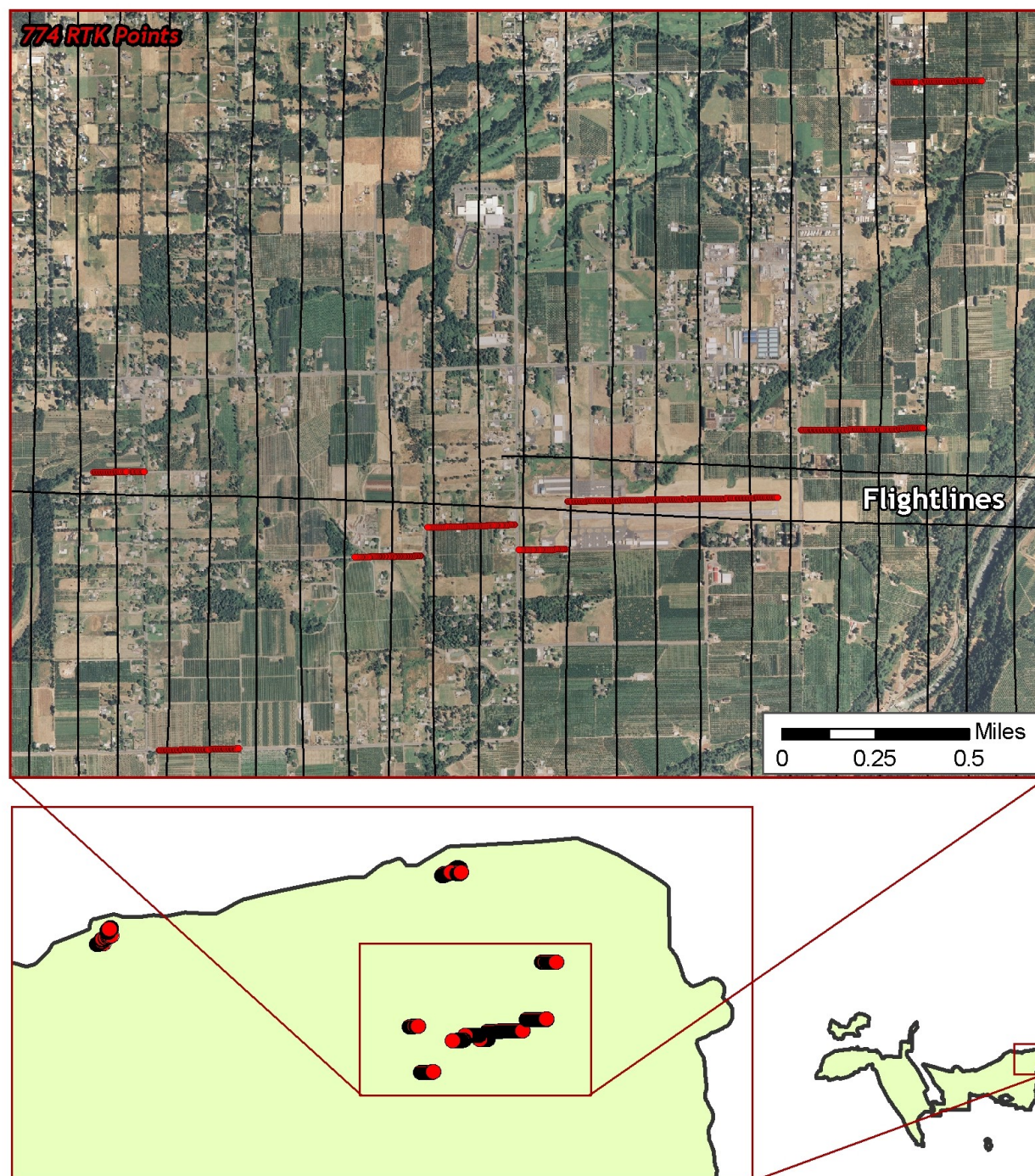


Figure 2.28. RTK point locations in the DOGAMI study area; color images are NAIP Orthoimages.

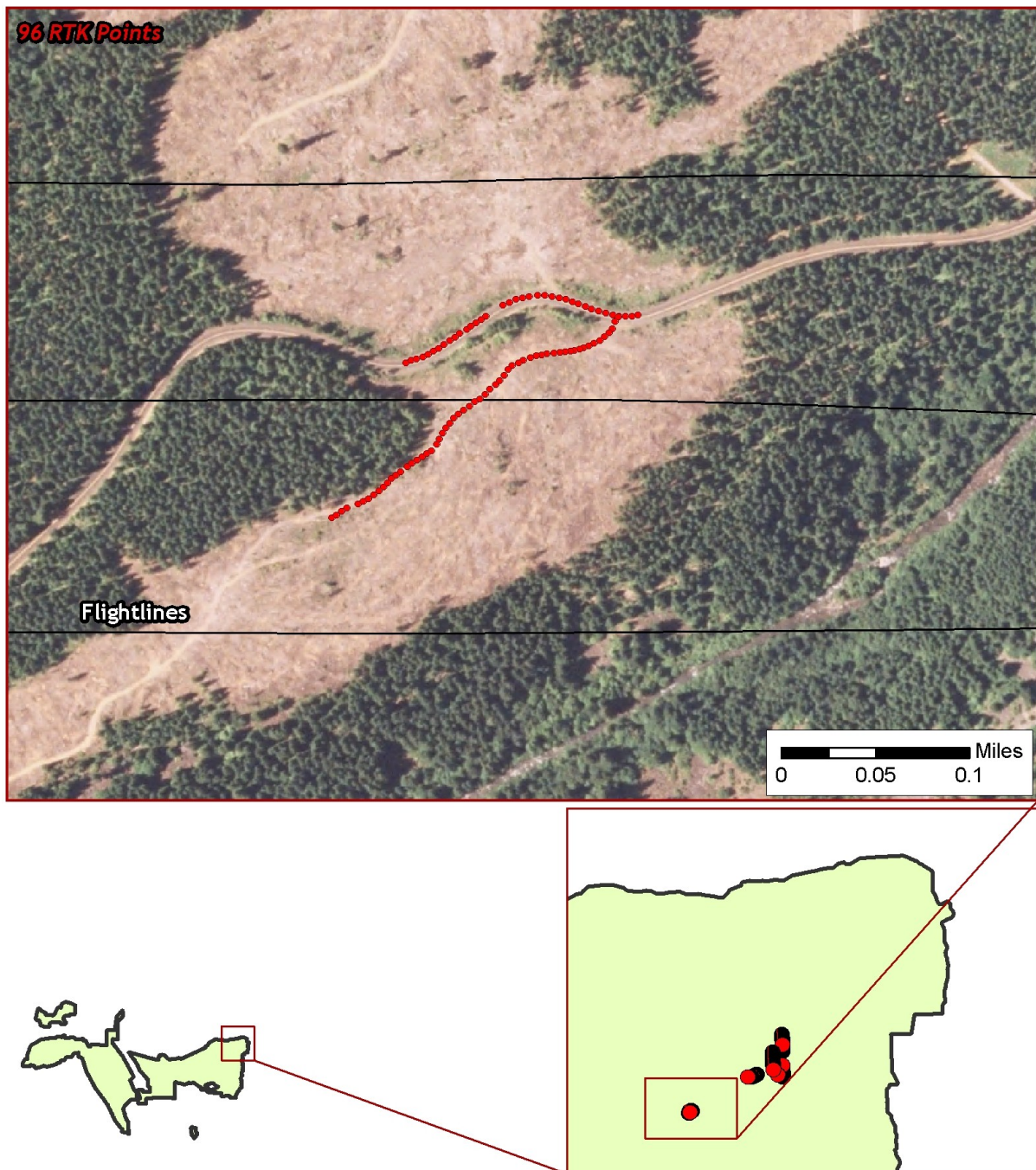
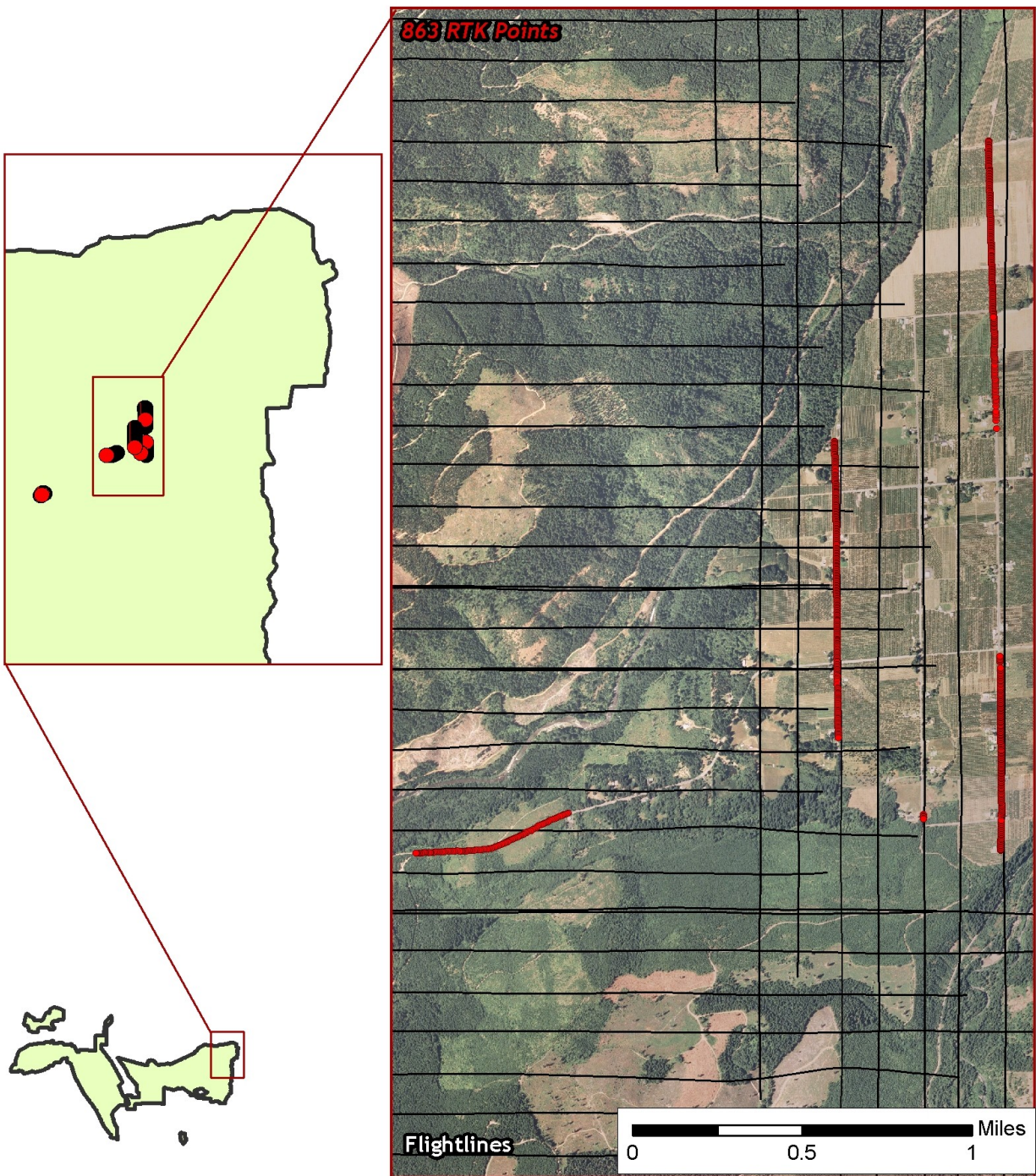


Figure 2.29. RTK point locations in the DOGAMI study area; color images are NAIP Orthoimages.



3. LiDAR Data Processing

3.1 Applications and Work Flow Overview

1. Resolve kinematic corrections for aircraft position data using kinematic aircraft GPS and static ground GPS data.
Software: Waypoint GPS v.8.10, Trimble Geomatics Office v.1.62
2. Develop a smoothed best estimate of trajectory (SBET) file that blends the post-processed aircraft position with attitude data. Sensor head position and attitude are calculated throughout the survey. The SBET data are used extensively for laser point processing.
Software: IPAS v.1.4
3. Calculate laser point position by associating the SBET position to each laser point return time, scan angle, intensity, etc. Creates raw laser point cloud data for the entire survey in *.las (ASPRS v1.1) format.
Software: ALS Post Processing Software
4. Import raw laser points into manageable blocks (less than 500 MB) to perform manual relative accuracy calibration and filter for pits/birds. Ground points are then classified for individual flight lines (to be used for relative accuracy testing and calibration).
Software: TerraScan v.9.001
5. Using ground classified points per each flight line, the relative accuracy is tested. Automated line-to-line calibrations are then performed for system attitude parameters (pitch, roll, heading), mirror flex (scale) and GPS/IMU drift. Calibrations are performed on ground classified points from paired flight lines. Every flight line is used for relative accuracy calibration.
Software: TerraMatch v.9.001
6. Position and attitude data are imported. Resulting data are classified as ground and non-ground points. Statistical absolute accuracy is assessed via direct comparisons of ground classified points to ground RTK survey data. Data are then converted to orthometric elevations (NAVD88) by applying a Geoid03 correction. Ground models are created as a triangulated surface and exported as ArcInfo ASCII grids at a 3-foot pixel resolution.
Software: TerraScan v.9.001, ArcMap v9.3, TerraModeler v.9.001

3.2 Aircraft Kinematic GPS and IMU Data

LiDAR survey datasets are referenced to 1 Hz static ground GPS data collected over pre-surveyed monuments with known coordinates. While surveying, the aircraft collects 2 Hz kinematic GPS data. The onboard inertial measurement unit (IMU) collects 200 Hz aircraft attitude data. Waypoint GPS v.7.80 is used to process the kinematic corrections for the aircraft. The static and kinematic GPS data are then post-processed after the survey to obtain an accurate GPS solution and aircraft positions. IPAS v.1.4 is used to develop a trajectory file that includes corrected aircraft position and attitude information. The trajectory data for the entire flight survey session are incorporated into a final smoothed best estimated trajectory (SBET) file that contains accurate and continuous aircraft positions and attitudes.

3.3 Laser Point Processing

Laser point coordinates are computed using the IPAS and ALS Post Processor software suites based on independent data from the LiDAR system (pulse time, scan angle), and aircraft trajectory data (SBET). Laser point returns (first through fourth) are assigned an associated (x, y, z) coordinate along with unique intensity values (0-255). The data are output into large LAS v. 1.1 files; each point maintains the corresponding scan angle, return number (echo), intensity, and x, y, z (easting, northing, and elevation) information.

These initial laser point files are too large to process. To facilitate laser point processing, bins (polygons) are created to divide the dataset into manageable sizes (< 500 MB). Flightlines and LiDAR data are then reviewed to ensure complete coverage of the study area and positional accuracy of the laser points.

Once the laser point data are imported into bins in TerraScan, a manual calibration is performed to assess the system offsets for pitch, roll, heading and mirror scale. Using a geometric relationship developed by Watershed Sciences, each of these offsets is resolved and corrected if necessary.

The LiDAR points are then filtered for noise, pits and birds by screening for absolute elevation limits, isolated points and height above ground. Each bin is then inspected for pits and birds manually; spurious points are removed. For a bin containing approximately 7.5-9.0 million points, an average of 50-100 points are typically found to be artificially low or high. These spurious non-terrestrial laser points must be removed from the dataset. Common sources of non-terrestrial returns are clouds, birds, vapor, and haze.

The internal calibration is refined using TerraMatch. Points from overlapping lines are tested for internal consistency and final adjustments are made for system misalignments (i.e., pitch, roll, heading offsets and mirror scale). Automated sensor attitude and scale corrections yield 3-5 cm improvements in the relative accuracy. Once the system misalignments are corrected, vertical GPS drift is then resolved and removed per flight line, yielding a slight improvement (<1 cm) in relative accuracy. At this point in the workflow, data have passed a robust calibration designed to reduce inconsistencies from multiple sources (i.e. sensor attitude offsets, mirror scale, GPS drift) using a procedure that is comprehensive (i.e. uses all of the overlapping survey data). Relative accuracy screening is complete.

The TerraScan software suite is designed specifically for classifying near-ground points (Soininen, 2004). The processing sequence begins by 'removing' all points that are not 'near' the earth based on geometric constraints used to evaluate multi-return points. The resulting bare earth (ground) model is visually inspected and additional ground point modeling is performed in site-specific areas (over a 50-meter radius) to improve ground detail. This is only done in areas with known ground modeling deficiencies, such as: bedrock outcrops, cliffs, deeply incised stream banks, and dense vegetation. In some cases, ground point classification includes known vegetation (i.e., understory, low/dense shrubs, etc.) and these points are manually reclassified as non-grounds. Ground surface rasters are developed from triangulated irregular networks (TINs) of ground points.

4. LiDAR Accuracy and Resolution

4.1 Laser Point Accuracy

Laser point absolute accuracy is largely a function of internal consistency (measured as relative accuracy) and laser noise:

- **Laser Noise:** For any given target, laser noise is the breadth of the data cloud per laser return (i.e., last, first, etc.). Lower intensity surfaces (roads, rooftops, still/calm water) experience higher laser noise. The laser noise range for this mission is approximately 0.02 meters.
- **Relative Accuracy:** Internal consistency refers to the ability to place a laser point in the same location over multiple flight lines, GPS conditions, and aircraft attitudes.
- **Absolute Accuracy:** RTK GPS measurements taken in the study areas compared to LiDAR point data.

Statements of statistical accuracy apply to fixed terrestrial surfaces only, not to free-flowing or standing water surfaces, moving automobiles, et cetera.

Table 4.1. *LiDAR accuracy is a combination of several sources of error. These sources of error are cumulative. Some error sources that are biased and act in a patterned displacement can be resolved in post processing.*

| Type of Error | Source | Post Processing Solution |
|---------------------------|------------------------------|---|
| GPS (Static/Kinematic) | Long Base Lines | None |
| | Poor Satellite Constellation | None |
| | Poor Antenna Visibility | Reduce Visibility Mask |
| Relative Accuracy | Poor System Calibration | Recalibrate IMU and sensor offsets/settings |
| | Inaccurate System | None |
| Laser Noise | Poor Laser Timing | None |
| | Poor Laser Reception | None |
| | Poor Laser Power | None |
| | Irregular Laser Shape | None |

4.1.1 Relative Accuracy

Relative accuracy refers to the internal consistency of the data set and is measured as the divergence between points from different flight lines within an overlapping area. Divergence is most apparent when flight lines are opposing. When the LiDAR system is well calibrated the line to line divergence is low (<10 cm). Internal consistency is affected by system attitude offsets (pitch, roll and heading), mirror flex (scale), and GPS/IMU drift.

Operational measures taken to improve relative accuracy:

1. Low Flight Altitude: Terrain following was targeted at a flight altitude of 900 meters above ground level (AGL). Laser horizontal errors are a function of flight altitude above ground (i.e., $\sim 1/3000^{\text{th}}$ AGL flight altitude). Lower flight altitudes decrease laser noise on surfaces with even the slightest relief.
2. Focus Laser Power at narrow beam footprint: A laser return must be received by the system above a power threshold to accurately record a measurement. The strength of the laser return is a function of laser emission power, laser footprint, flight altitude and the reflectivity of the target. While surface reflectivity cannot be controlled, laser power can be increased and low flight altitudes can be maintained.
3. Reduced Scan Angle: Edge-of-scan data can become inaccurate. The scan angle was reduced to a maximum of $\pm 14^\circ$ from nadir, creating a narrow swath width and greatly reducing laser shadows from trees and buildings.
4. Quality GPS: Flights took place during optimal GPS conditions (e.g., 6 or more satellites and PDOP [Position Dilution of Precision] less than 3.0). Before each flight, the PDOP was determined for the survey day. During all flight times, a dual frequency DGPS base station recording at 1-second epochs was utilized and a maximum baseline length between the aircraft and the control points was less than 19 km (11.5 miles) at all times.
5. Ground Survey: Ground survey point accuracy (i.e., <1.5 cm RMSE) occurs during optimal PDOP ranges and targets a minimal baseline distance of 4 miles between GPS rover and base. Robust statistics are, in part, a function of sample size (n) and distribution.
6. 50% Side-Lap (100% Overlap): Overlapping areas are optimized for relative accuracy testing. Laser shadowing is minimized to help increase target acquisition from multiple scan angles. Ideally, with a 50% side-lap, the most nadir portion of one flight line coincides with the edge (least nadir) portion of overlapping flight lines. A minimum of 50% side-lap with terrain-followed acquisition prevents data gaps.
7. Opposing Flight Lines: All overlapping flight lines are opposing. Pitch, roll and heading errors are amplified by a factor of two relative to the adjacent flight line(s), making misalignments easier to detect and resolve.

Relative Accuracy Calibration Methodology

1. Manual System Calibration: Calibration procedures for each mission require solving geometric relationships that relate measured swath-to-swath deviations to misalignments of system attitude parameters. Corrected scale, pitch, roll and heading offsets are calculated and applied to resolve misalignments. The raw divergence between lines is computed after the manual calibration is completed and reported for each study area.
2. Automated Attitude Calibration: All data are tested and calibrated using TerraMatch automated sampling routines. Ground points are classified for each individual flight line and used for line-to-line testing. System misalignment offsets (pitch, roll and heading) and mirror scale are solved for each individual mission. The application of attitude misalignment offsets (and mirror scale) occurs for each individual mission. The data from each mission are then blended when imported together to form the entire area of interest.
3. Automated Z Calibration: Ground points per line are utilized to calculate the vertical divergence between lines caused by vertical GPS drift. Automated Z calibration is the final step employed for relative accuracy calibration.

Relative Accuracy Calibration Results

2007 Acquisition Areas

Relative accuracies have been determined for all portions of the DOGAMI & ODF study areas **acquired in 2007** and delivered; the statistics are based on the comparison of 1,157 flightlines and over 12 billion points. For flightline coverage, see **Figure 2.1** in Section 2.1.

- Project Average = 0.057 m
- Median Relative Accuracy = 0.079 m
- 1 σ Relative Accuracy = 0.106 m
- 2 σ Relative Accuracy = 0.173 m

Figure 4.1. Distribution of relative accuracies, non slope-adjusted.

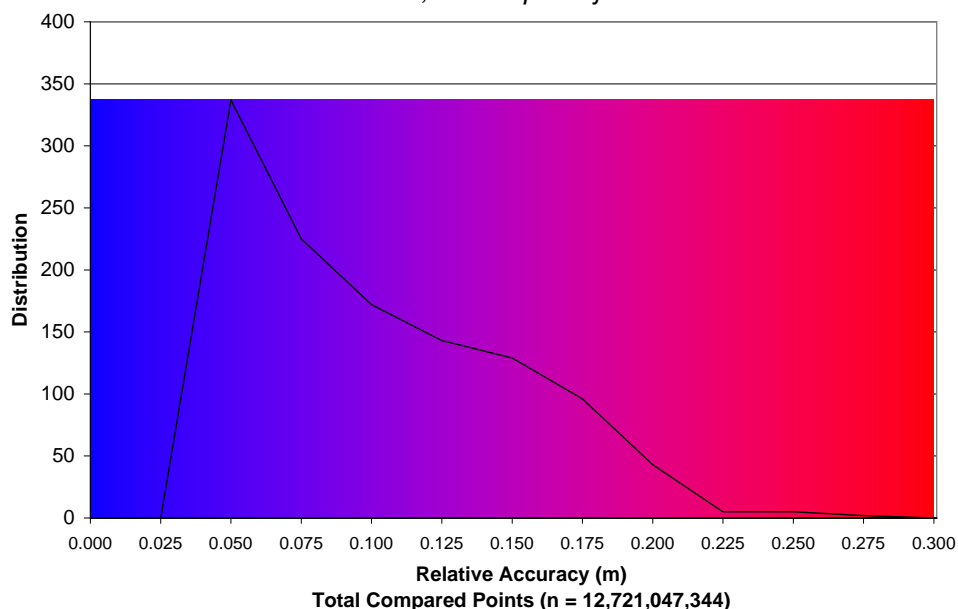
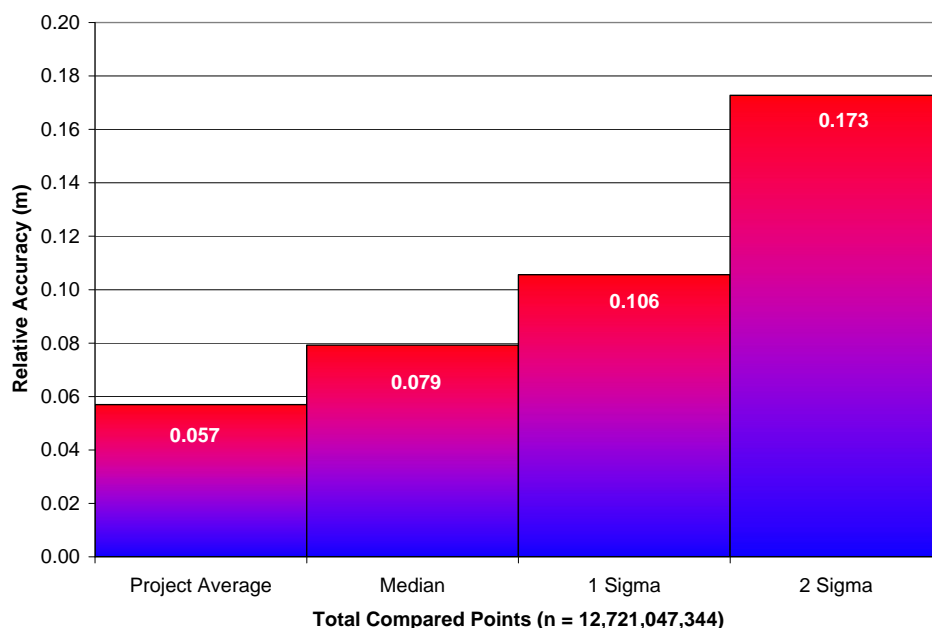


Figure 4.2. Statistical relative accuracies, non slope-adjusted.



2008 Acquisition Area

Relative accuracies have been determined for the entire DOGAMI study area **acquired in 2008**; the statistics are based on the comparison of 708 flightlines and over 3 billion points. For flightline coverage, see **Figure 2.1** in Section 2.1.

- Project Average = 0.067 m
- Median Relative Accuracy = 0.066 m
- 1σ Relative Accuracy = 0.072 m
- 2σ Relative Accuracy = 0.090 m

Figure 4.3. Distribution of relative accuracies, non slope-adjusted.

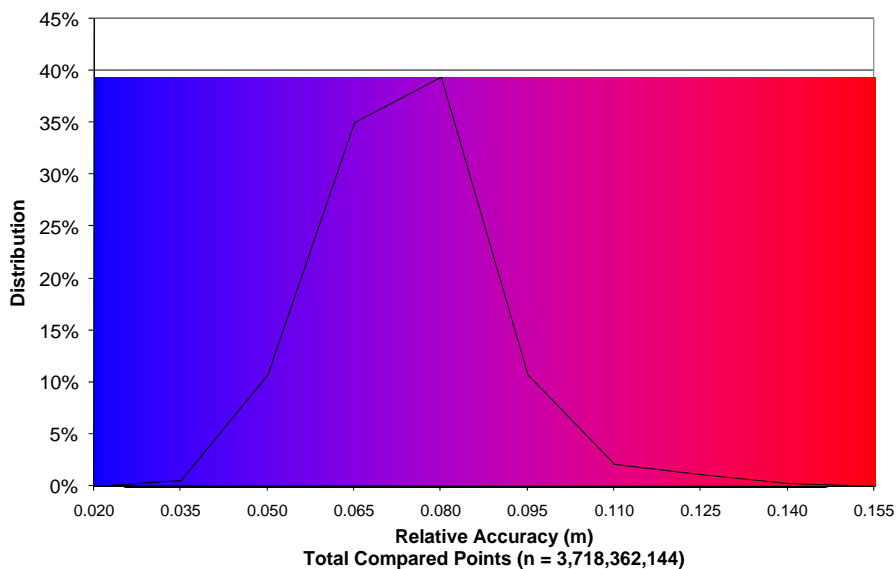
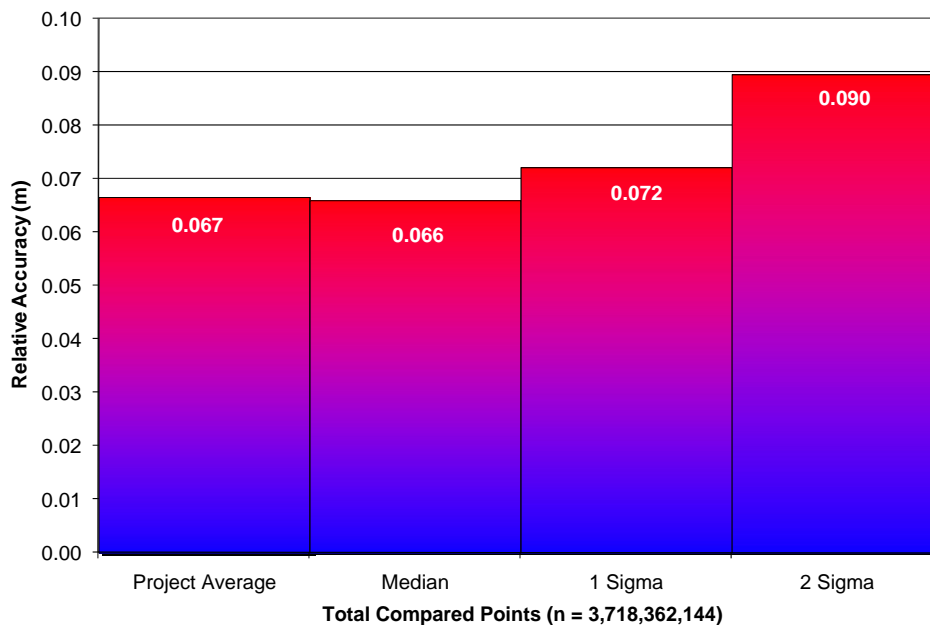


Figure 4.4. Statistical relative accuracies, non slope-adjusted.



4.1.2 Absolute Accuracy

2007 Acquisition Area

The final quality control measure is a statistical accuracy assessment that compares known RTK ground survey points to the closest laser point. For the DOGAMI and ODF study areas **acquired in 2007** and delivered, 11,969 RTK points were collected. Accuracy statistics are reported in **Table 4.2** and shown in Figures 4.5-4.6.

Table 4.2. Absolute Accuracy – Deviation between laser points and RTK survey points.

| Sample Size (n): 11,969 | |
|---|---------------------------------|
| Root Mean Square Error (RMSE): 0.11feet | |
| Standard Deviations | Deviations |
| 1 sigma (s): 0.11 feet | Minimum Δz : -0.52 feet |
| 2 sigma (s): 0.23 feet | Maximum Δz : 0.45 feet |
| | Average Δz : 0.00 feet |

Figure 4.5. Study Area: Histogram Statistics

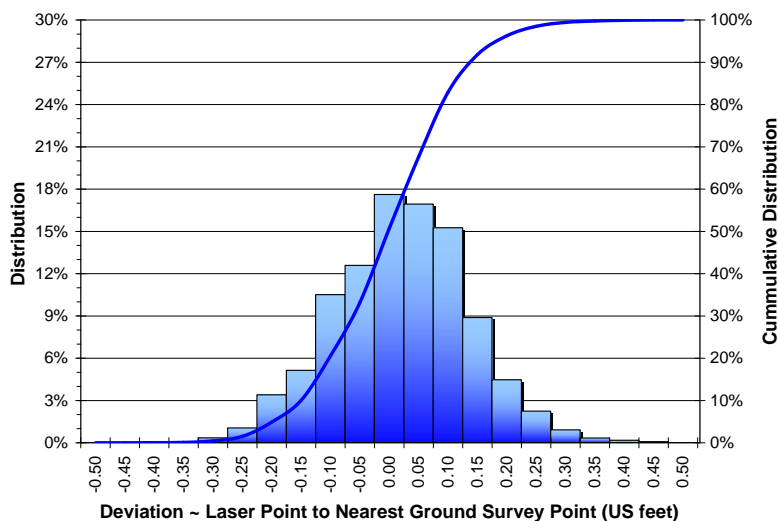
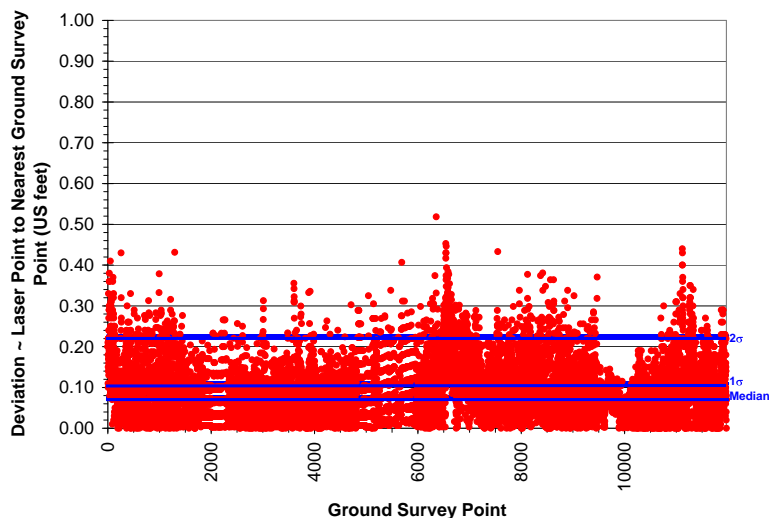


Figure 4.6. Study Area: Point Absolute Deviation Statistics



2008 Acquisition Area

The final quality control measure is a statistical accuracy assessment that compares known RTK ground survey points to the closest laser point. For the DOGAMI and ODF study areas **acquired in 2008**, 5,193 RTK points were collected. Accuracy statistics are reported in **Table 4.3** and shown in Figures 4.7-4.8.

Table 4.3. Absolute Accuracy – Deviation between laser points and RTK survey points.

| Sample Size (n): 5193 | |
|--|---------------------------------|
| Root Mean Square Error (RMSE): 0.13 feet | |
| Standard Deviations | Deviations |
| 1 sigma (s): 0.11 feet | Minimum Δz : -0.51 feet |
| 2 sigma (s): 0.27 feet | Maximum Δz : 0.84 feet |
| | Average Δz : -0.02 feet |

Figure 4.7. Study Area: Histogram Statistics

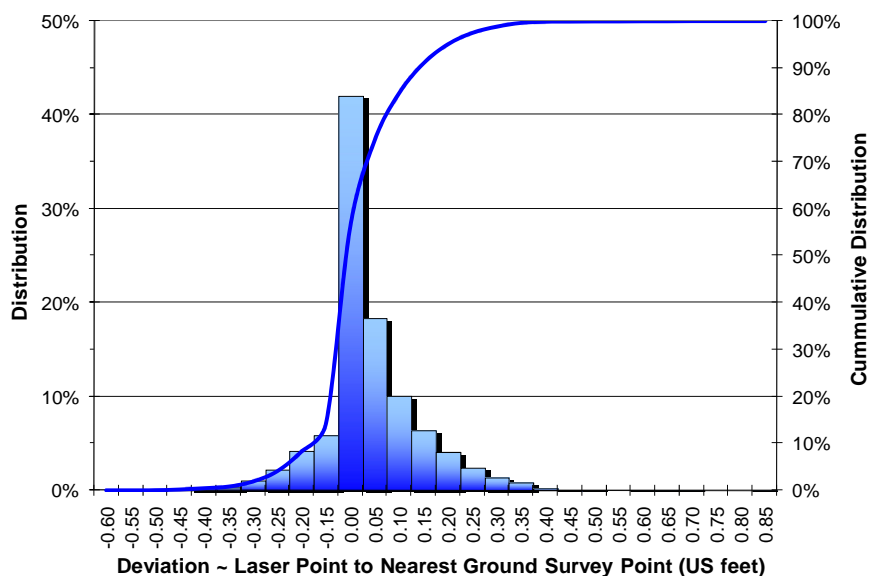
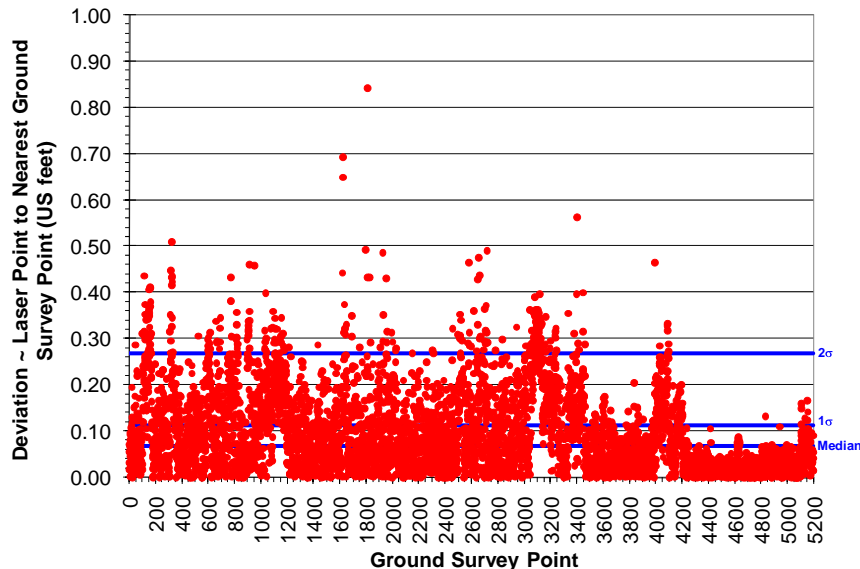


Figure 4.8. Study Area: Point Absolute Deviation Statistics

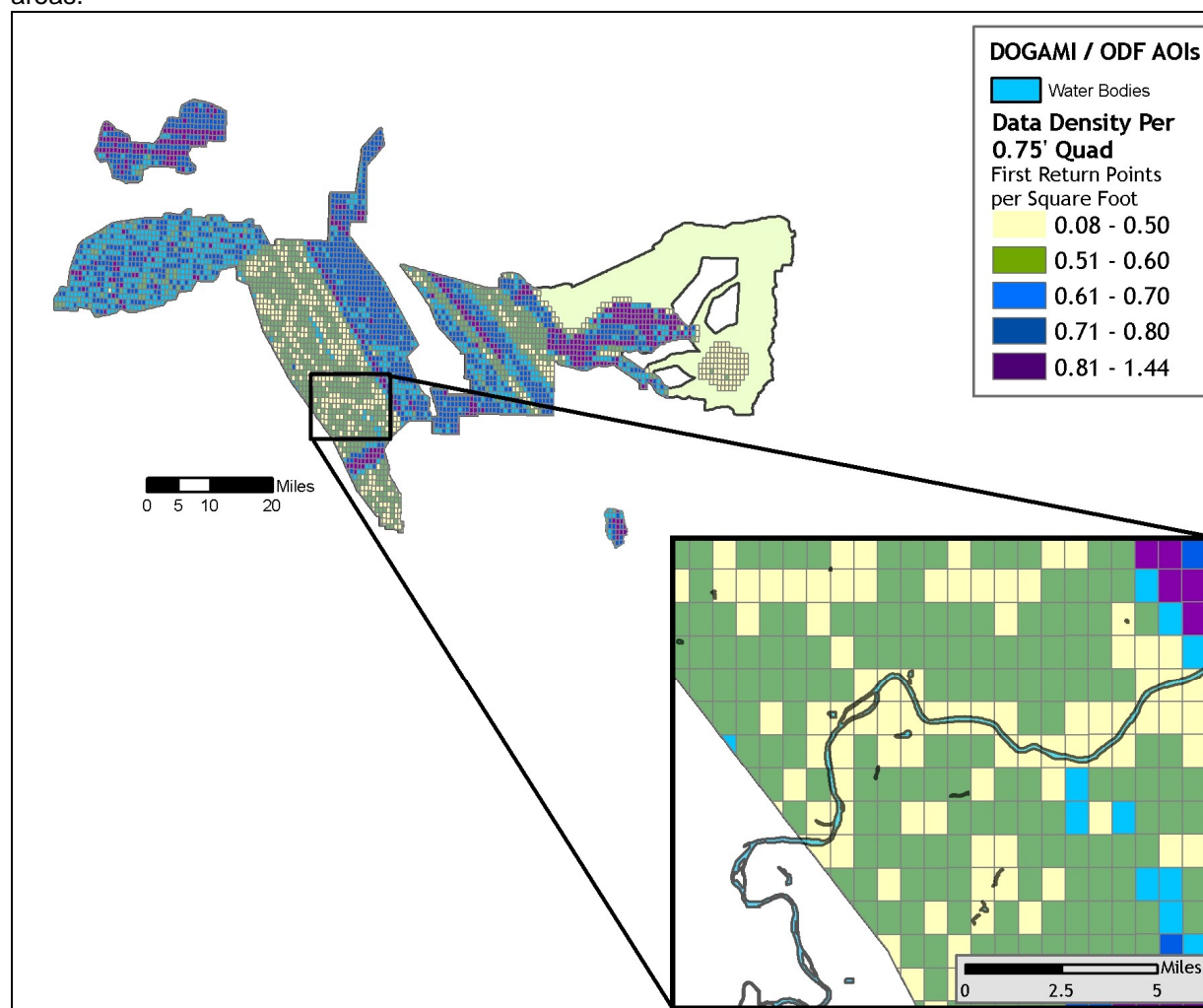


4.2 Data Density/Resolution

Some types of surfaces (i.e., dense vegetation or water) may return fewer pulses than the laser originally emitted. Therefore, the delivered density can be less than the native density and lightly variable according to distributions of terrain, land cover and water bodies (**Figure 4.9**). Density histograms and maps (**Figures 4.10-4.21**) have been calculated based on first return laser point density and ground-classified laser point density (see Section 4.3 for discussion of density per AIO).

| | Total Pulse Density | Ground Pulse Density |
|--|---|---|
| 2007 ODF Data Acquisition Processing Complete | 7.71 points per square meter 0.72 points per square foot | 0.71 points per square meter 0.07 points per square foot |
| 2007 DoGAMI Data Acquisition Processing Complete | 6.90 points per square meter 0.64 points per square foot | 1.28 points per square meter 0.12 points per square foot |
| 2008 DoGAMI Data Acquisition Processing Complete | 7.75 points per square meter 0.72 points per square foot | 0.76 points per square meter 0.07 points per square foot |

Figure 4.9. Illustration of the location of water bodies and the corresponding lower-density data areas.



4.2.1 First Return Laser Pulses per Square Foot

Figure 4.10. Histogram of first return laser point data density in both of ODF's AOIs, per 0.75' USGS Quad.

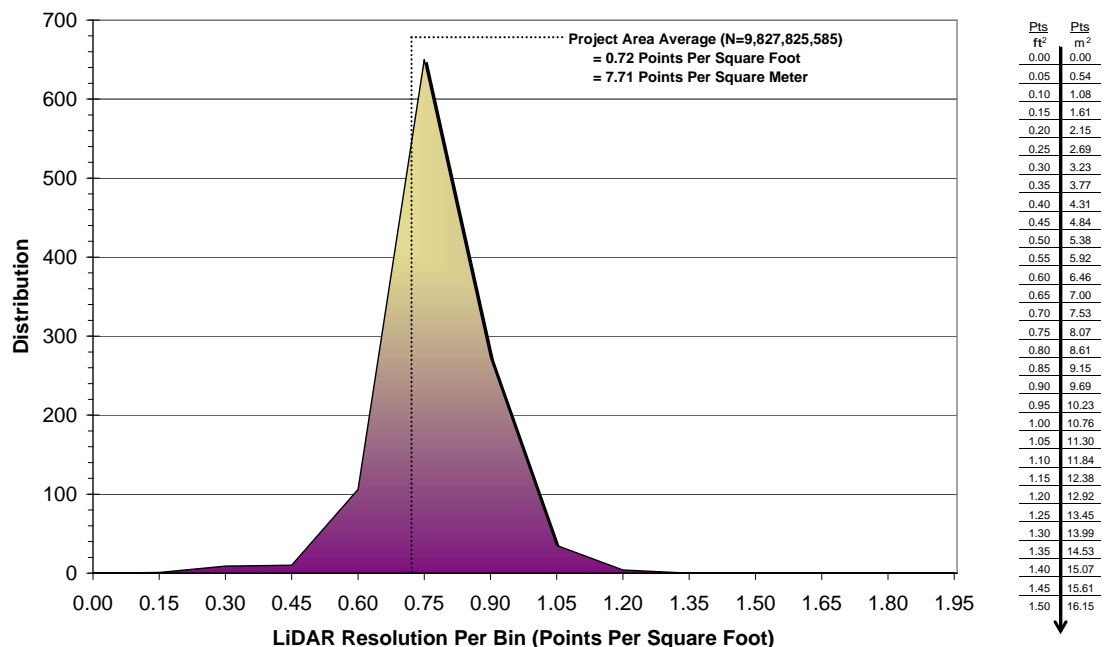


Figure 4.11. Image shows first return laser point data density in both of ODF's AOIs, per 0.75' USGS Quad.

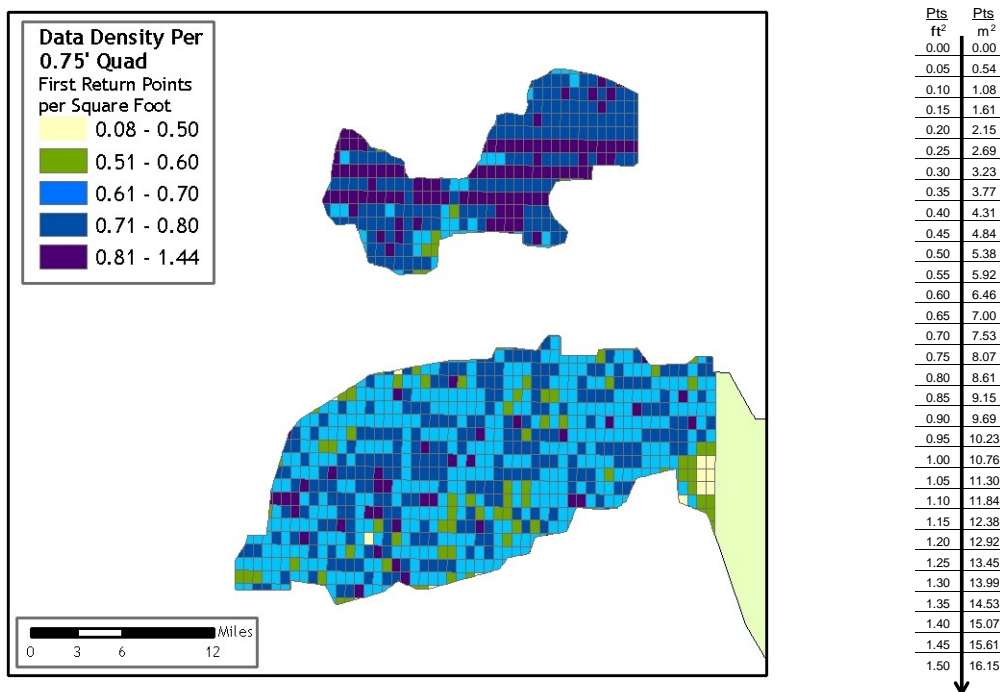


Figure 4.12. Histogram of first return laser point data density in **all Portland Area quads acquired in 2007**, per 0.75' USGS Quad.

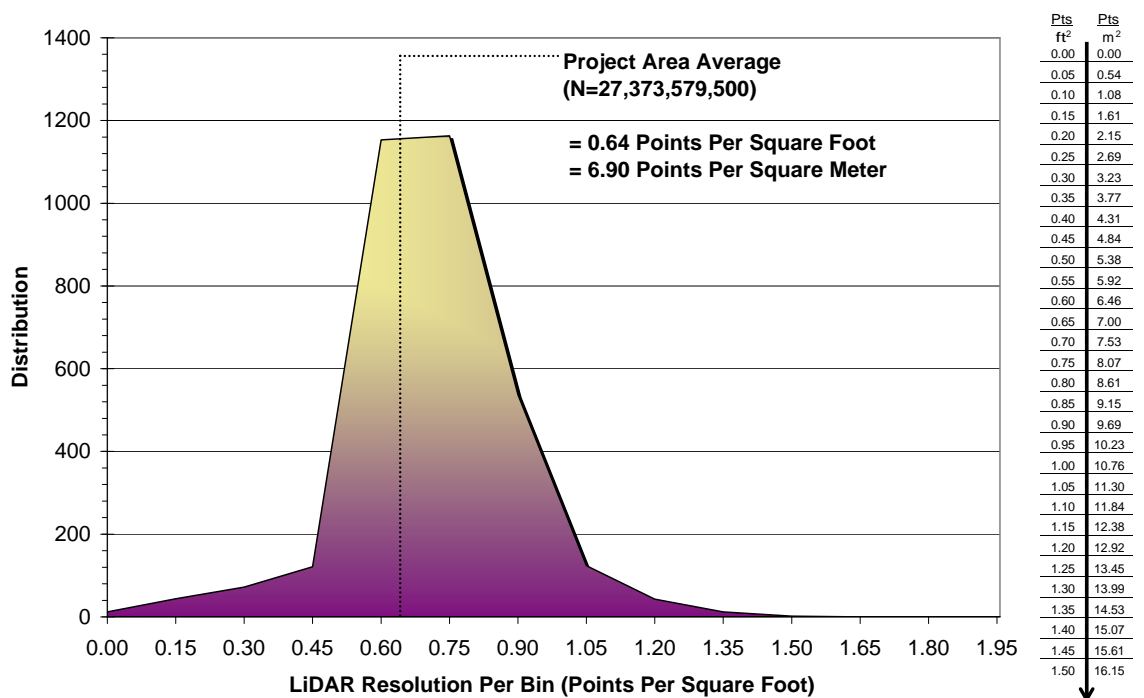


Figure 4.13. Image shows first return laser point data density in **all Portland Area quads acquired in 2007**, per 0.75' USGS Quad.

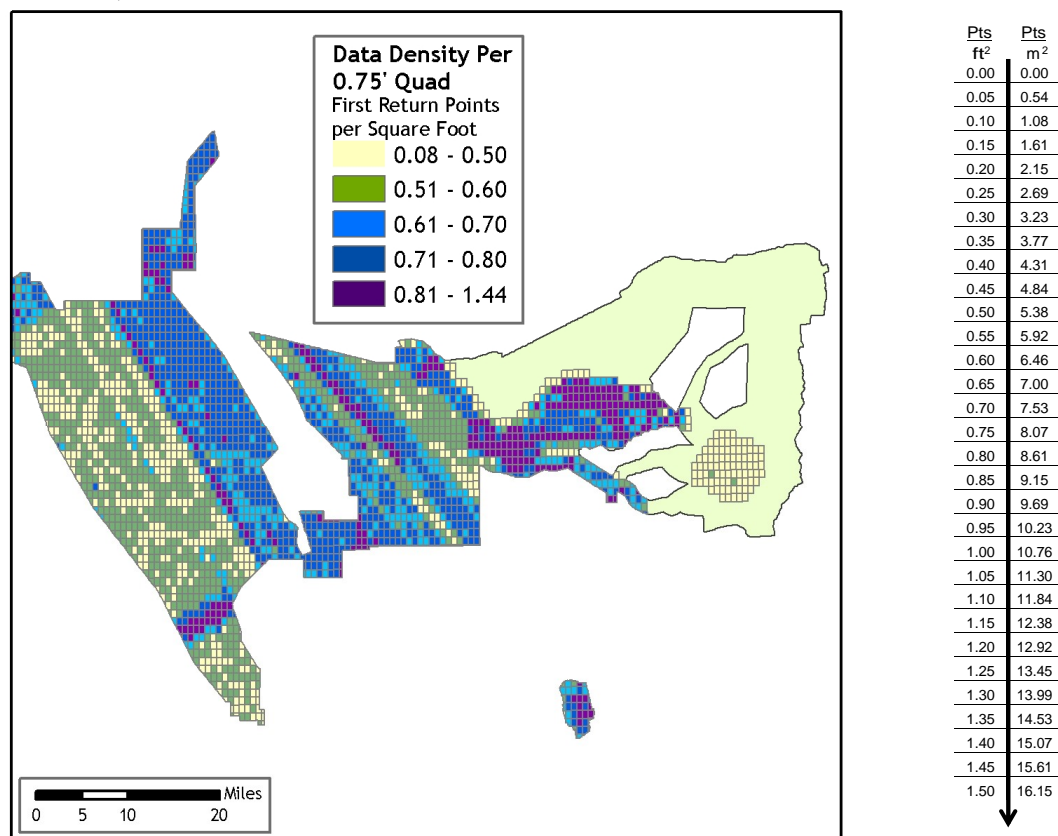


Figure 4.14. Histogram of first return laser point data density in *all Portland Area quads acquired in 2008*, per 0.75' USGS Quad.

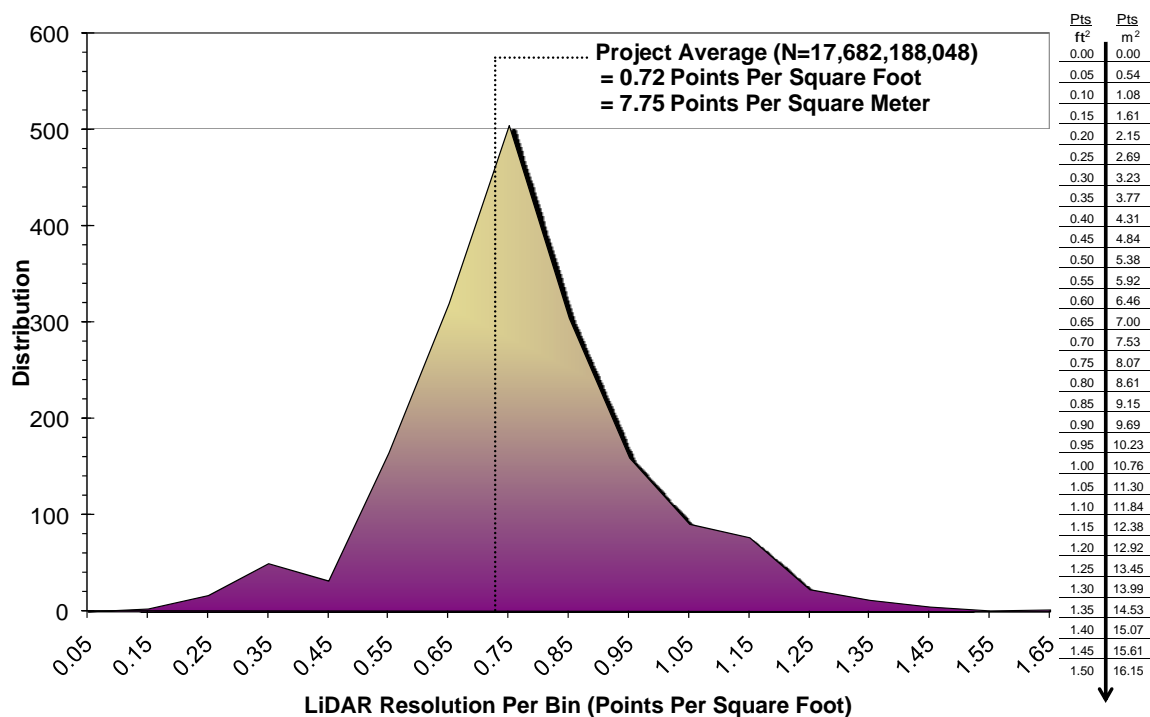
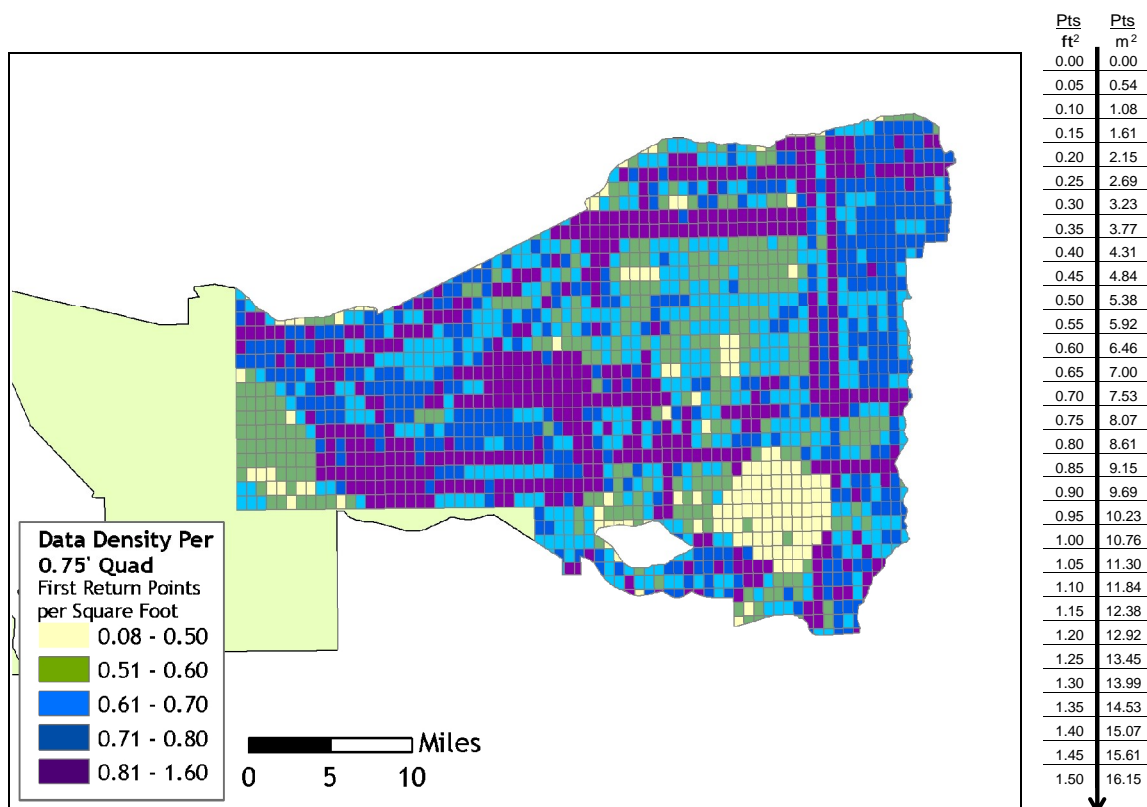


Figure 4.15. Image shows first return laser point data density in *all Portland Area quads acquired in 2008*, per 0.75' USGS Quad.



4.2.2 Classified Ground Points per Square Foot

Ground classifications are derived from ground surface modeling. Supervised classifications were performed by reseeded of the ground model where it is determined that the ground model has failed, usually under dense vegetation and/or at breaks in terrain, steep slopes and at bin boundaries.

Figure 4.16. Histogram of ground-classified laser point data density in both **ODF's AOIs**, per 0.75' USGS Quad.

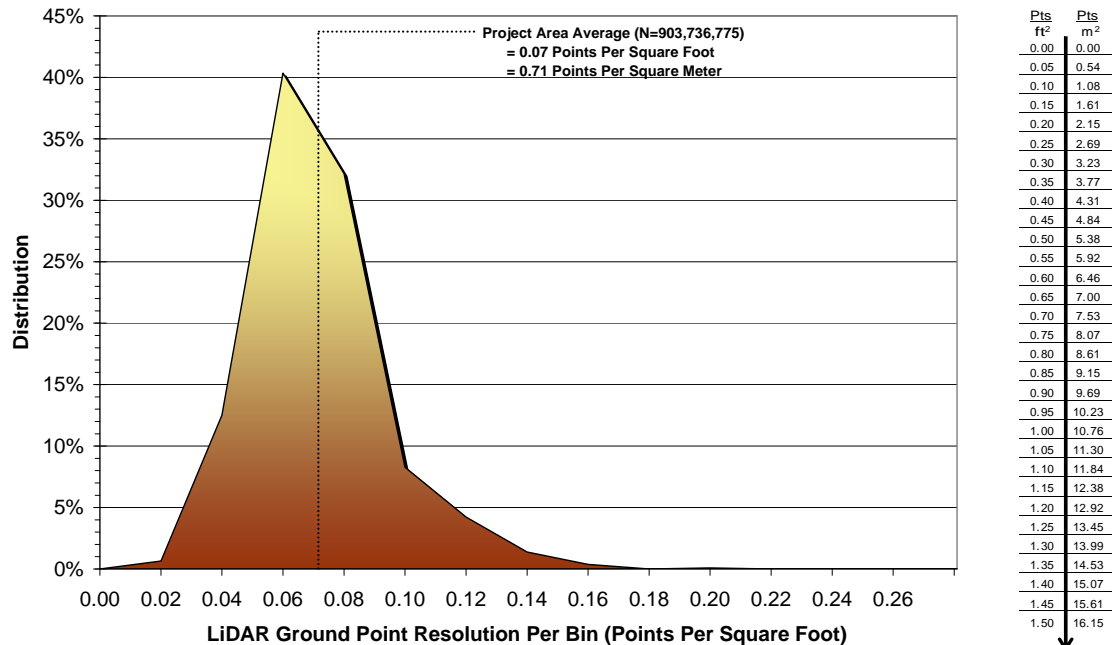


Figure 4.17. Image shows ground-classified laser point data density per 0.75' USGS Quad in both **ODF's AOIs**.

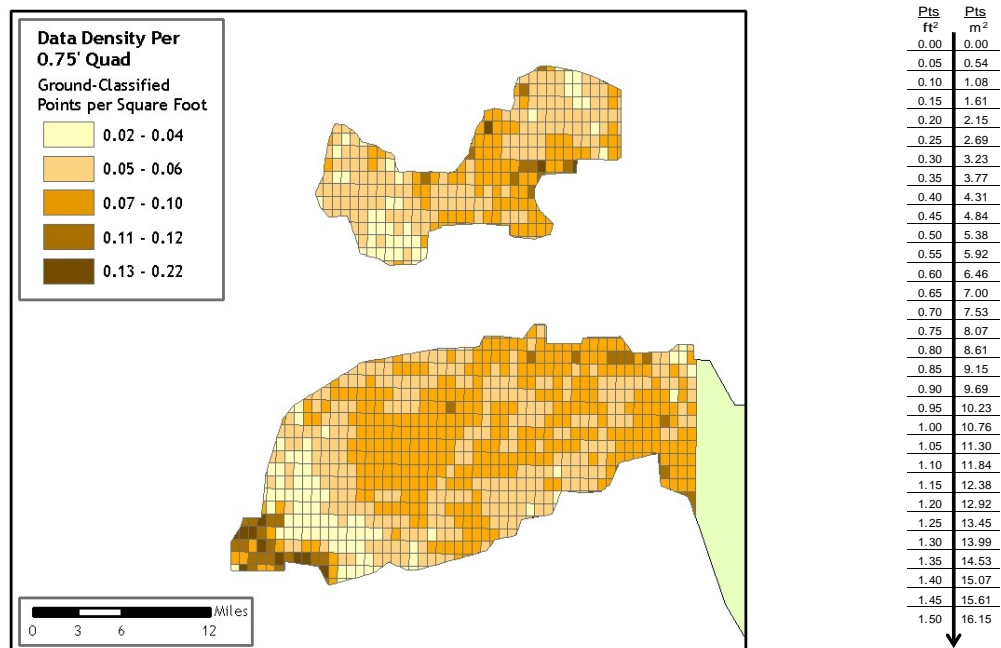


Figure 4.18. Histogram of ground-classified laser point data density in *all Portland Area data* acquired in 2007, per 0.75' USGS Quad.

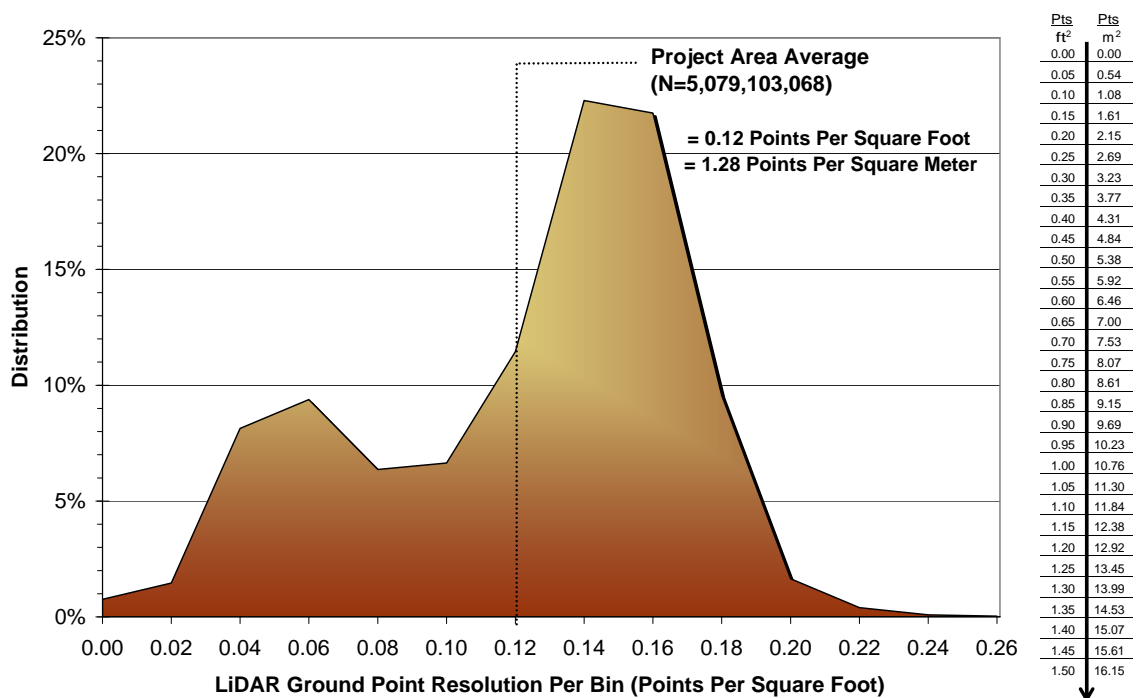


Figure 4.19. Image shows ground-classified laser point data density in *all Portland Area data* acquired in 2007, per 0.75' USGS Quad.

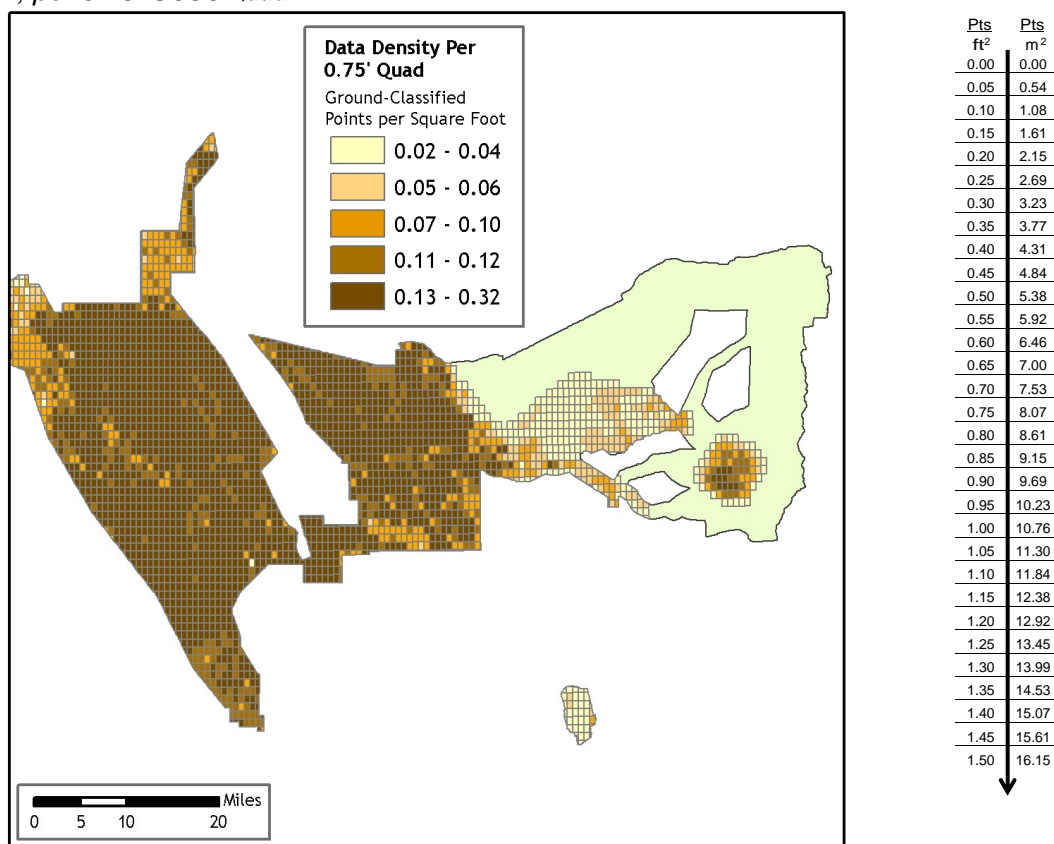


Figure 4.20. Histogram of ground-classified laser point data density in *all Portland Area data* acquired in 2008, per 0.75' USGS Quad.

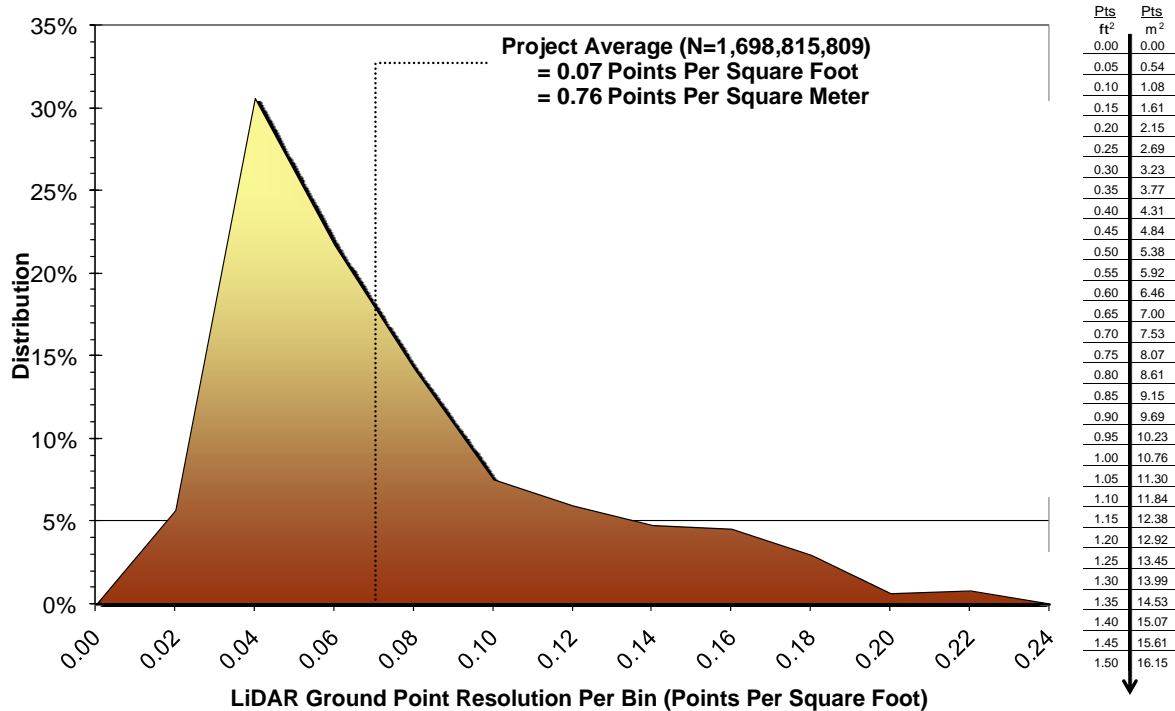
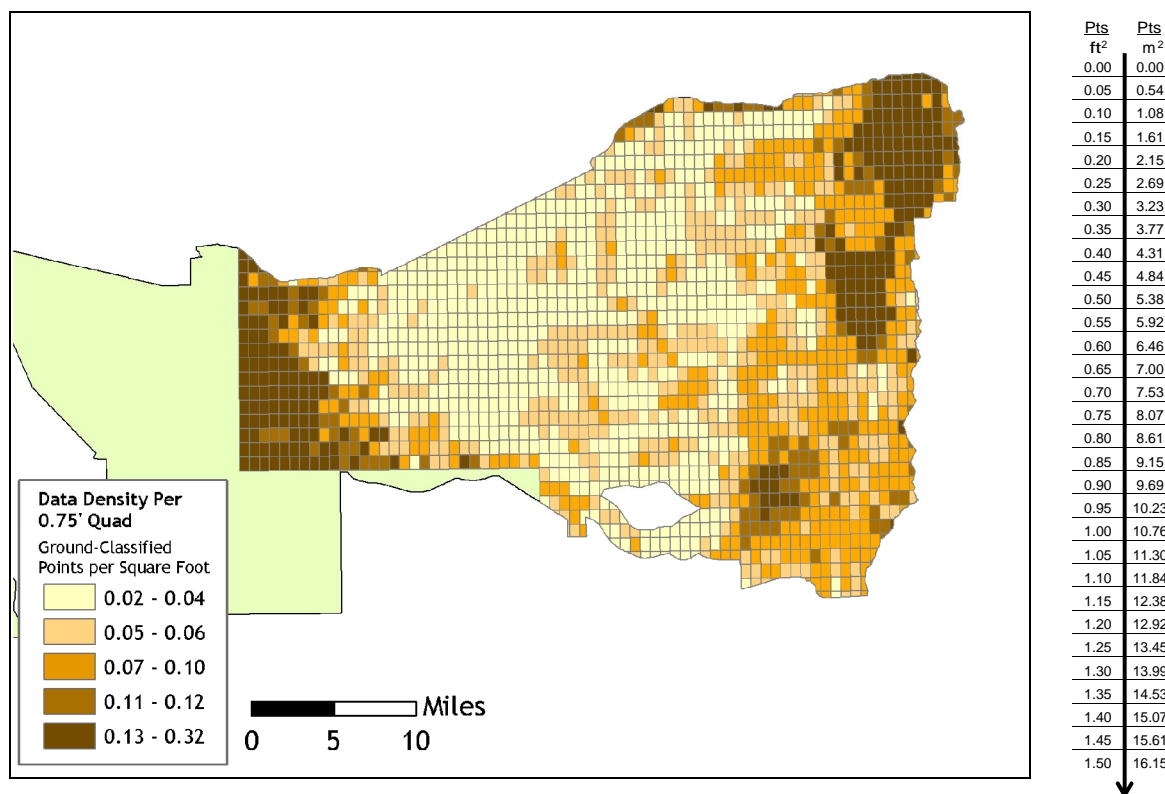


Figure 4.21. Image shows ground-classified laser point data density in *all Portland Area data* acquired in 2008, per 0.75' USGS Quad.



4.3 Data Density/Resolution per AOI

Table 4.4. Average Pulse Densities per AOI in the DOGAMI/ODF Study Areas.

| AOI | Name | Average Pulse Density (ft) | Average Pulse Density (m) |
|-------|-------------------|----------------------------|---------------------------|
| 1 | Portland | 0.62 | 6.66 |
| 2 | ODF | 0.72 | 7.71 |
| 3 | Upper Sandy River | 0.70 | 7.56 |
| 4 | Collawash | 0.69 | 7.46 |
| 5 | Lower Sandy River | 0.78 | 8.38 |
| 6 & 7 | Mt. Hood | 0.27 | 2.91 |
| 8 | Bull Run | 0.83 | 8.92 |
| 9 | Hood / Gorge | 0.76 | 7.75 |

4.3.1 Portland AOI

The Portland AOI was acquired with both an Optech 3100 and a Leica ALS50 LiDAR system, resulting in different acquisition densities per laser (**Figure 4.22**). In areas of flightline overlap, higher data densities occur (**Figure 4.23**). The average pulse density for the Portland AOI is 0.62 pulses per square foot (6.66 pulses per square meter).

Figure 4.22. Illustration of difference in data density between two different LiDAR systems used.

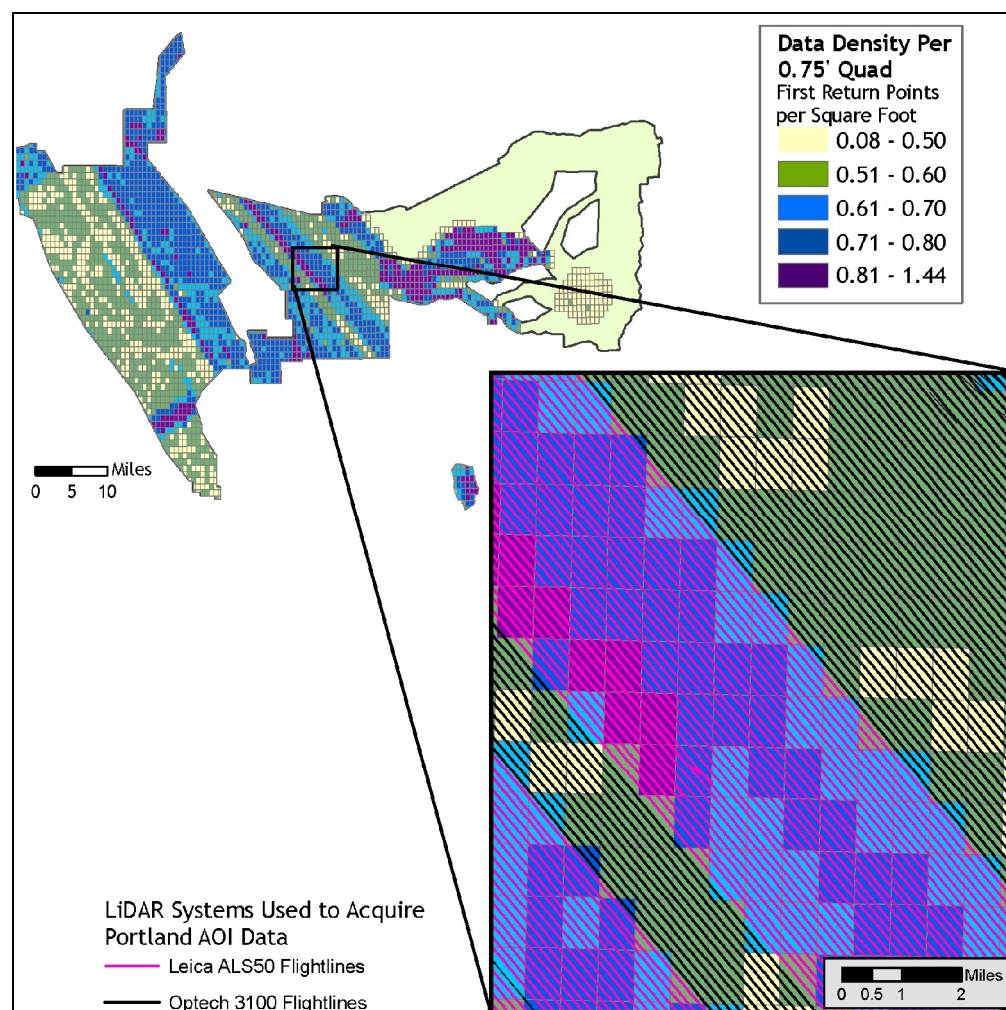
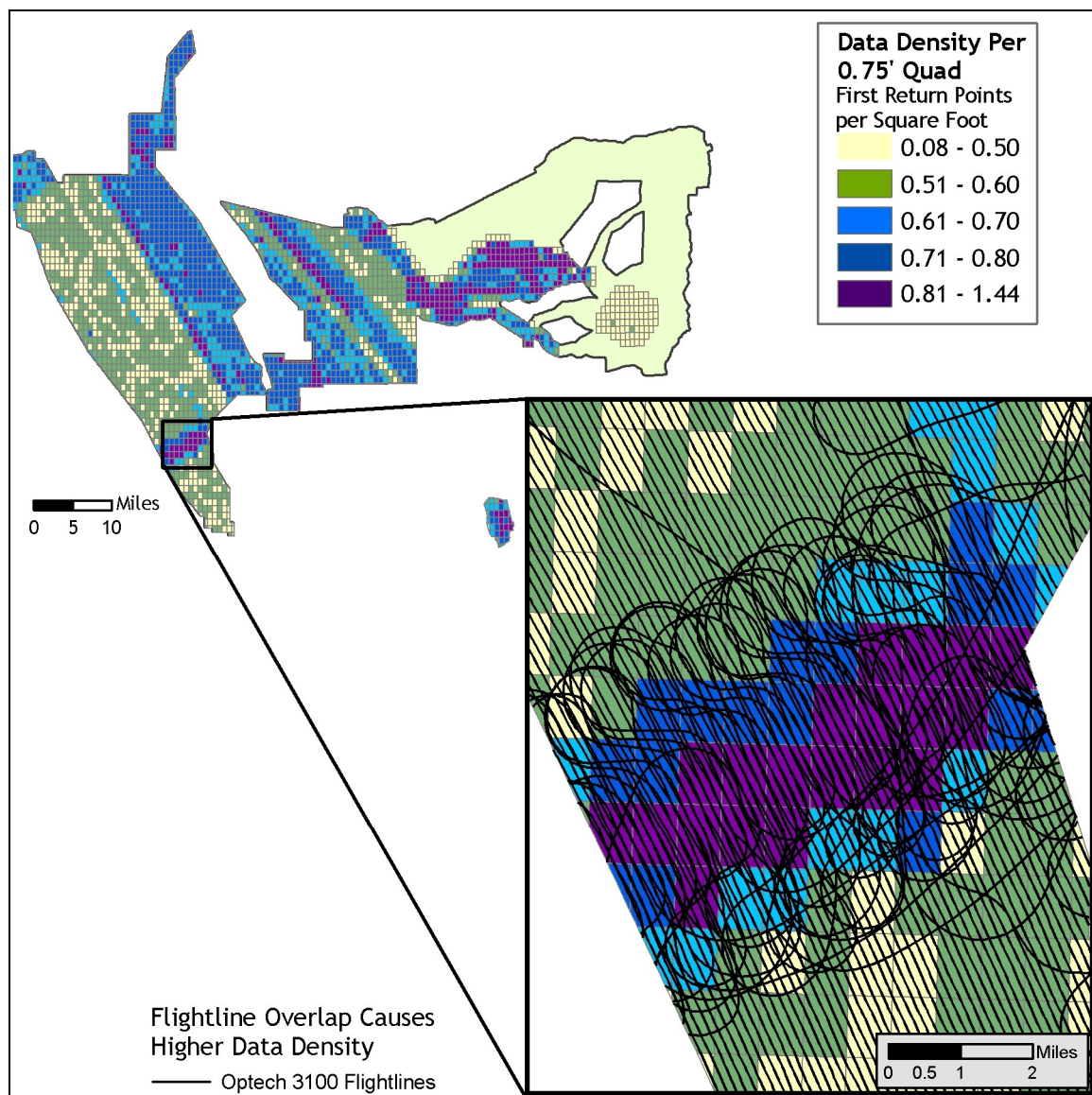


Figure 4.23. Illustration of higher data density in areas of overlapping flightlines.



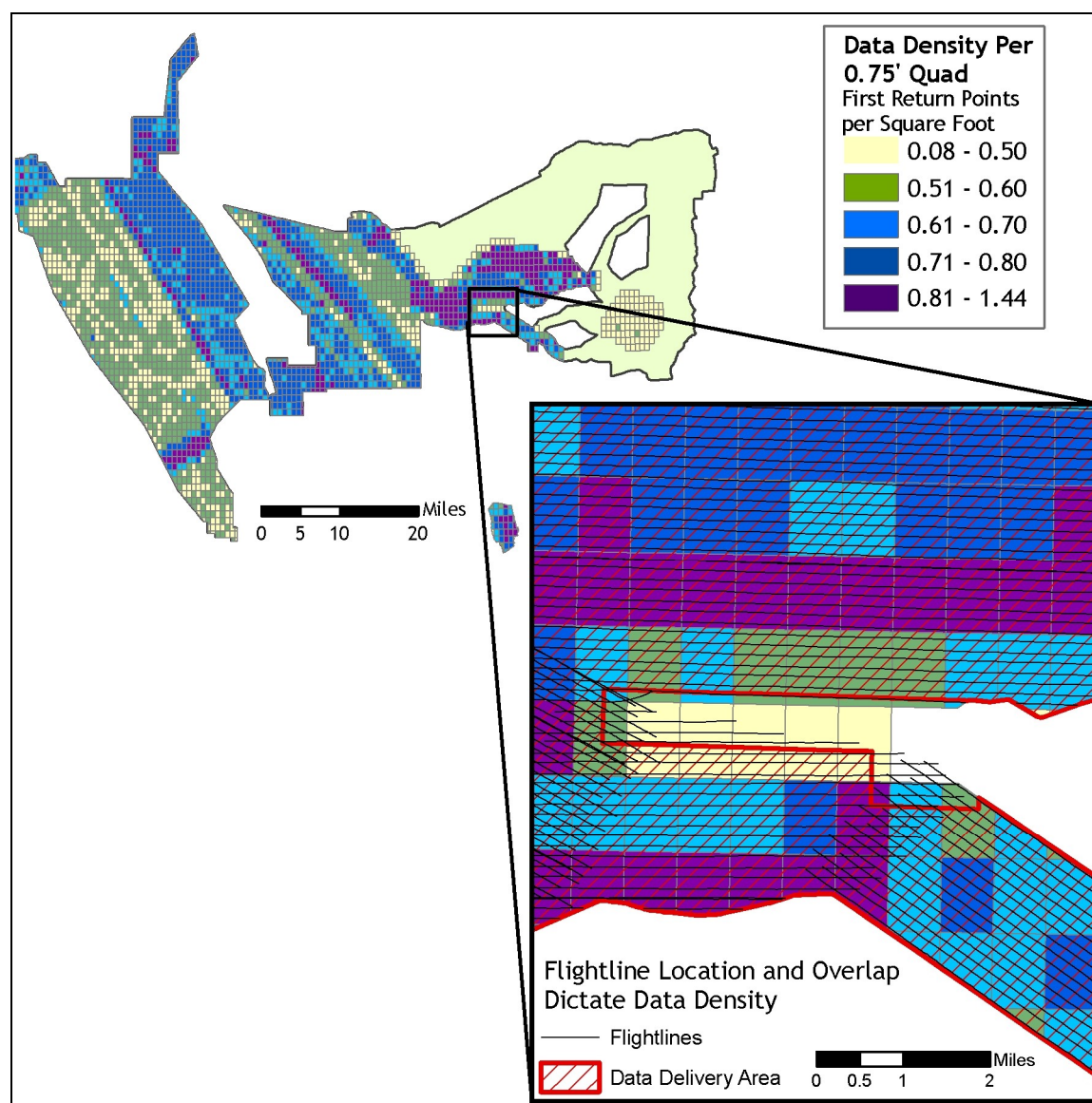
4.3.2 ODF AOI

The average pulse density for the ODF AOI is 0.72 pulses per square foot (7.71 pulses per square meter). See Figure 4.11 in Section 4.2.1 for illustration of density coverage in the ODF study area.

4.3.3 Upper Sandy / Bull Run AOIs

Due to the shapes and locations of the Upper Sandy and Bull Run study areas, an area of incomplete data coverage occurred between the two acquisition polygons (**Figure 4.24**), resulting in a lower data density. The average pulse density for the Upper Sandy AOI is 0.70 pulses per square foot (7.56 pulses per square meter). The average pulse density for the Bull Run AOI is 0.83 pulses per square foot (8.92 pulses per square meter).

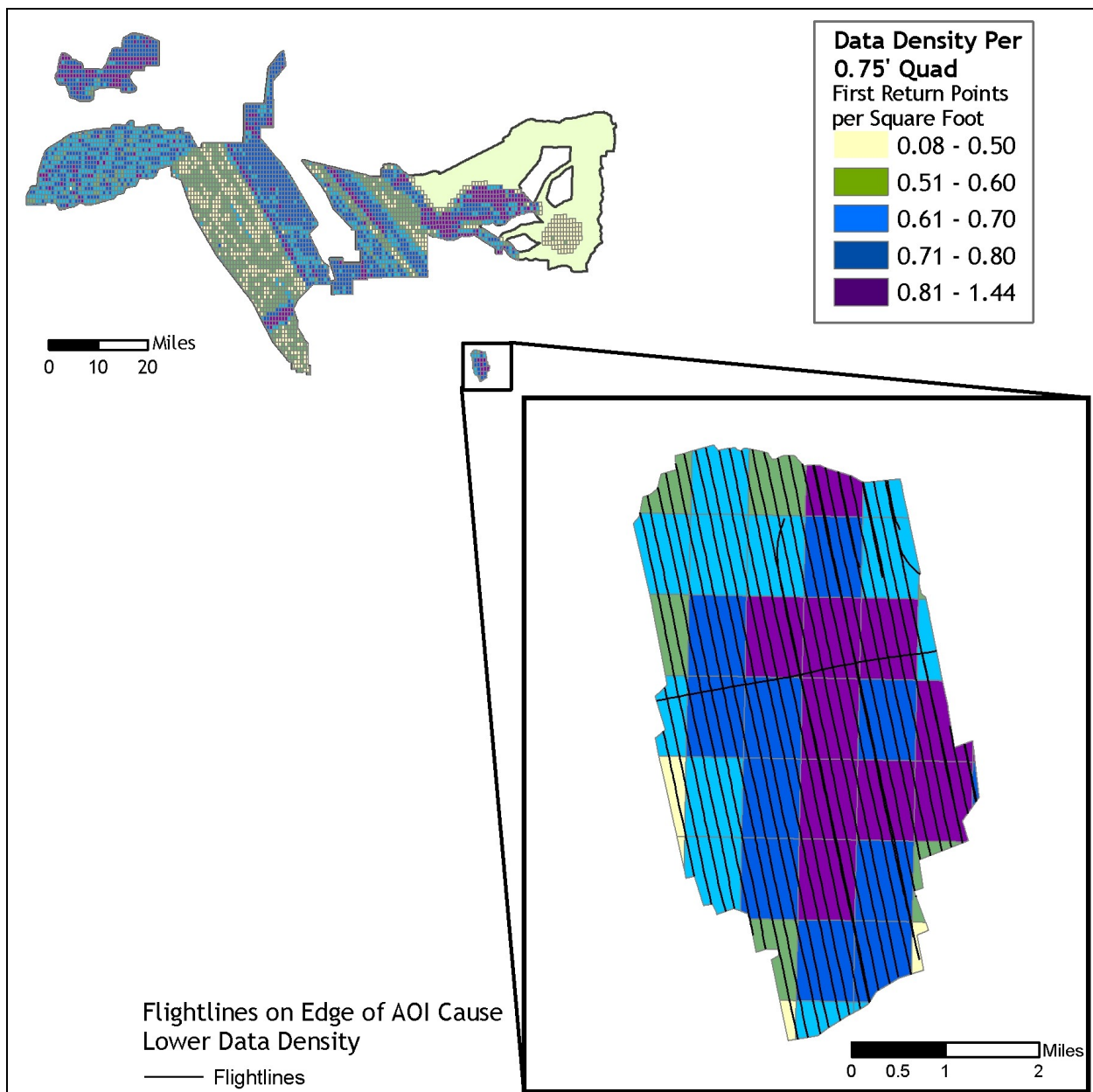
Figure 4.24. Illustration of lower-density data blocks caused by sparse or no flightlines.



4.3.4 Collawash AOI

The Collawash study area was an isolated survey, and as a result, the edges of the AOI experienced a lower data density due to single flightline edges. The average pulse density for the Collawash AOI is 0.69 pulses per square foot (7.46 pulses per square meter).

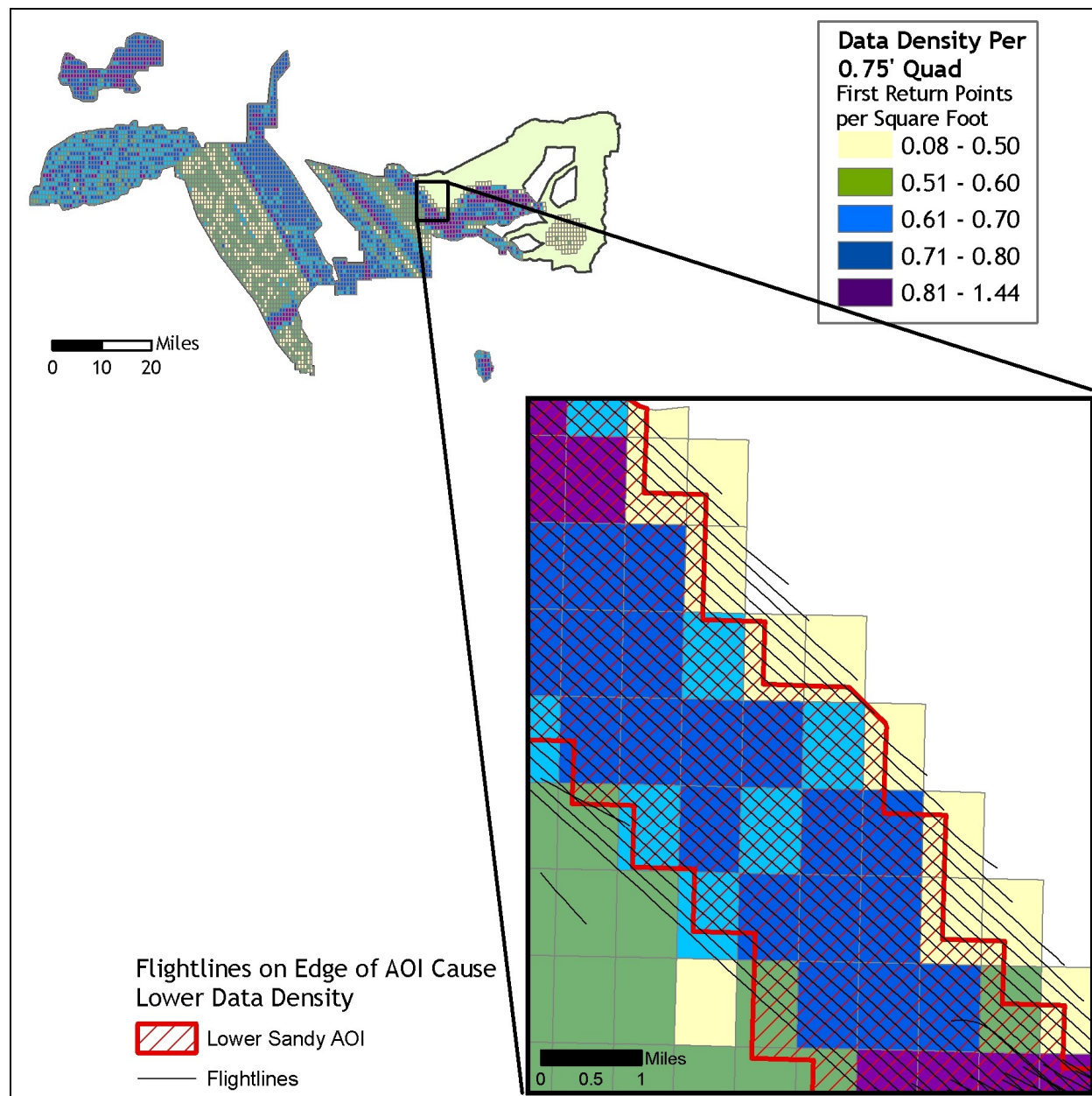
Figure 4.25. Image illustrating the lower data density caused by edge flightlines along the border of the Collawash study area.



4.3.5 Lower Sandy AOI

The lower sandy survey is on the edge of the acquired data; therefore, the edge data blocks experience a lower density due to single flightline edges. The average pulse density for the Lower Sandy AOI is 0.78 pulses per square foot (8.38 pulses per square meter).

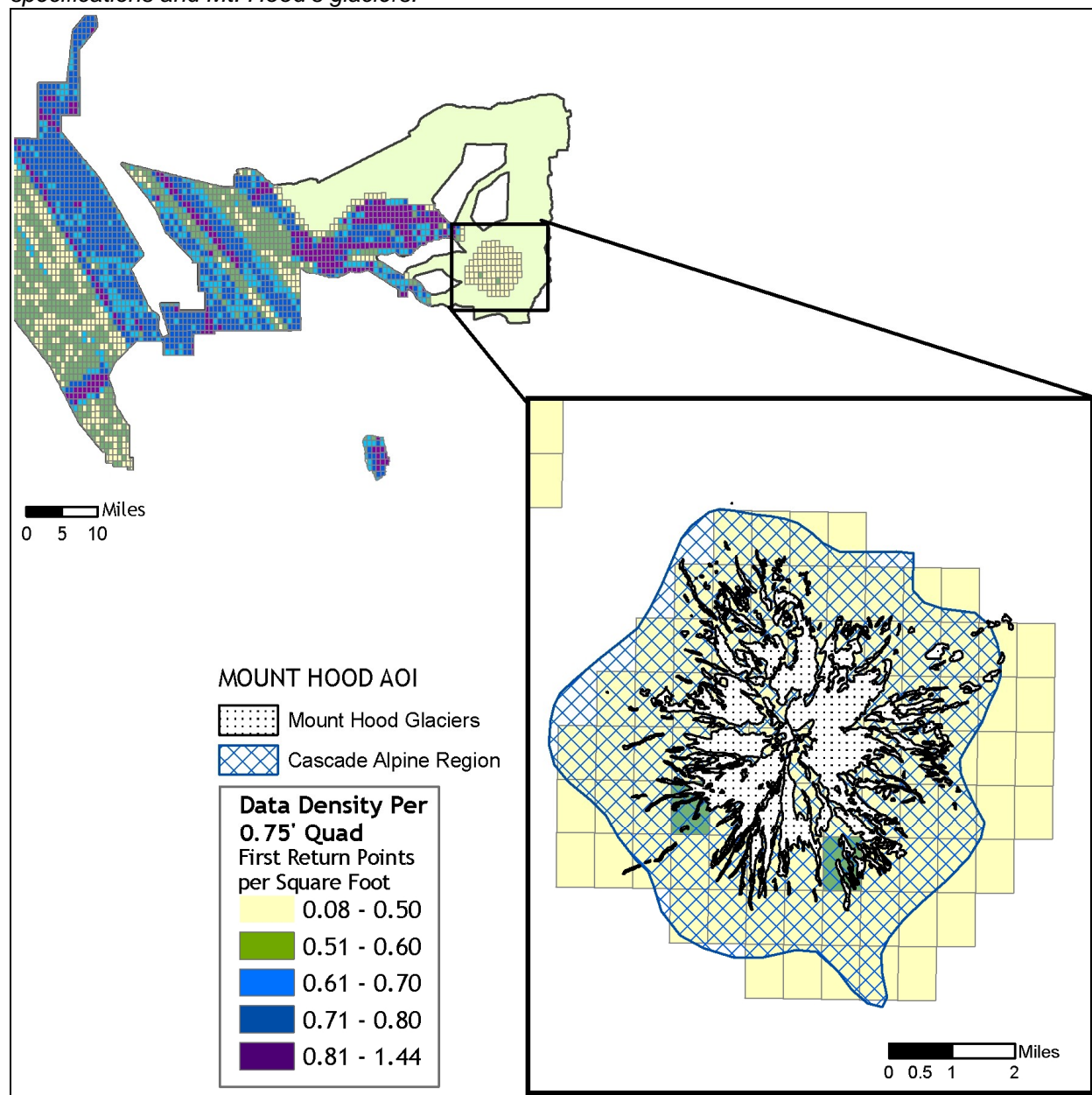
Figure 4.26. Image illustrating the lower data density caused by edge flightlines along the border of the Lower Sandy study area.



4.3.6 Mount Hood AOI

The Mount Hood AOI data has a lower data density than the project average; this was due to the data collection specifications tailored for high-relief (see **Table 2.1**). As the laser range increases, the available pulse rate frequency decreases. The survey aircraft cannot terrain follow Mount Hood easily or safely, and therefore, requires a larger operational range. Lower pulse rates result, causing lower data densities. The average pulse density for the Mount Hood AOI is 0.27 pulses per square foot (2.91 pulses per square meter).

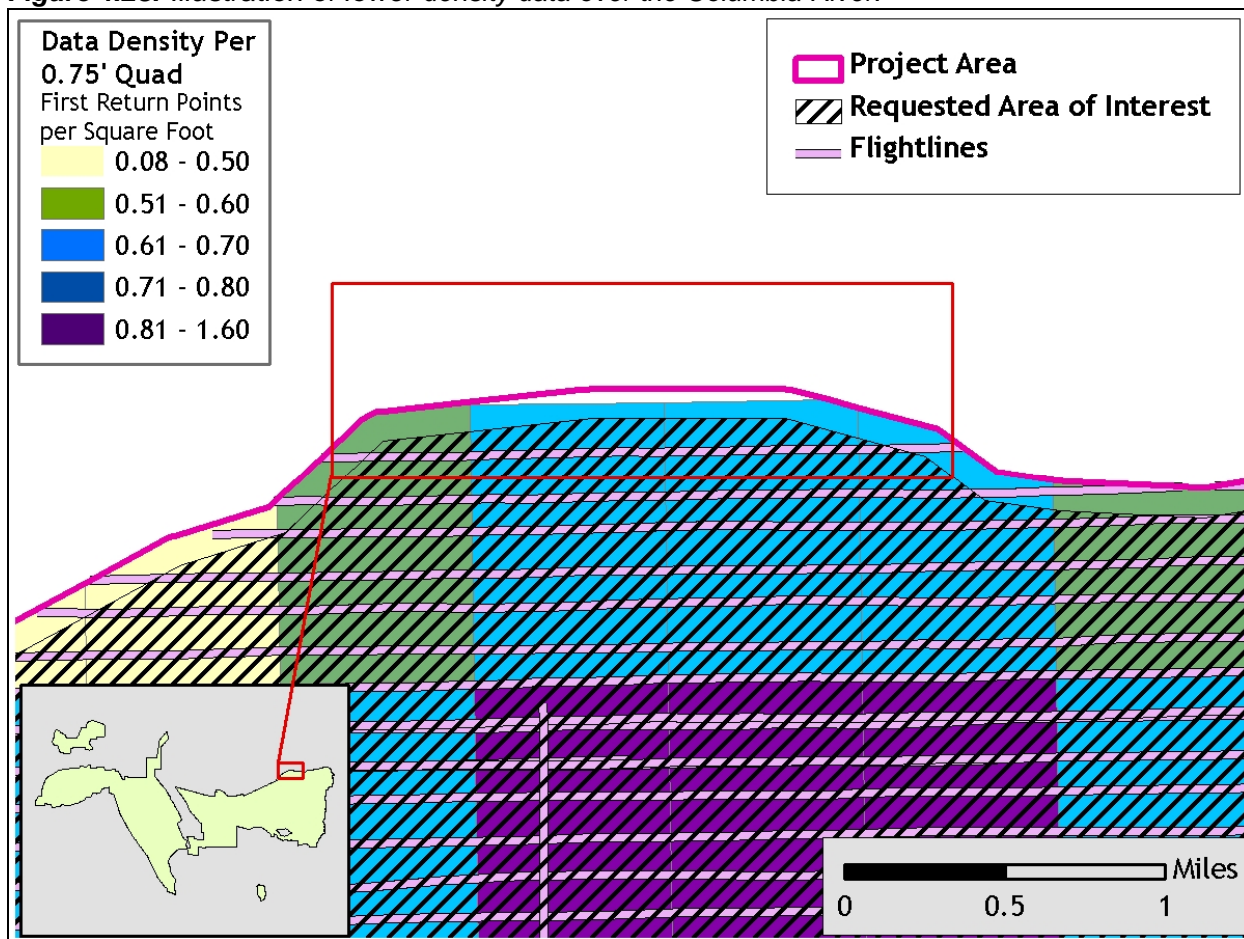
Figure 4.27. Illustration of lower data density in the Mt. Hood AOI as a result of acquisition specifications and Mt. Hood's glaciers.



4.3.7 Columbia River Gorge AOI

The northern border of the Gorge portion of the Portland AOI coincides with the Columbia River. Owing to the variable response of laser returns over open water, the point density on the northern edge of the study area is lower than the project average. In some cases, no returns were captured over the river, leaving a gap in the expected data collection border; however, the data collected still fully covers the area of interest requested by the client.

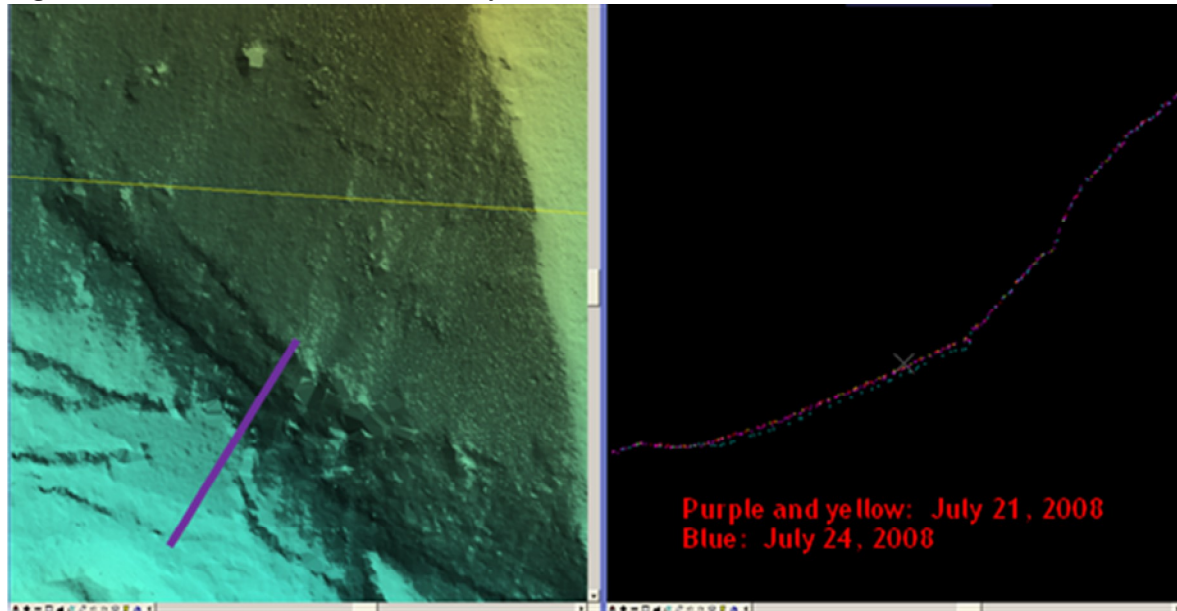
Figure 4.28. Illustration of lower density data over the Columbia River.



5. Mt. Hood / Columbia River Gorge Acquisition Discussion

The 2008 LiDAR acquisition follows a record year for snowfall in the Mt. Hood region. Snow persists in this dataset in sheltered canyons, heavily timbered acreage, and lee slopes. **Figure 5.1**, below, depicts a cross-section above timberline on the southeast flank of Mt. Hood. The image to the right is colored by flightline. Pink and yellow point data were collected July 21, 2008, while the blue data were collected July 24. The point data are in agreement on upper and exposed surfaces. Between these surfaces, an apparent snow-filled swale exhibits elevation displacement. Elevation differences between the two dates (approximately 4 cm) is attributed to snowmelt.

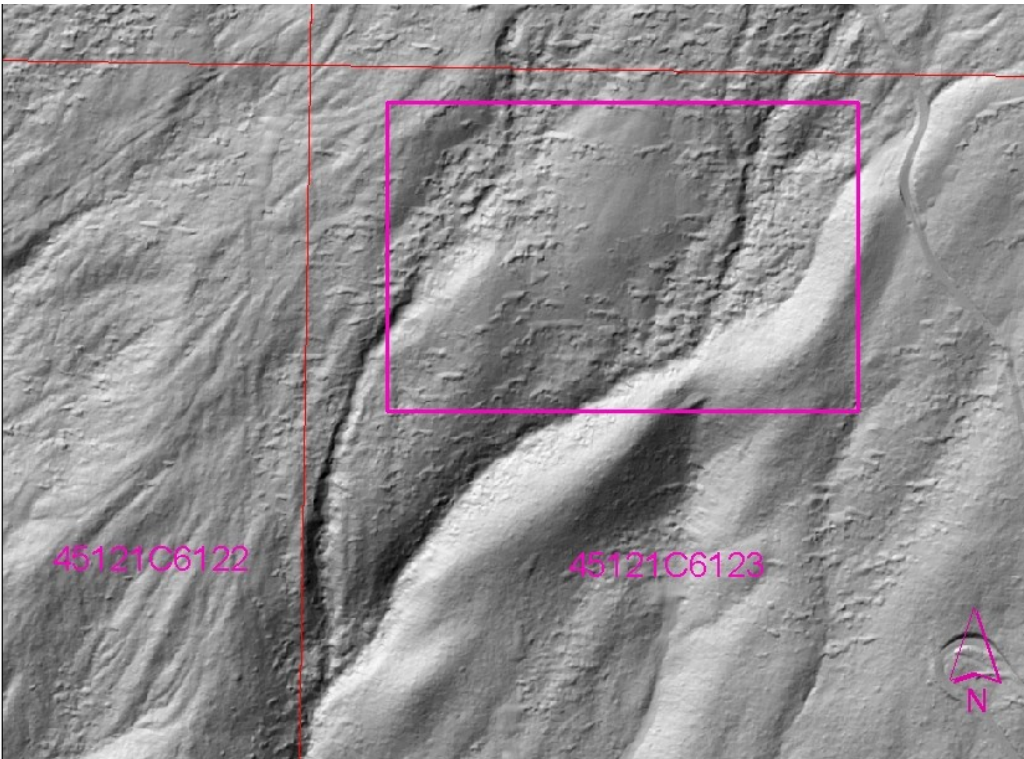
Figure 5.1. *Snow melt in sheltered canyon.*



Snow is present in timbered areas, manifesting as lobed surface features. **Figure 5.2** illustrates snow features in a forested area near Timberline Ski Area.

Figure 5.2. Lobed snow features on forested lee slopes. a. Bare-earth DEM. b. Highest Hit DEM.

a.



b.



Artifacts resulting from the difference in acquisition dates are evident in the data. The data from 2007 and 2008 surveys agree well on firm permanent surfaces (**Figure 5.3**). However, in some instances, topographic change is marked between the two acquisition periods. **Figure 5.4** illustrates the presence of a new surface feature at the south-eastern end of a parking lot servicing Mt. Hood Meadows ski area.

Figure 5.3. Cross section spanning 2007 and 2008 datasets (border demarcated by yellow line) on road surface near Mt. Hood Meadows ski area.

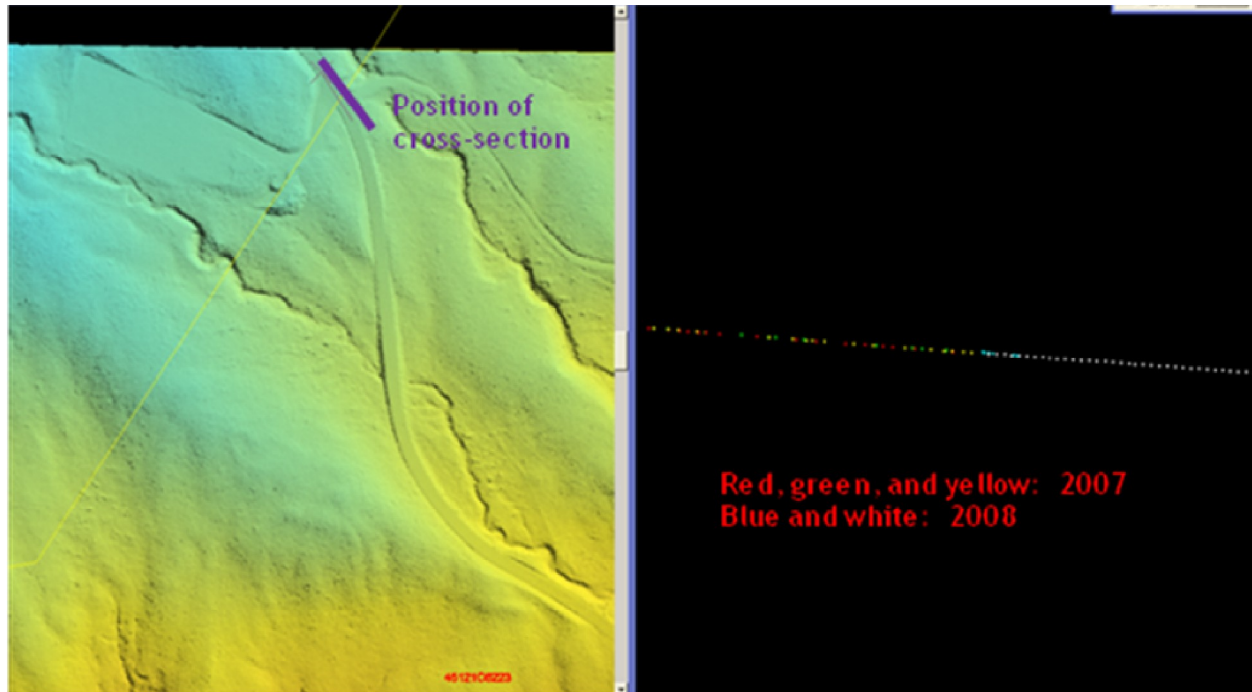


Figure 5.4. Cross-section illustrating new surface feature not present in the 2007 dataset

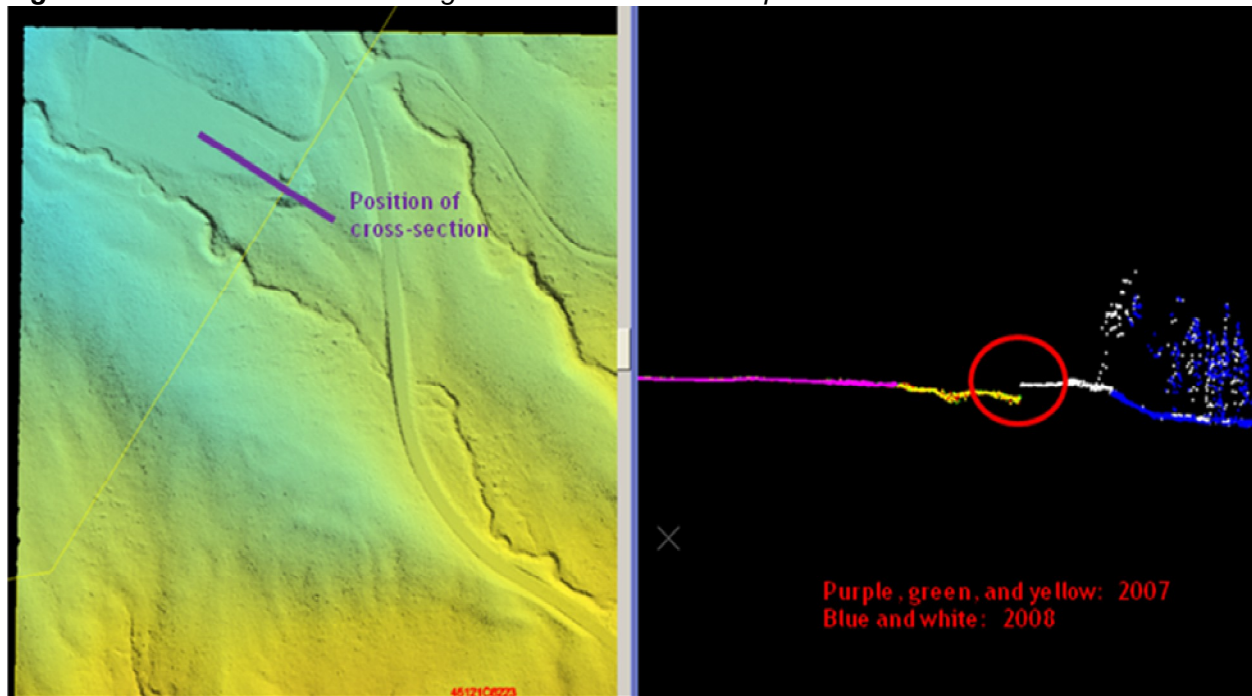
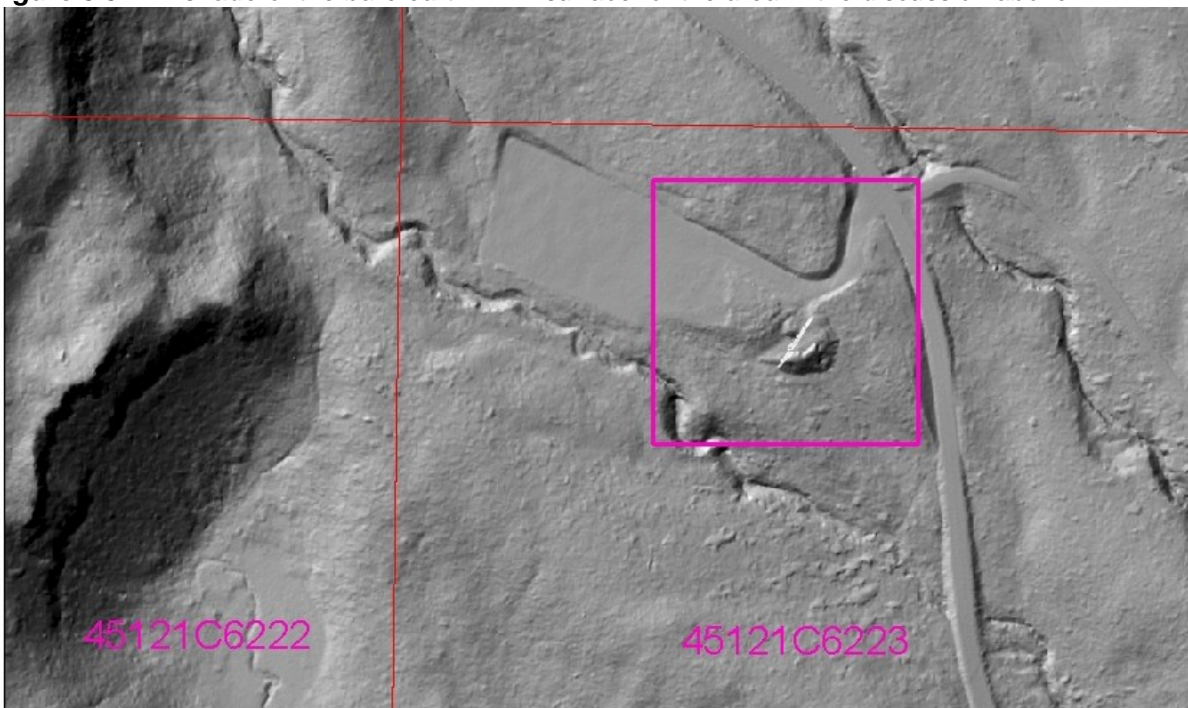
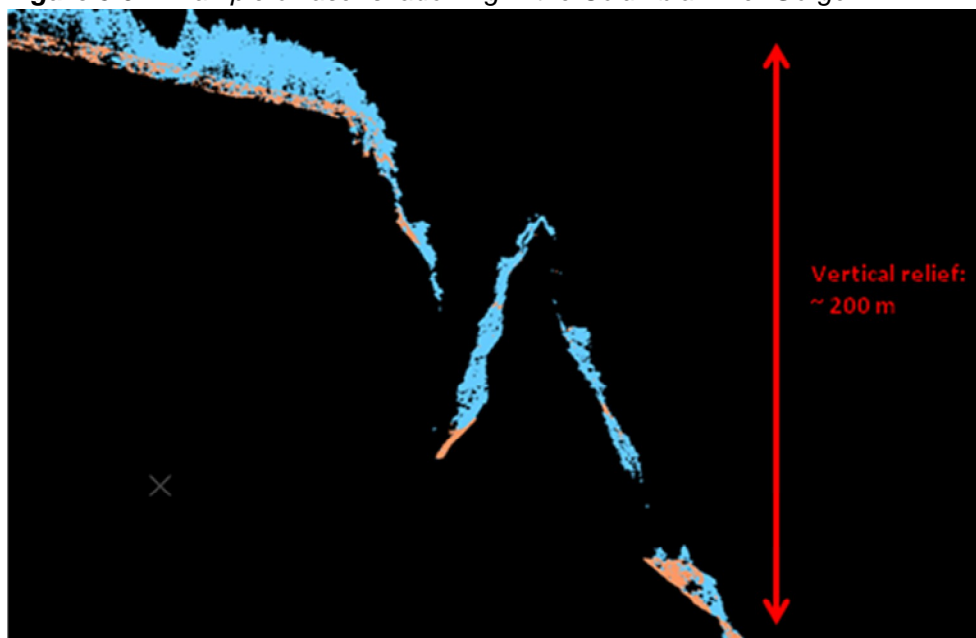


Figure 5.5. Hillshade of the bare earth DEM surface for the area in the discussion above.



Laser shadowing occurs when topographic or feature orientation relative to scan angle results in the occlusion of surface features. In areas of exceptional topographic variability, such as the ridgeline in the figure below (Tile 45121F7402), laser shadowing can result in voids in the LiDAR derived ground model. While flight planning attempts to minimize this acquisition artifact, terrain challenges present in the Columbia River Gorge prevented their elimination.

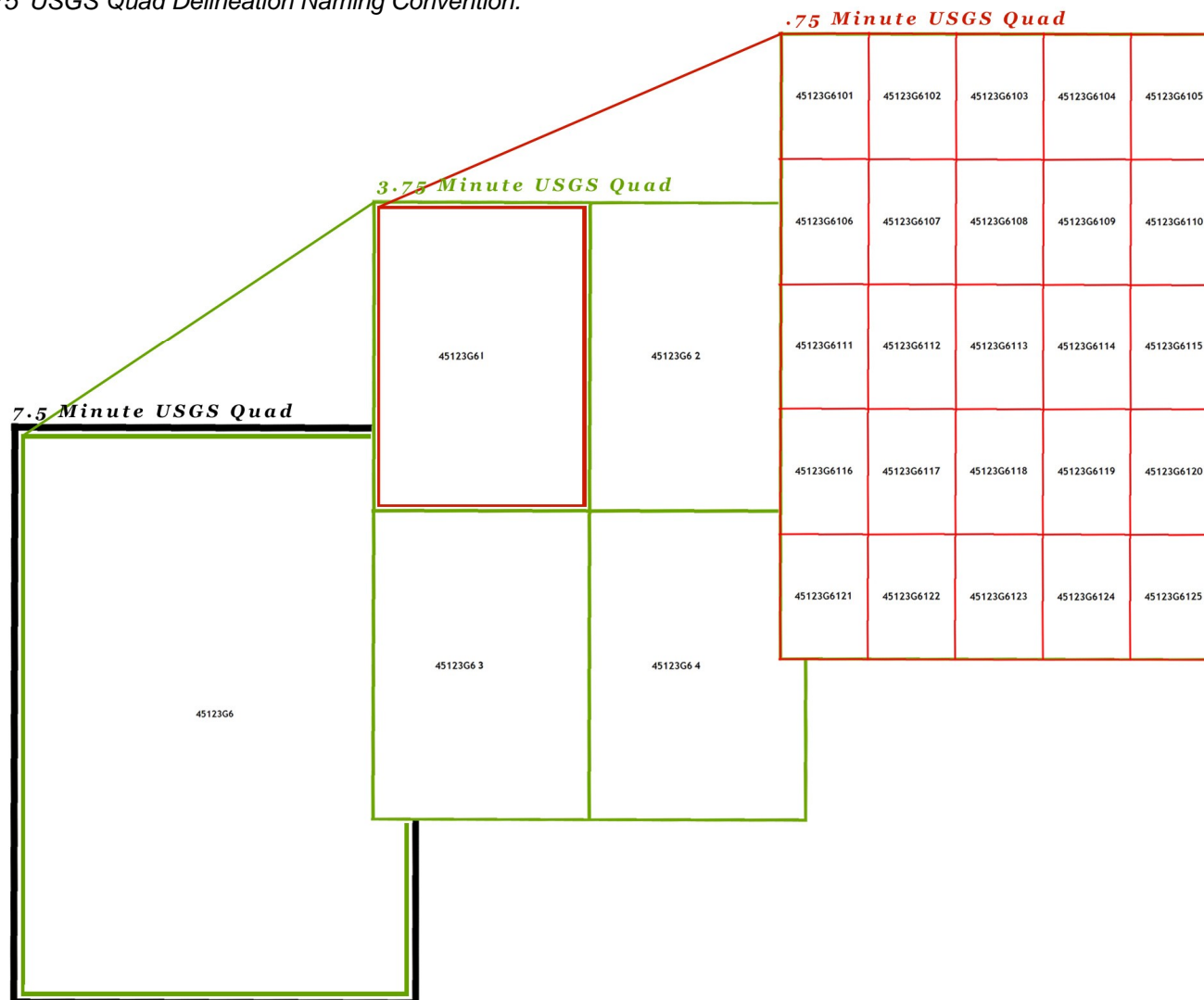
Figure 5.6. Example of laser shadowing in the Columbia River Gorge.



6. Deliverables

All Deliveries of DOGAMI and ODF Data conform to the following tiling scheme:

Figure 5.1. 0.75' USGS Quad Delineation Naming Convention.



6.1 Point Data (per 0.75' USGS Quad)

Data Fields: Number, X, Y, Z, Intensity, ReturnNumber, NumReturns, ScanDirection, EdgeOfFlightLine, Class, ScanAngleRank, FileMarker, UserBitField, GPSTime

- LAS v 1.1 Format
- ASCII Format
- Smoothed Best Estimate of Trajectory Point Files in ASCII format

6.2 Vector Data

- Total Area Flown
 - 7.5-minute quadrangle delineation in shapefile format
 - 0.75-minute quadrangle delineation in shapefile format (See **Figure 5.1** below for illustration)

6.3 Raster Data

- ESRI GRID of Bare Earth Modeled LiDAR data Points (3-foot resolution) delivered in 7.5' USGS Quad Delineation
- ESRI GRID of Above Ground Modeled LiDAR data Points (3-foot resolution) delivered in 7.5' USGS Quad Delineation
- Intensity Images in GeoTIFF format (1.5-foot resolution) delivered per 0.75' Quad

6.4 Data Report

- Full Report containing introduction, methodology, and accuracy.
 - Word Format (*.doc)
 - PDF Format (*.pdf)

6.5 Datum and Projection

The data were processed as ellipsoidal elevations and required a Geoid transformation to be converted into orthometric elevations (NAVD88). In TerraScan, the NGS published Geoid03 model is applied to each point. The data were processed using meters in the Universal Transverse Mercator (UTM) Zone 10 and NAD83 (CORS96)/NAVD88 datum and converted to the respective projections for each data set as specified below.

- ODF AOIs are delivered in Oregon Lambert, EPSG 2992, with horizontal units in International Feet and vertical units in US Survey Feet, in the NAD83/NAVD88 datum (Geoid 03).
- All other AOIs are delivered in Oregon State Plane North, with horizontal units in International Feet and vertical units in US Survey Feet, in the NAD83 HARN/NAVD88 datum (Geoid 03).

7. Selected Images

7.1 Three Dimensional Oblique View Data Pairs

Example areas are presented to show sample imagery (see **Figures 7.1-7.60**).

Figure 7.1. 3-d oblique view of LiDAR-derived surfaces in Quad 45123G6115, showing the North Fork Nehalem River and Hamlet Road in the ODF North Study Area (top image derived from all points, bottom image derived from ground-classified points).

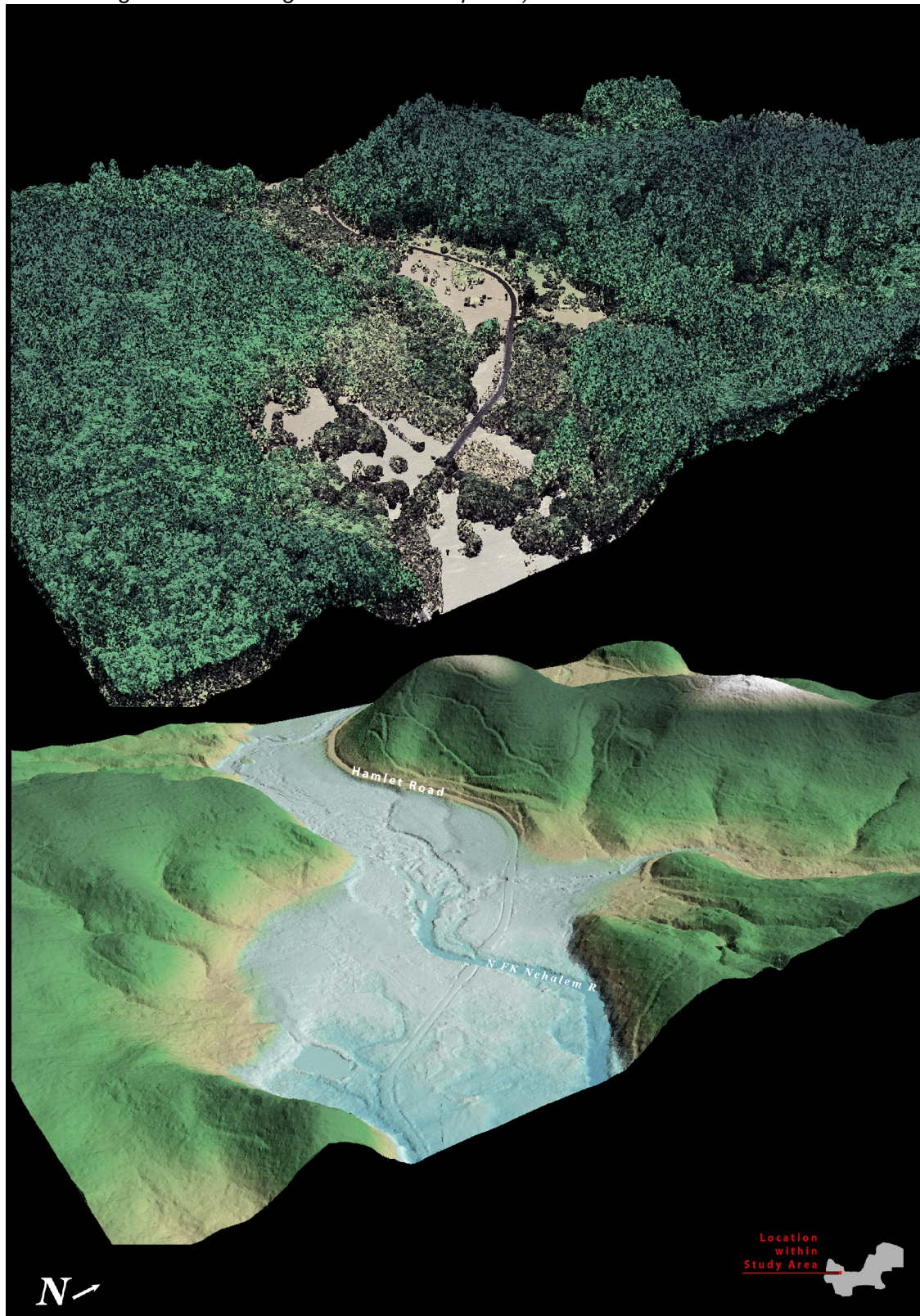


Figure 7.2. 3-d oblique view of LiDAR-derived surfaces in Quad 45123G6414, showing the Nehalem River and the Lower Nehalem Highway, just inside the Clatsop State Forest boundary in the ODF North Study Area. (Top image derived from all points, bottom image derived from ground-classified points).

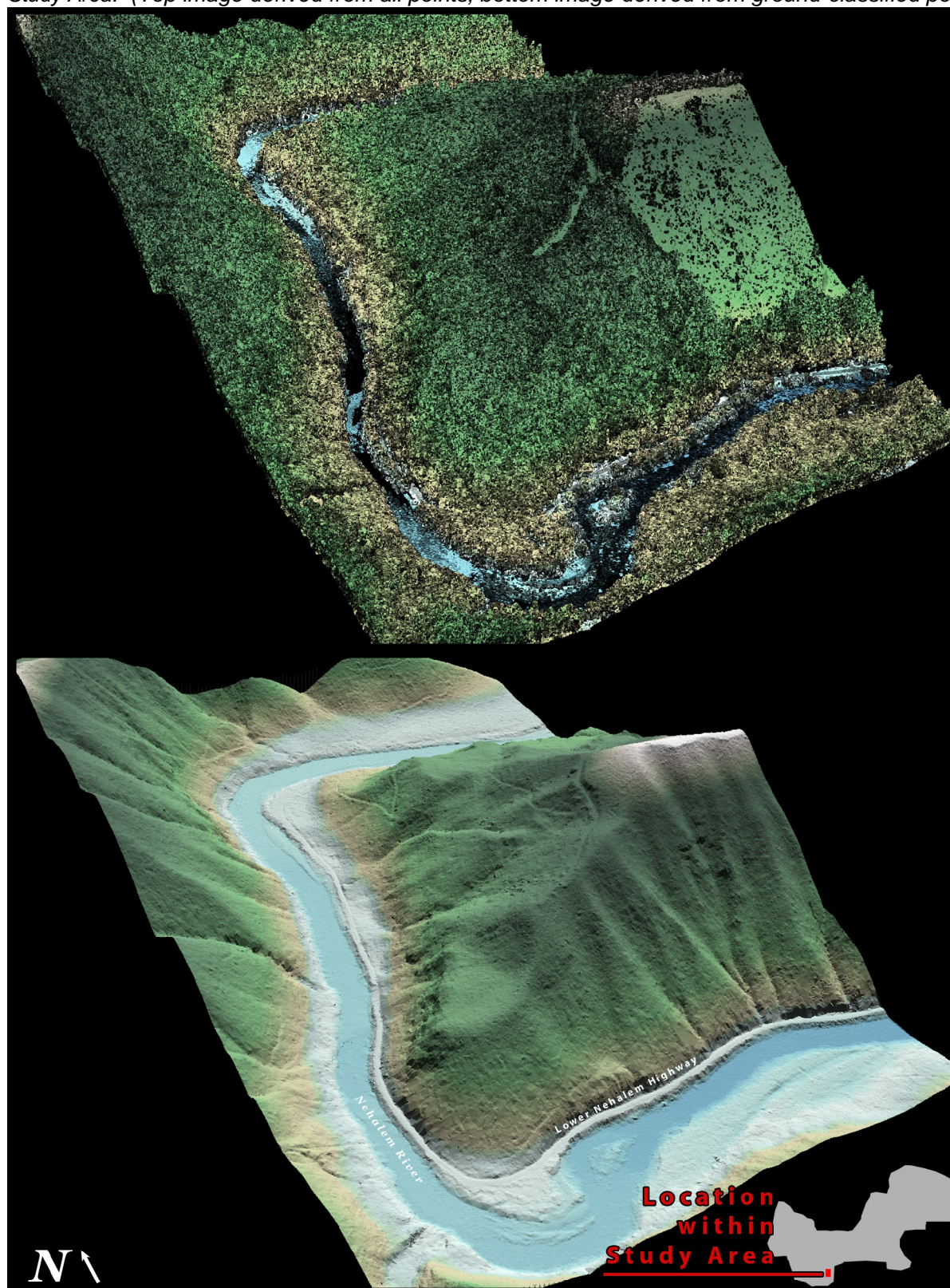


Figure 7.3. 3-d oblique view of LiDAR-derived surfaces in Quad 45123G6414, showing the confluence of Buster Creek with the Nehalem River, and Fishhawk Falls Road in the ODF North Study Area. (Top image derived from all points, bottom image derived from ground-classified points).

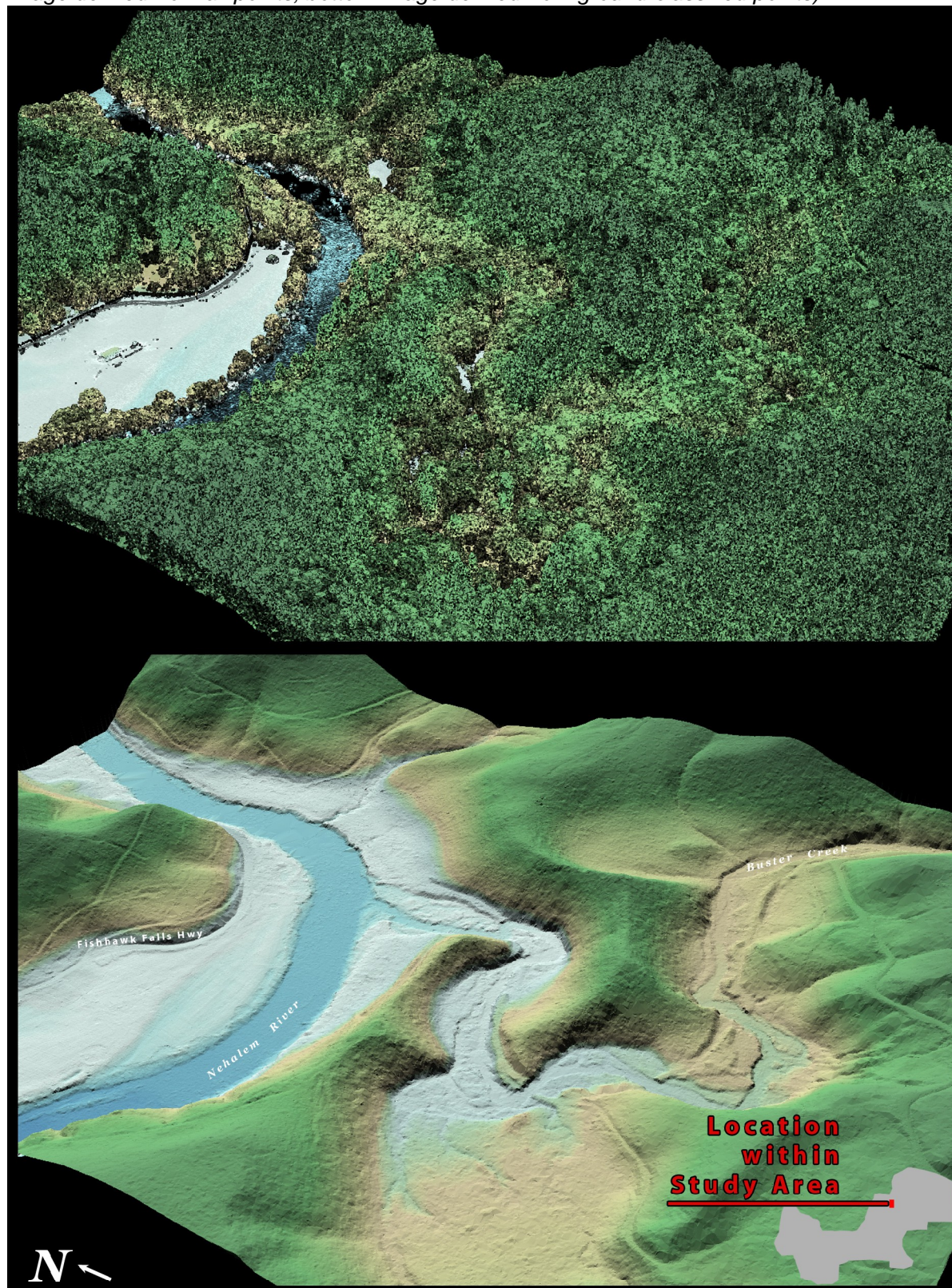


Figure 7.4. 3-d oblique view of LiDAR-derived surfaces in 0.75' Quad 45122A7223-224,403-404, showing the Mount Angel Abbey in the DOGAMI study area (top image derived from all points, bottom image derived from ground-classified points).

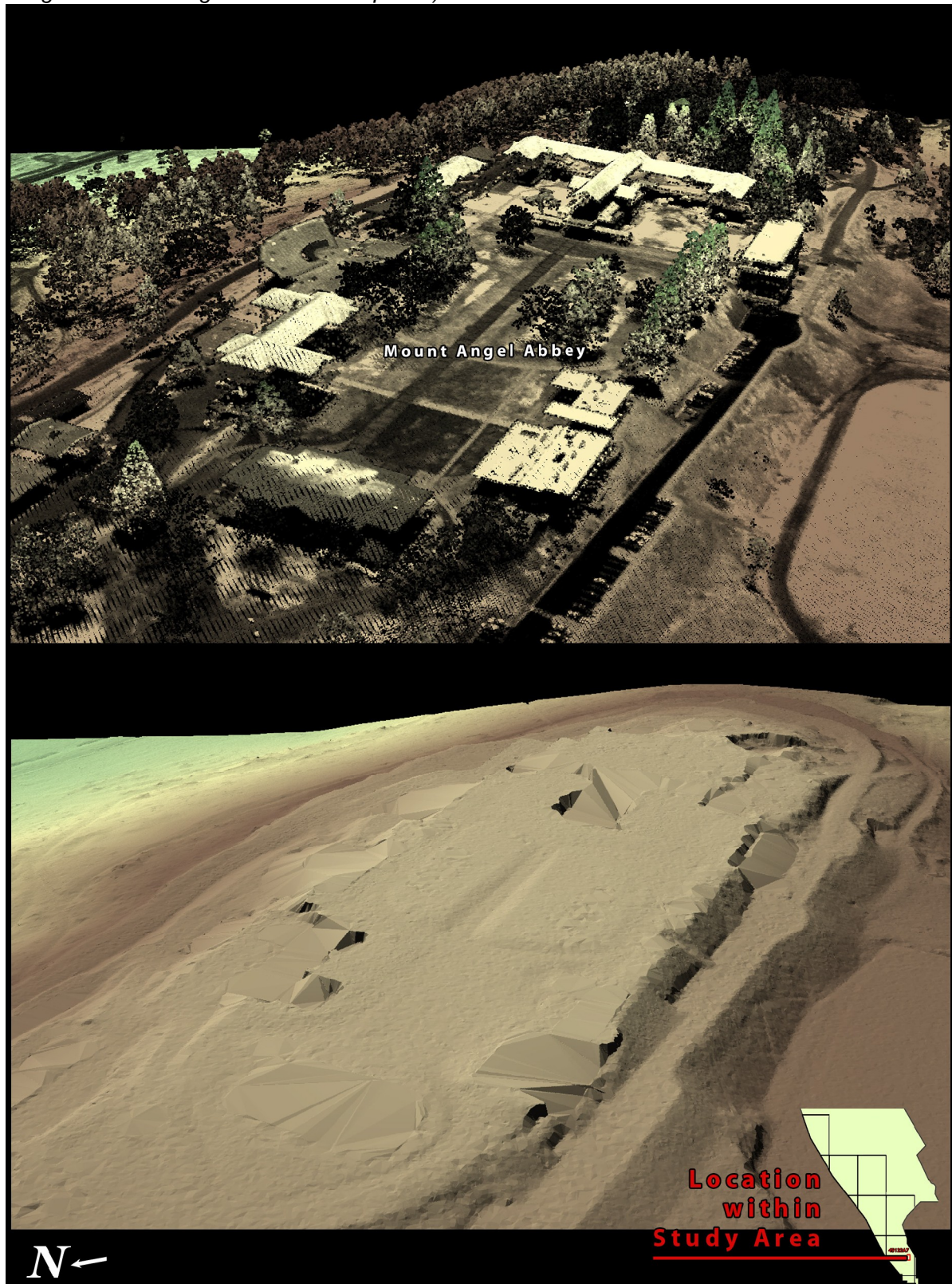


Figure 7.5. 3-d oblique view of LiDAR-derived surfaces in 0.75' Quad 45122A7108, showing a short reach of the Pudding River in the DOGAMI study area (top image derived from all points, bottom image derived from ground-classified points).

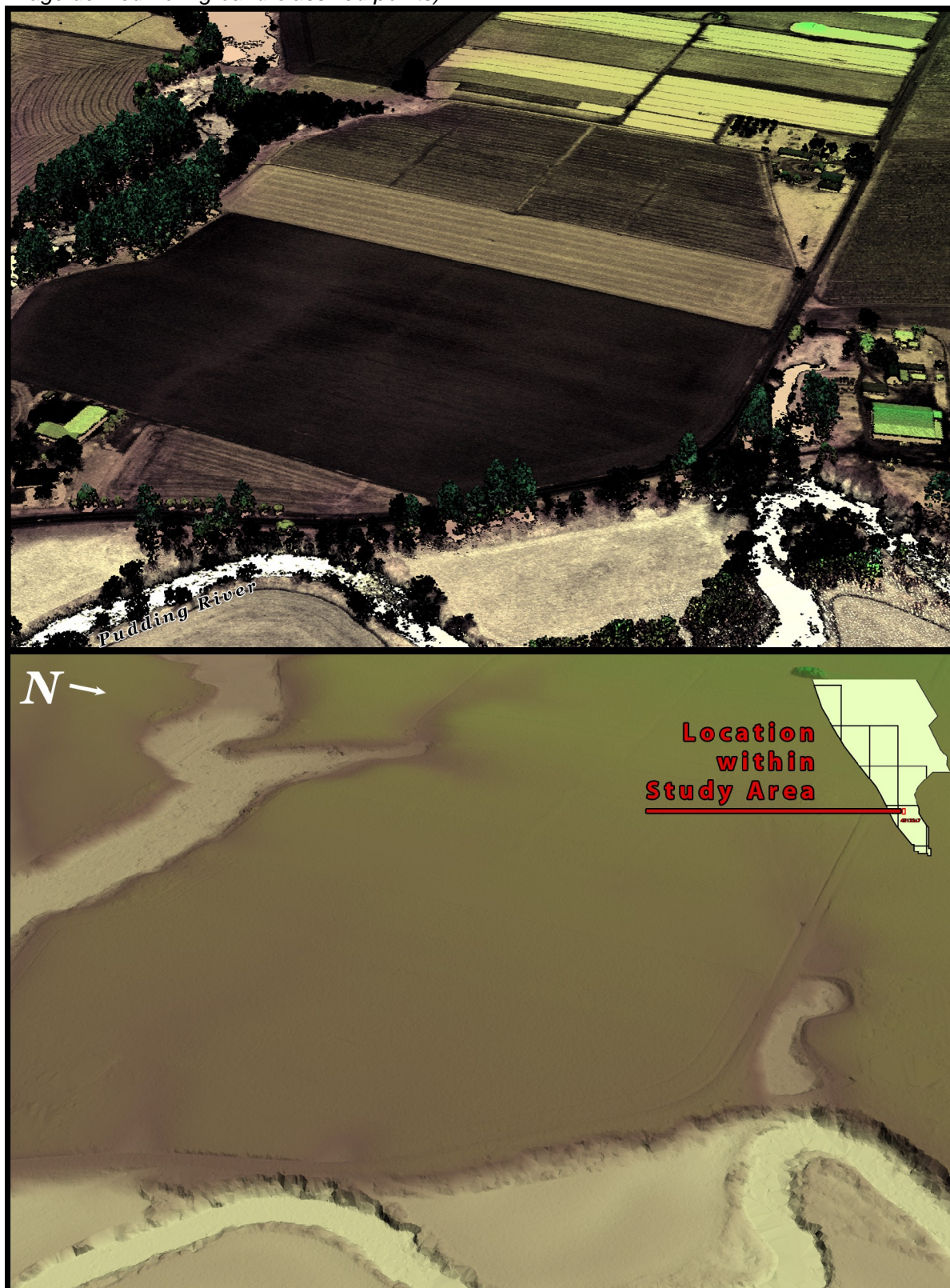


Figure 7.6. 3-d oblique view of LiDAR-derived surfaces in 0.75' Quad 45122C8307-308,312-313, showing the confluence of Chehalem Creek and the Willamette River, near the southwest edge of Newberg in the DOGAMI study area (top image derived from all points, bottom image derived from ground-classified points).

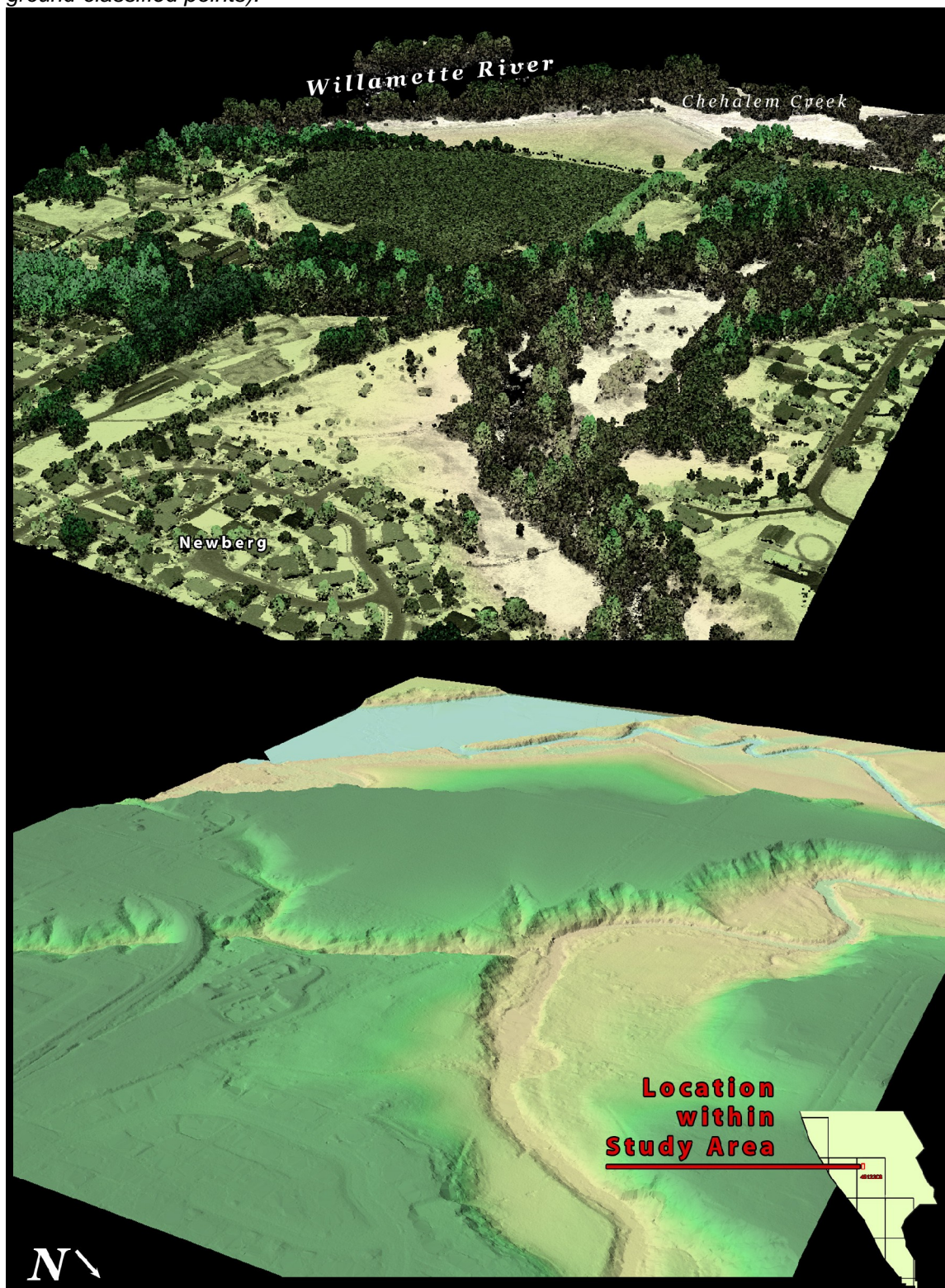


Figure 7.7. 3-d oblique view of LiDAR-derived surfaces in 0.75' Quad 45123D2109-110,114-115, showing Henry Hagg Lake and Scoggins Creek in the DOGAMI study area (top image derived from all points, bottom image derived from ground-classified points).

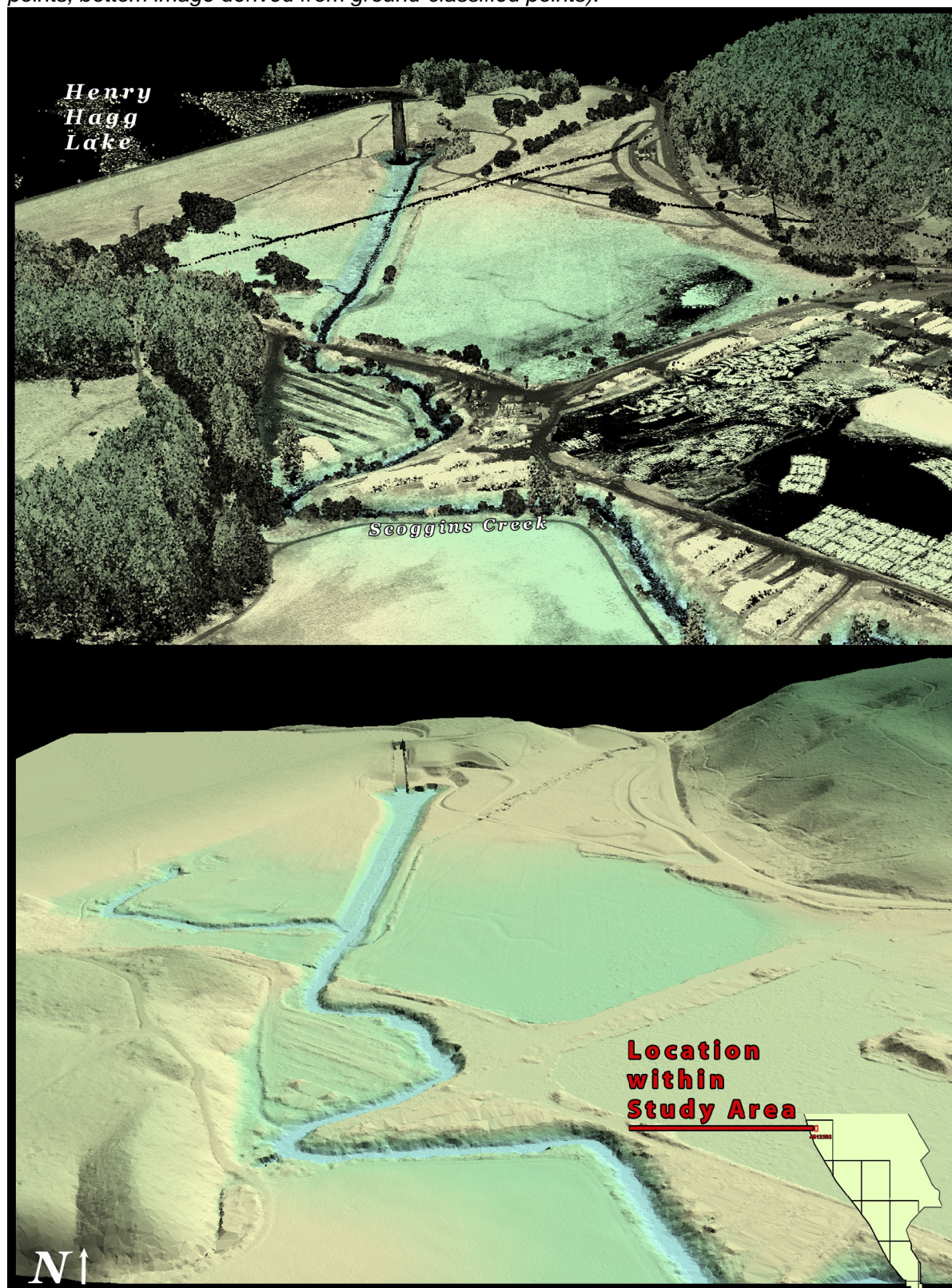


Figure 7.8. 3-d oblique view of LiDAR-derived surfaces in 7.5' Quad 45123D7, showing Kilchis and Wilson Rivers in the ODF South study area.

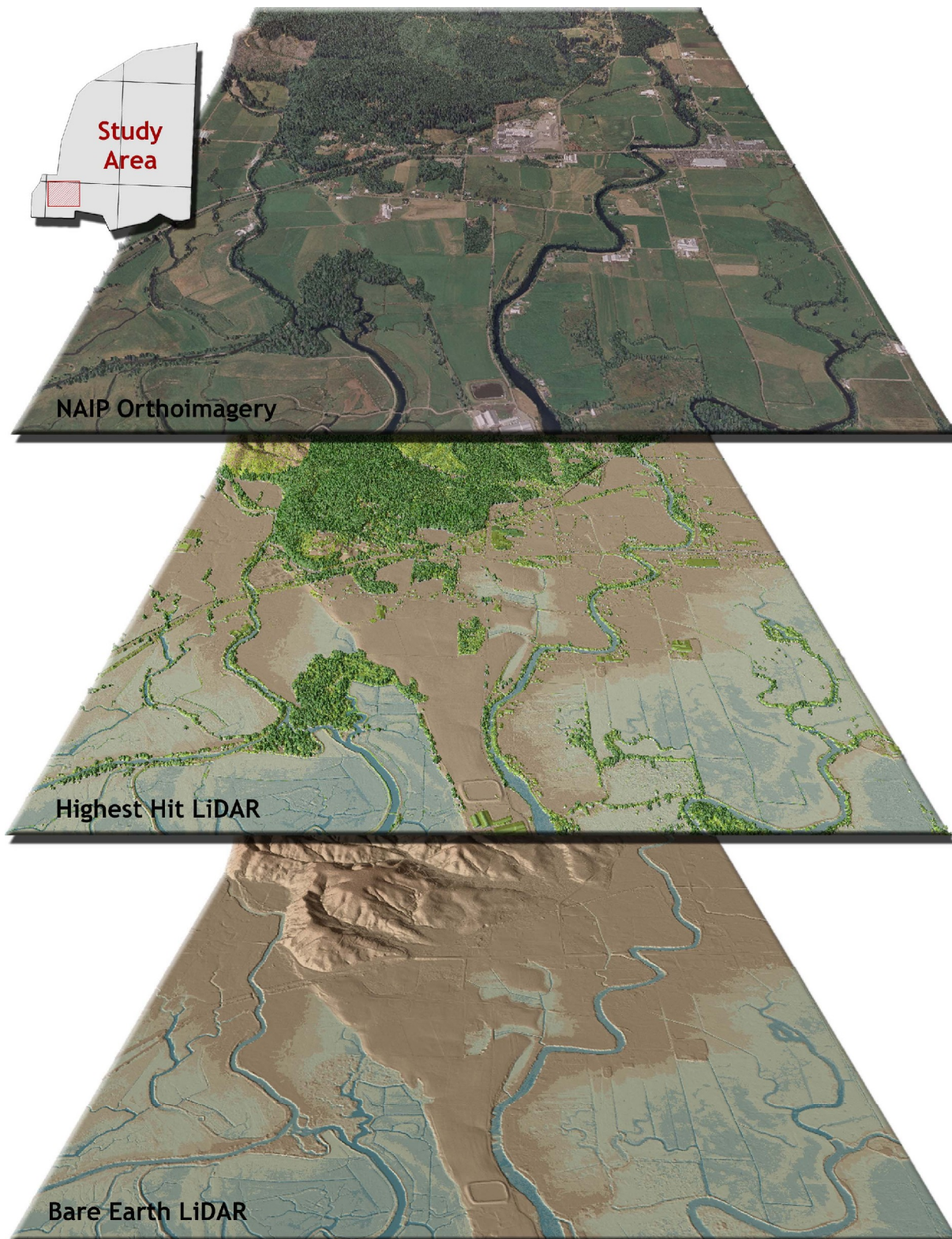


Figure 7.9. 3-d oblique view of LiDAR-derived surfaces in 7.5' Quad 45123D6, showing Wilson River near the Little North Fork confluence in the ODF South study area.

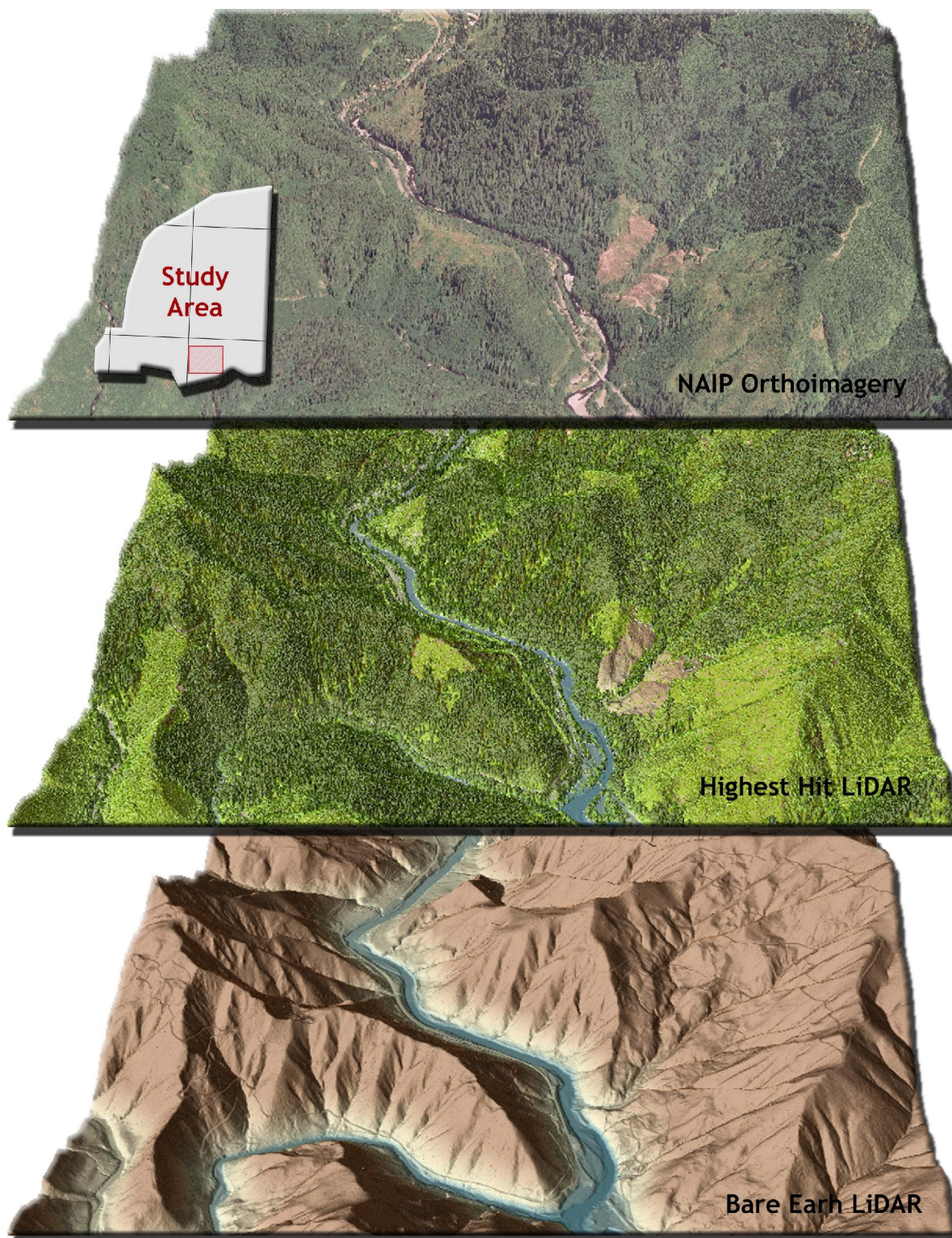


Figure 7.10. 3-d oblique view of LiDAR-derived surfaces in 7.5' Quad 45123D6, showing the confluence of the Wilson and Little North Fork Rivers in the ODF South study area.



Figure 7.11. 3-d oblique view of LiDAR-derived surfaces in 7.5' Quad 45123E6, showing the upper portion of the Little North Fork Wilson River watershed in the ODF South study area.

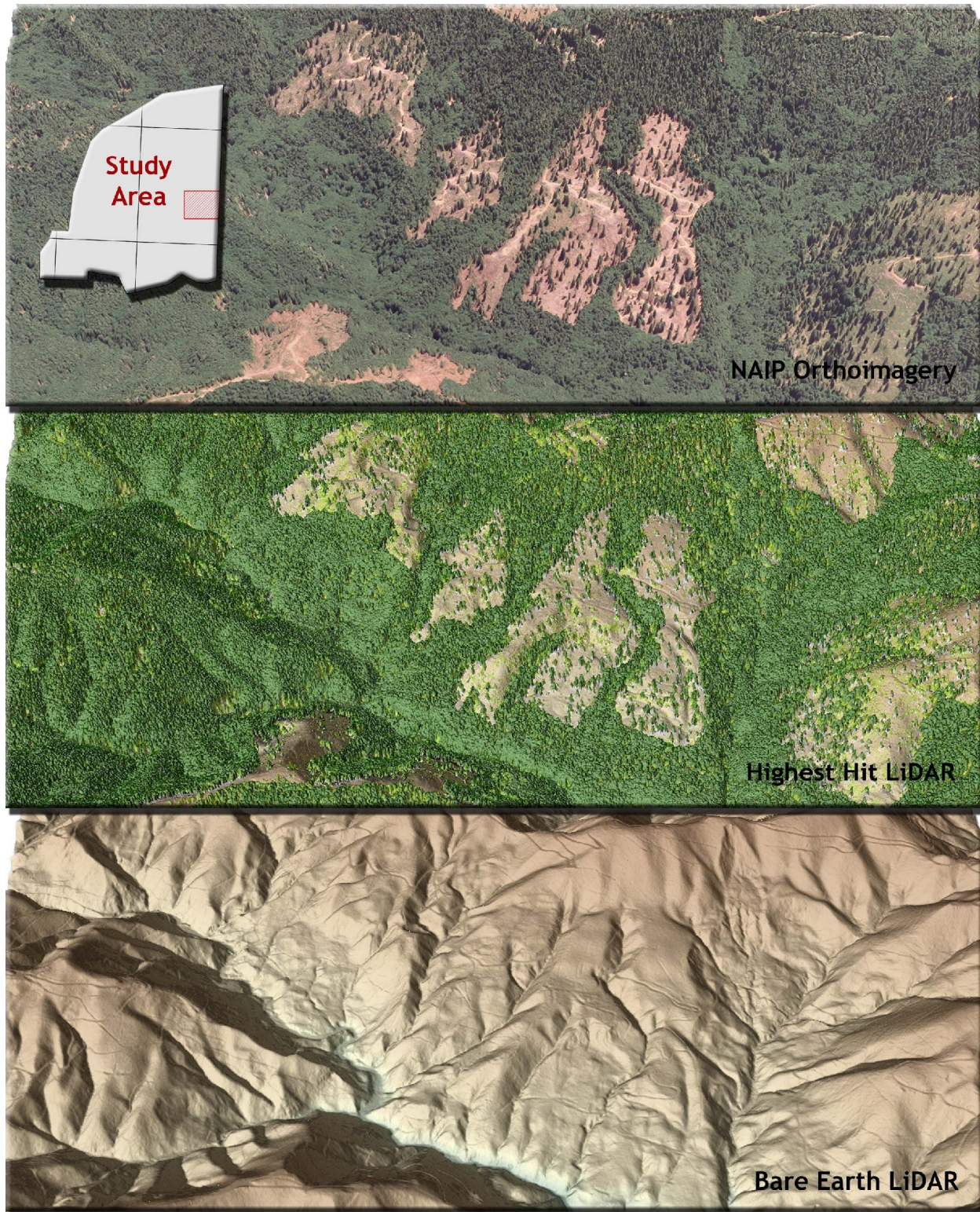


Figure 7.12. 3-d oblique view of LiDAR-derived surfaces showing a view of the Devils Lake Fork upper watershed.

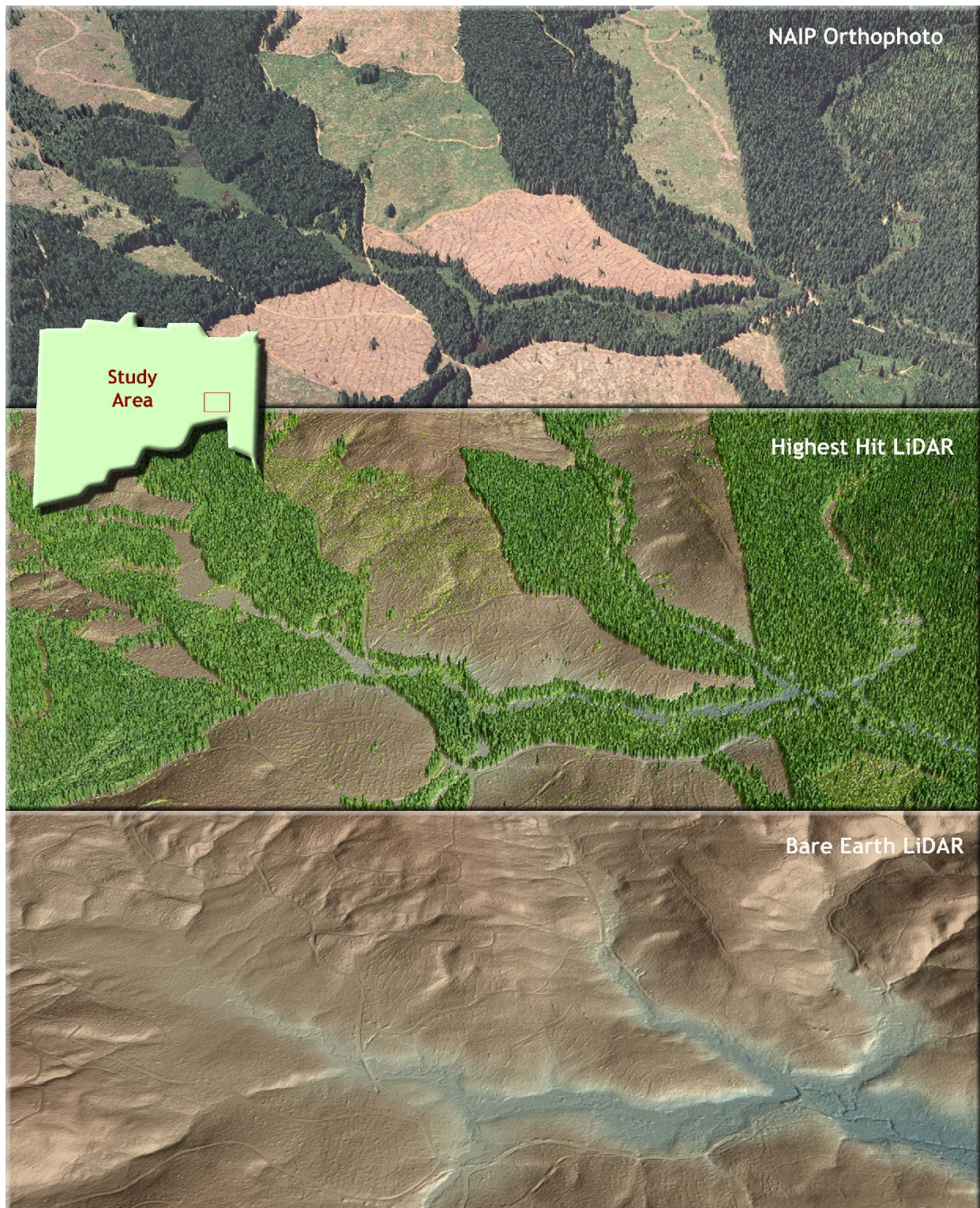


Figure 7.13. 3-d oblique view of LiDAR-derived surfaces looking south over the Wilson River near the North Fork confluence.

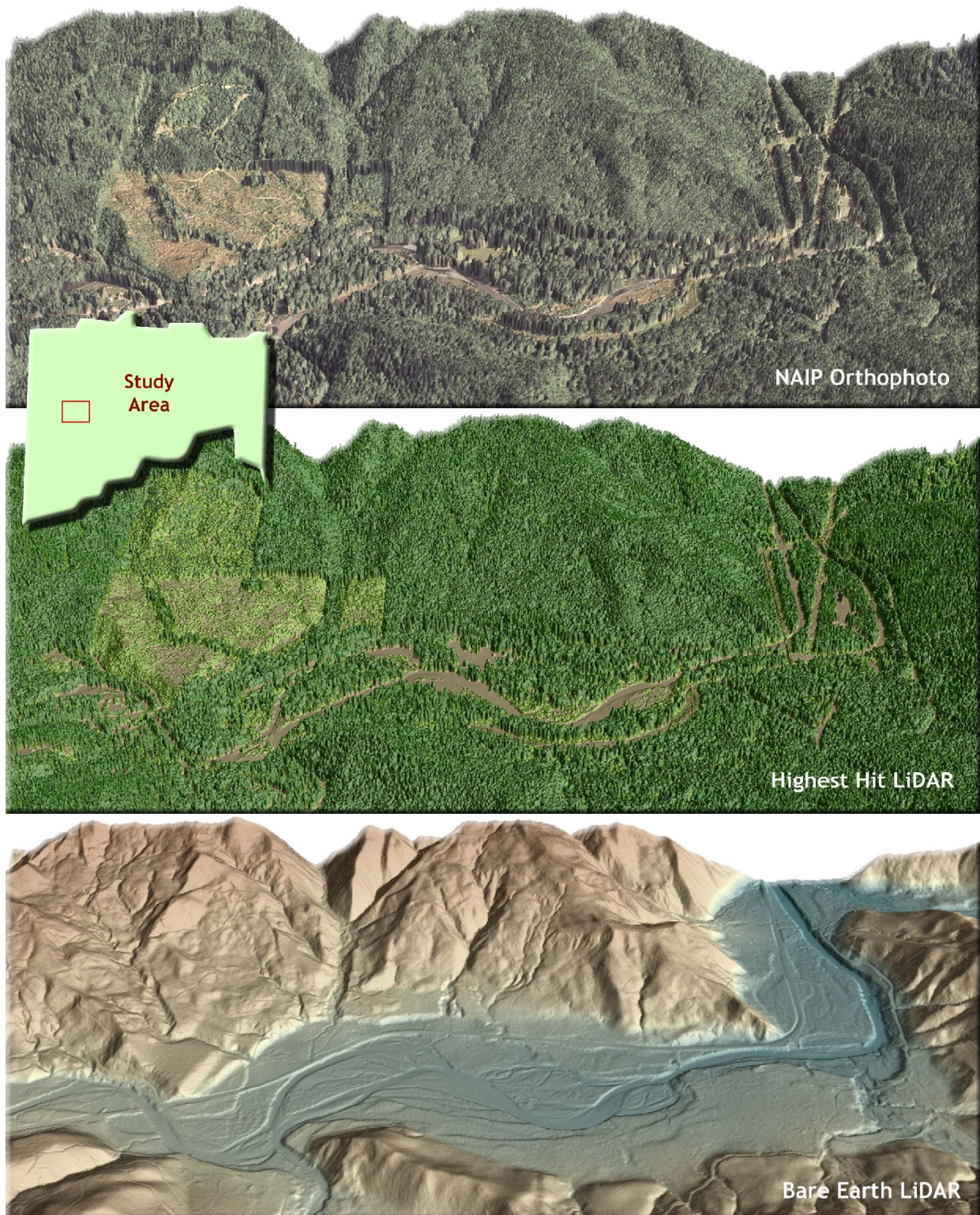


Figure 7.14. 3-d oblique view of LiDAR-derived surfaces looking south over the Wilson River near the North Fork confluence.

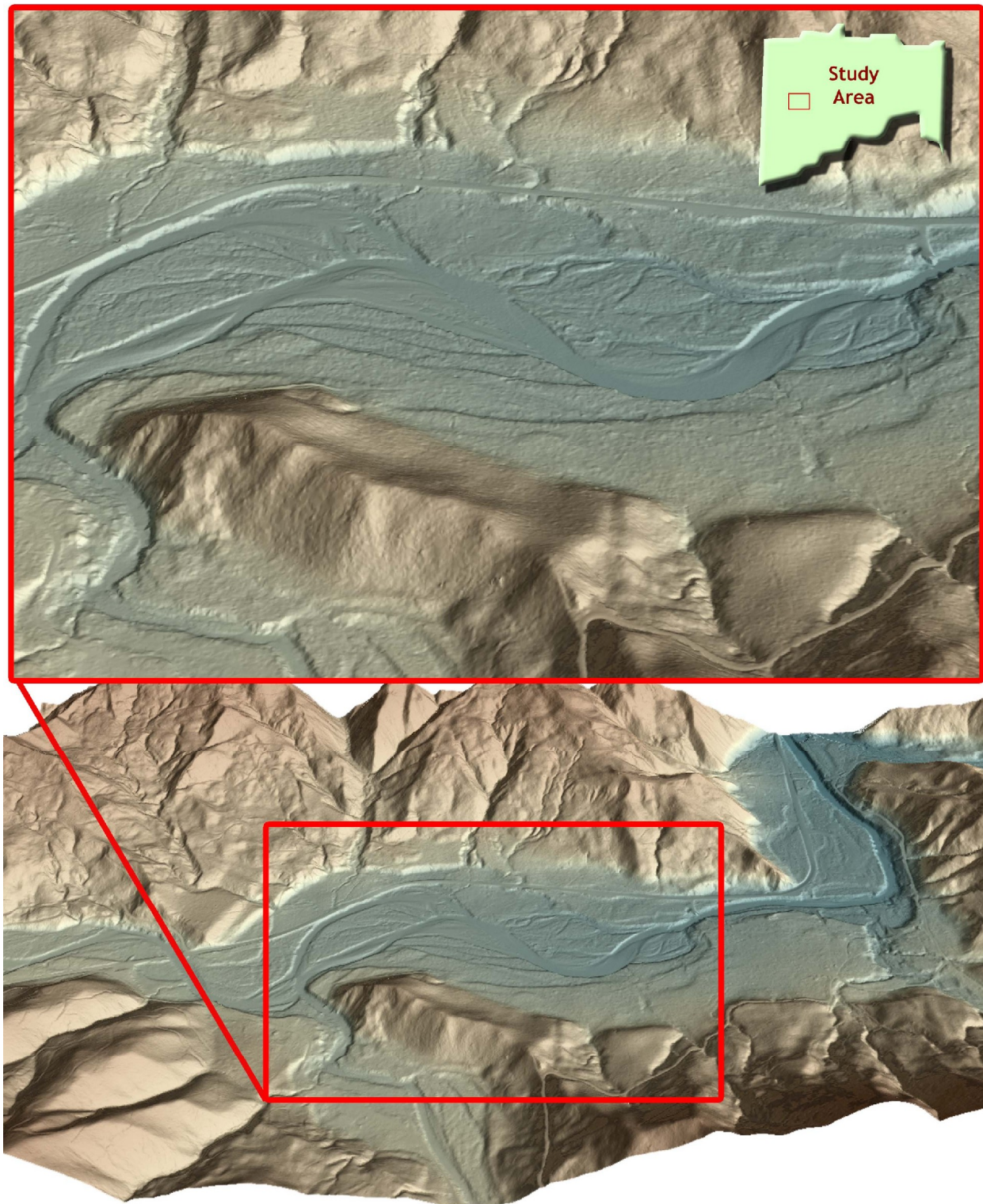


Figure 7.15. 3-d oblique view of LiDAR-derived surfaces showing an historic landslide along Devils Lake Fork, between Elliot Creek and Drift Creek.



Figure 7.16. 3-d oblique view of LiDAR-derived surfaces looking north across confluence of Gales Creek and Beaver Creek.

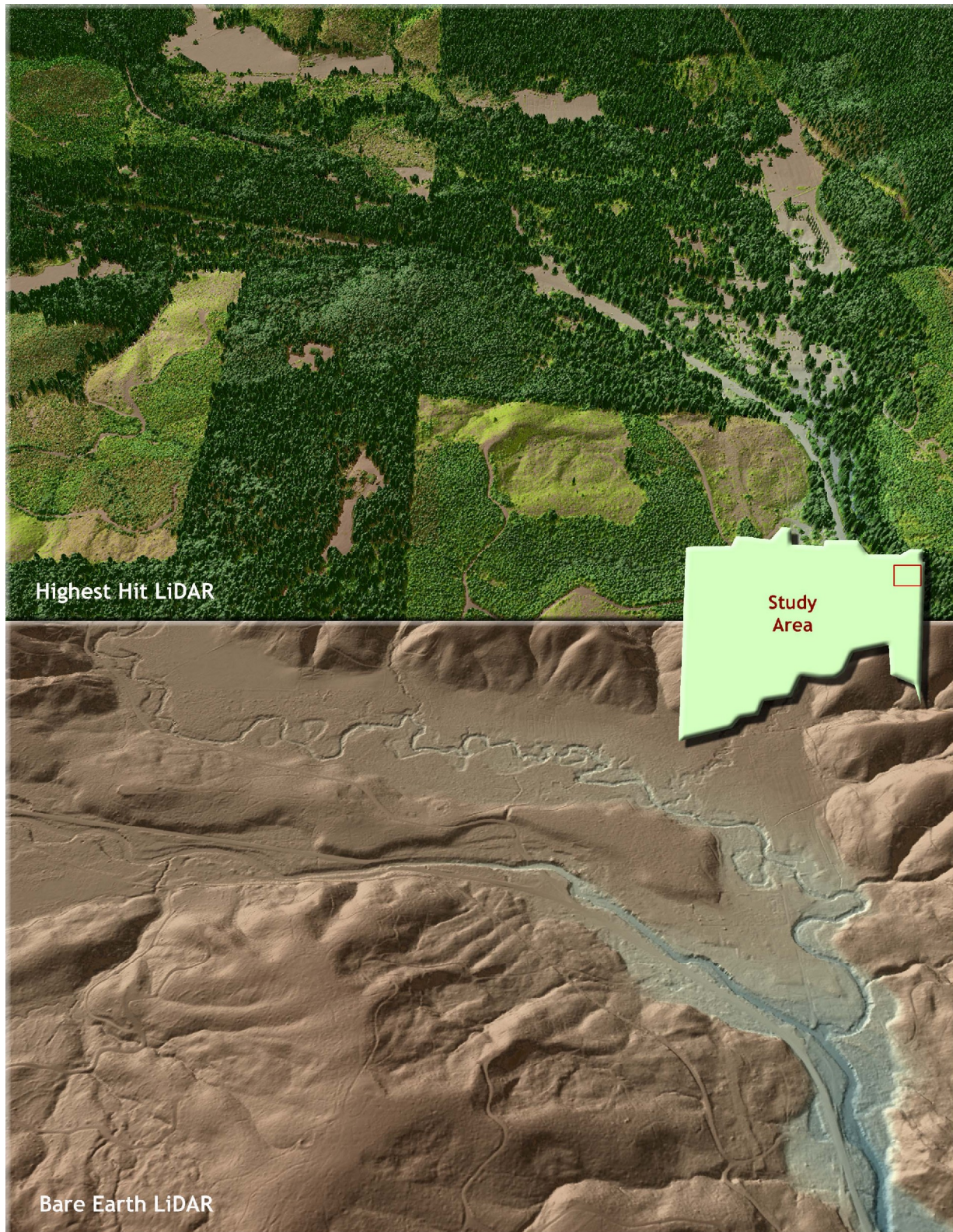


Figure 7.17. 3-d oblique view of LiDAR-derived surfaces showing the Wilson River at the Jordan Creek confluence.



Figure 7.18. 3-d oblique view of LiDAR-derived surfaces showing an historic landslide along Wolf Creek.

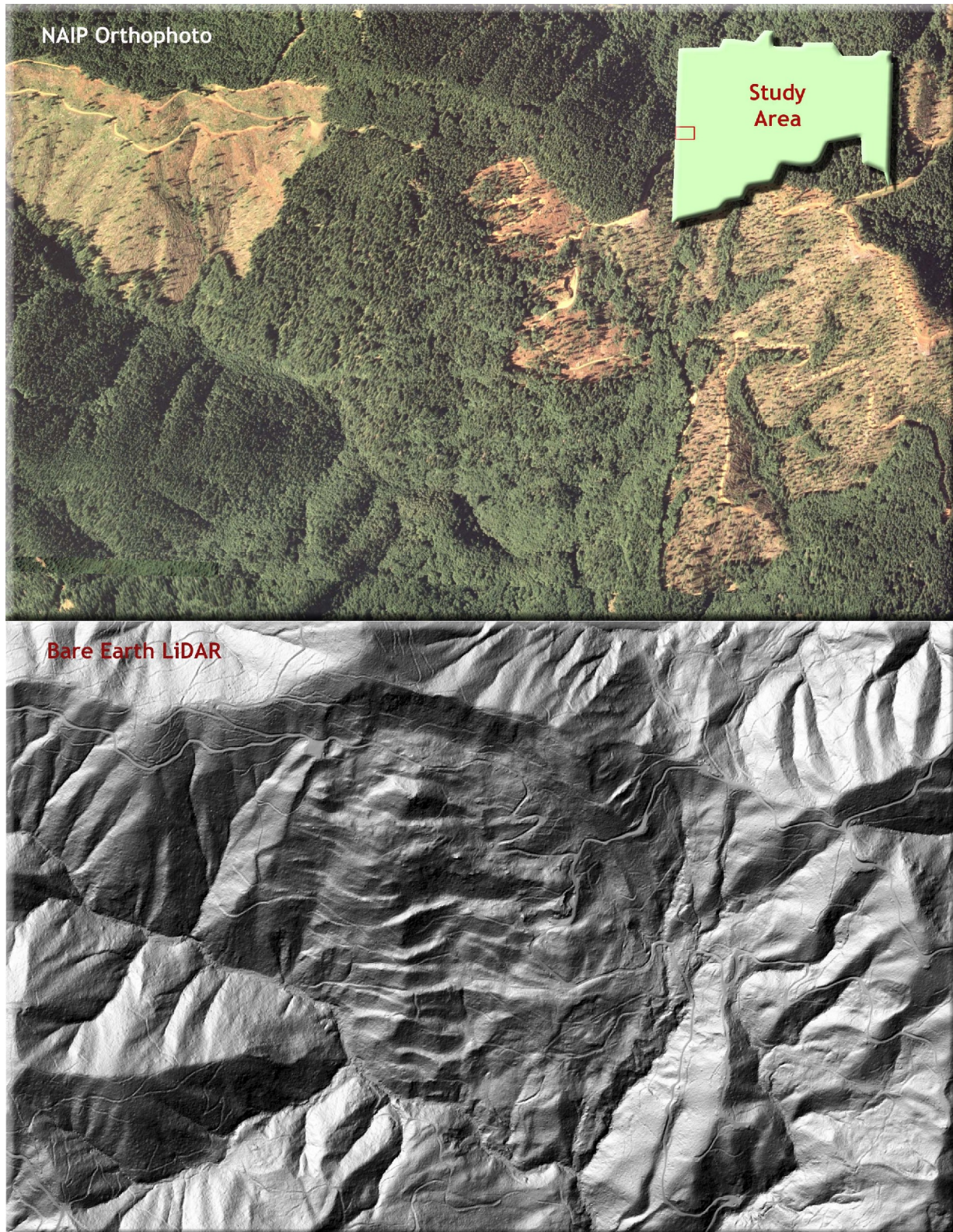


Figure 7.19. 3-d oblique view of LiDAR-derived images showing the highest hit surface of downtown Portland, looking eastward.

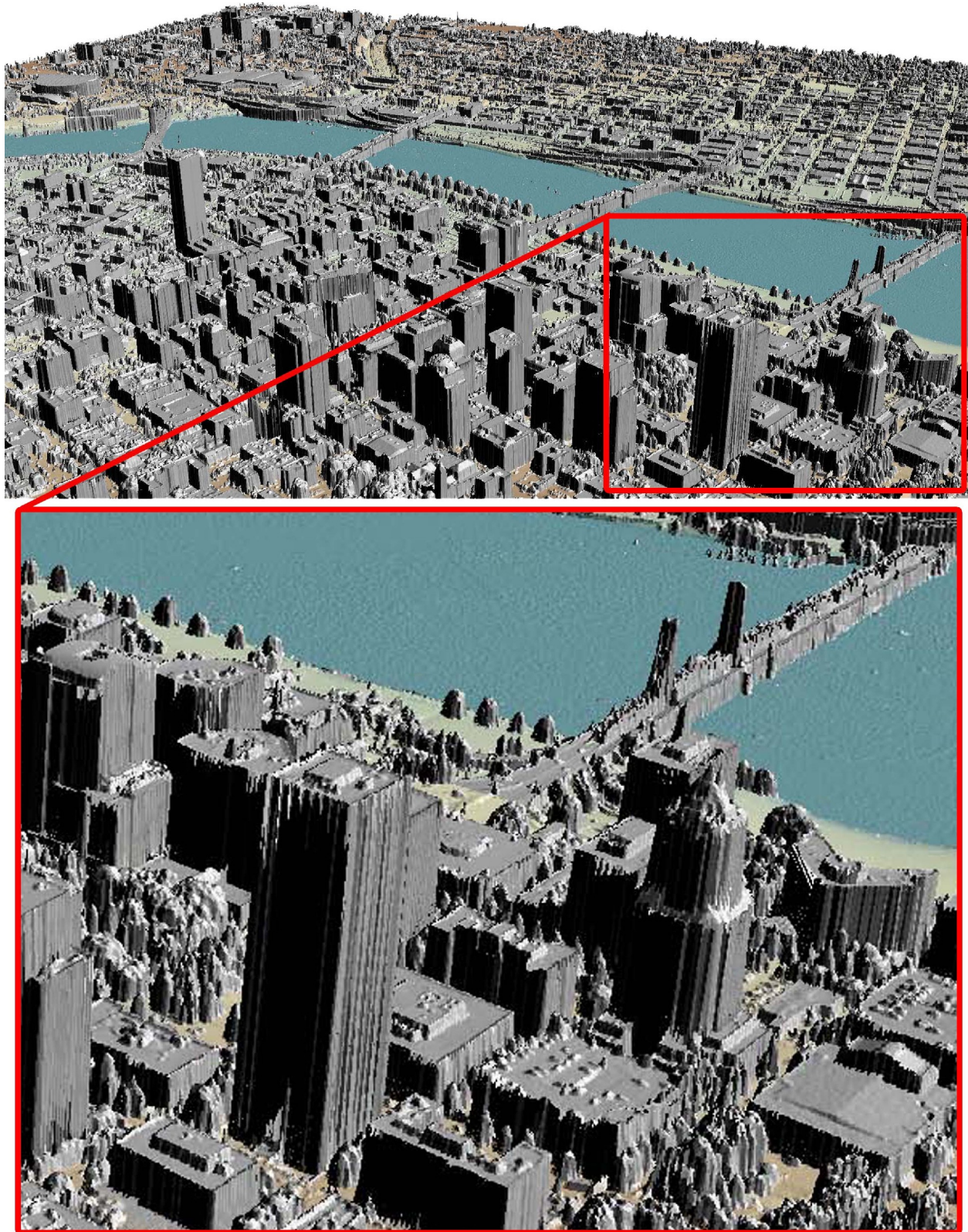


Figure 7.20. 3-d oblique view of LiDAR-derived surfaces showing the city of Portland, looking eastward.

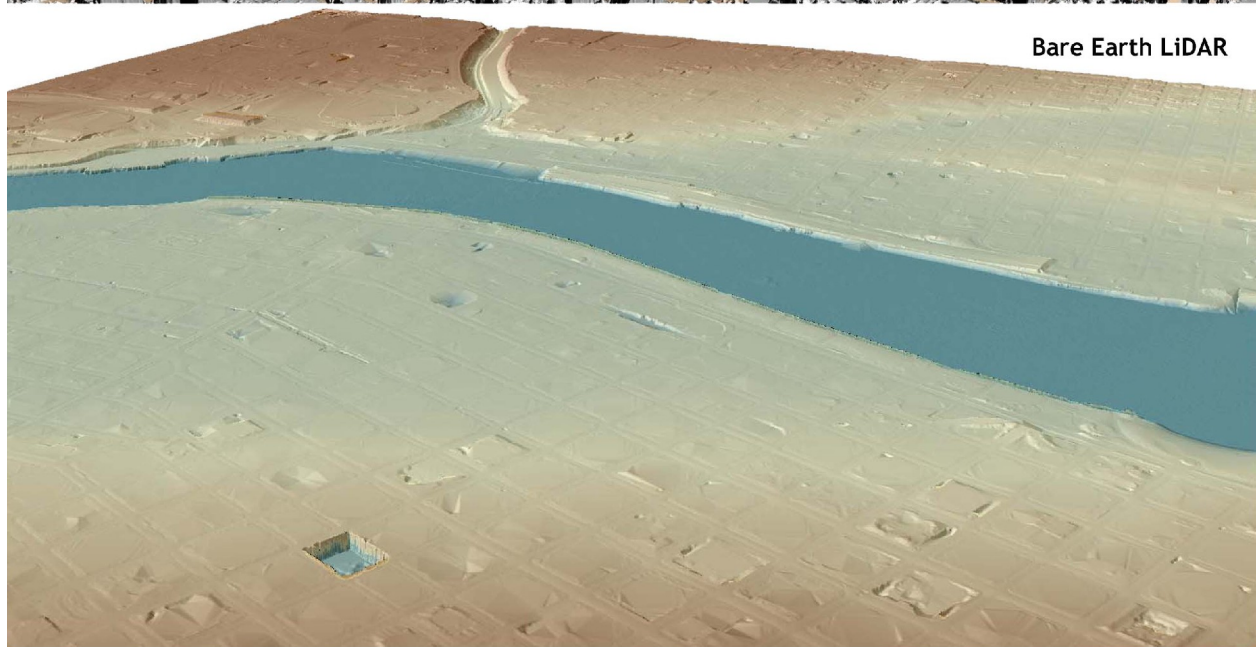
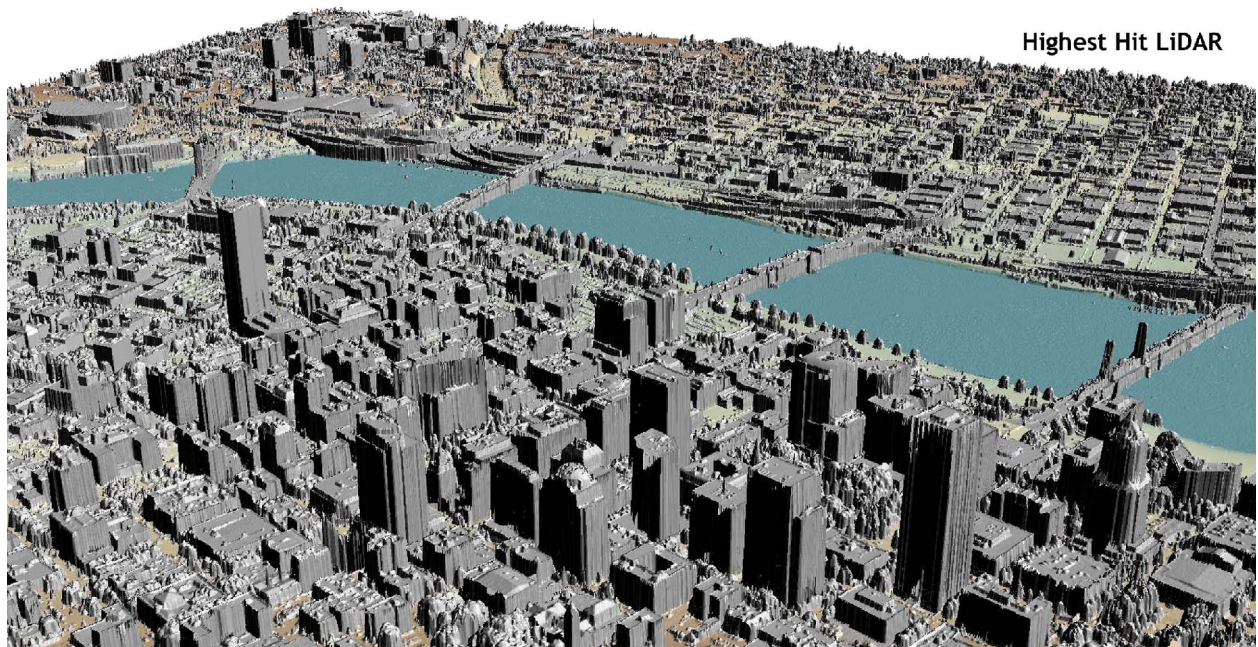


Figure 7.21. 3-d oblique view of downtown Portland, looking westward. Bottom image is of LiDAR-derived highest hit surface.

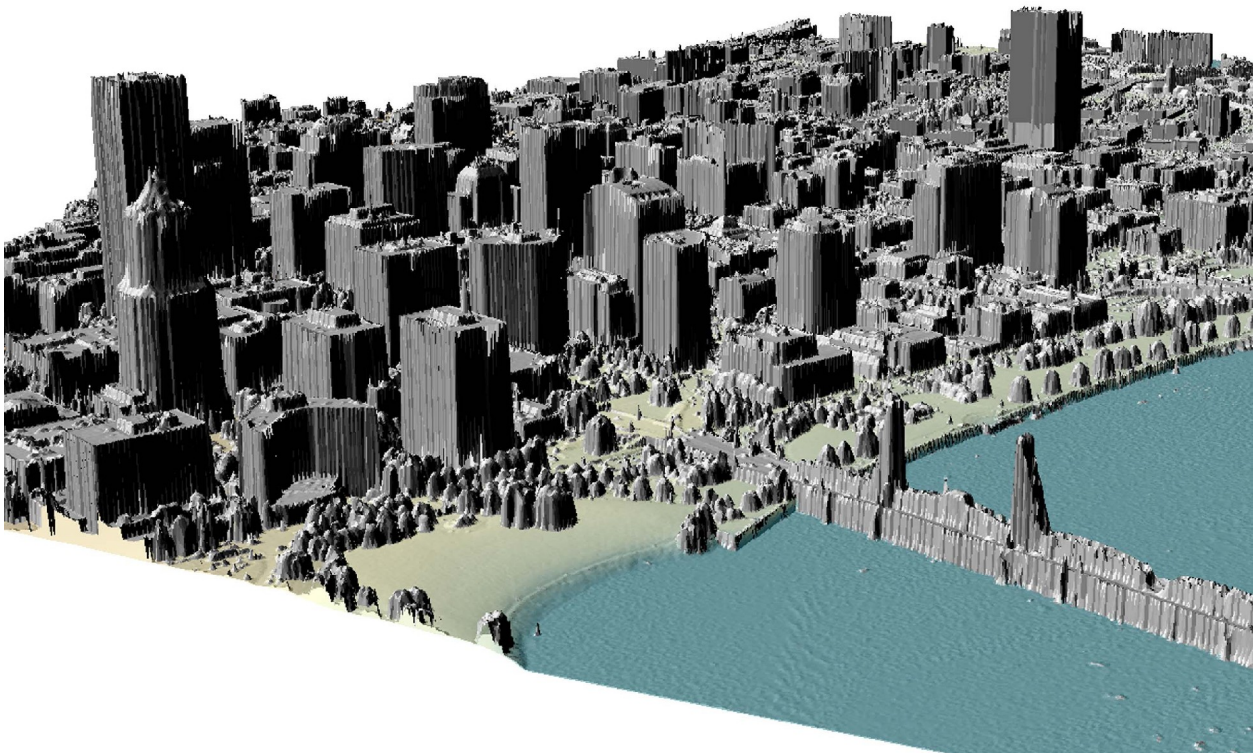


Figure 7.22. 3-d oblique view of Ladd's Addition in Southeast Portland.



Figure 7.23. 3-d oblique view North Willamette Boulevard, just east of the University of Portland.



Figure 7.24. 3-d oblique view of the I-5 and I-84 interchange near downtown Portland.

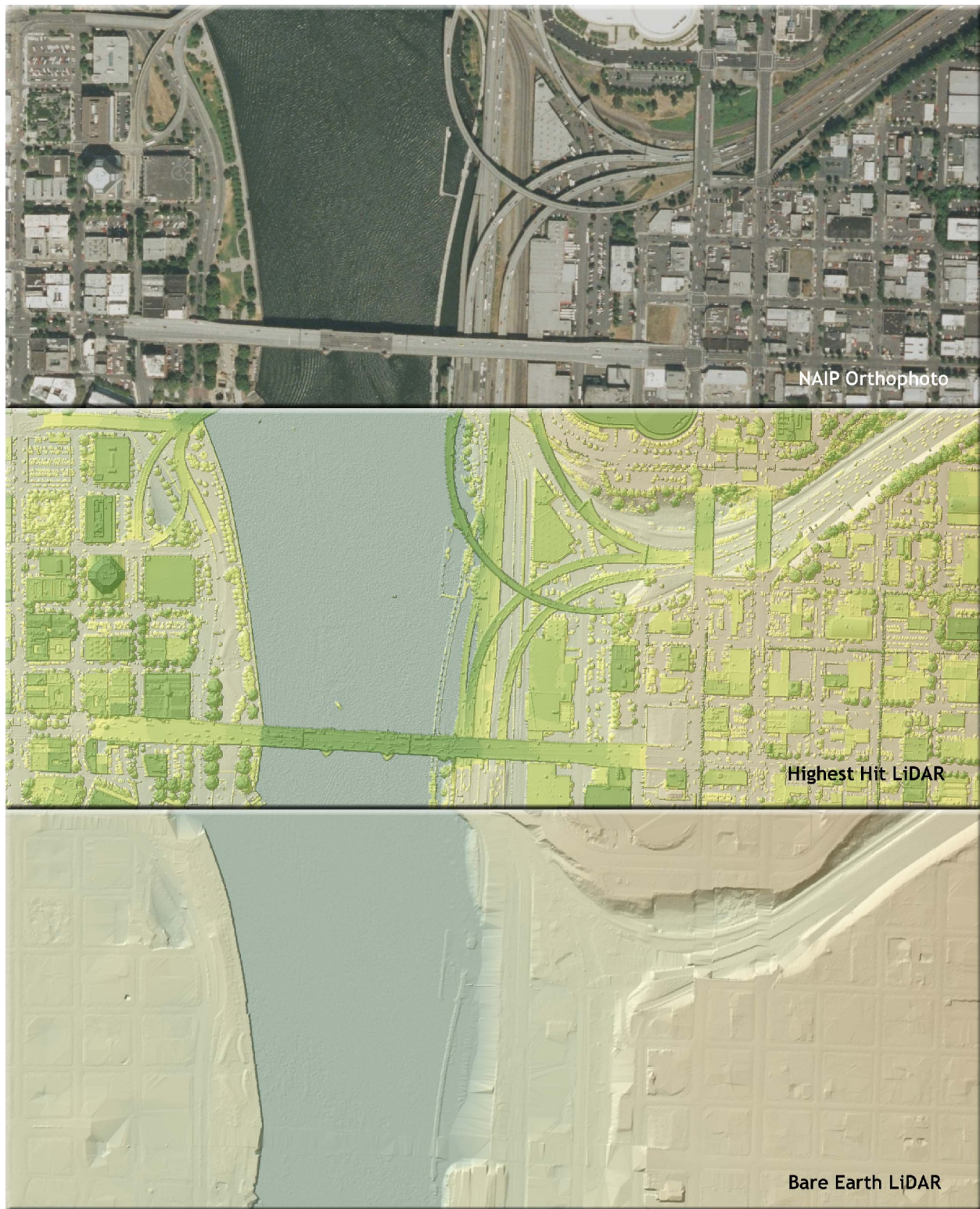


Figure 7.25. 3-d oblique view Looking southward at Willamette National Cemetery and nearby residential development.



Figure 7.26. 3-d oblique view of the Clackamas River, just downstream of Carver, OR (looking southward).



Figure 7.27. 3-d oblique view looking southward at Walters Hill and Johnson Creek in Gresham.



Figure 7.28. 3-d oblique view looking northward at Clear Creek near Redland.

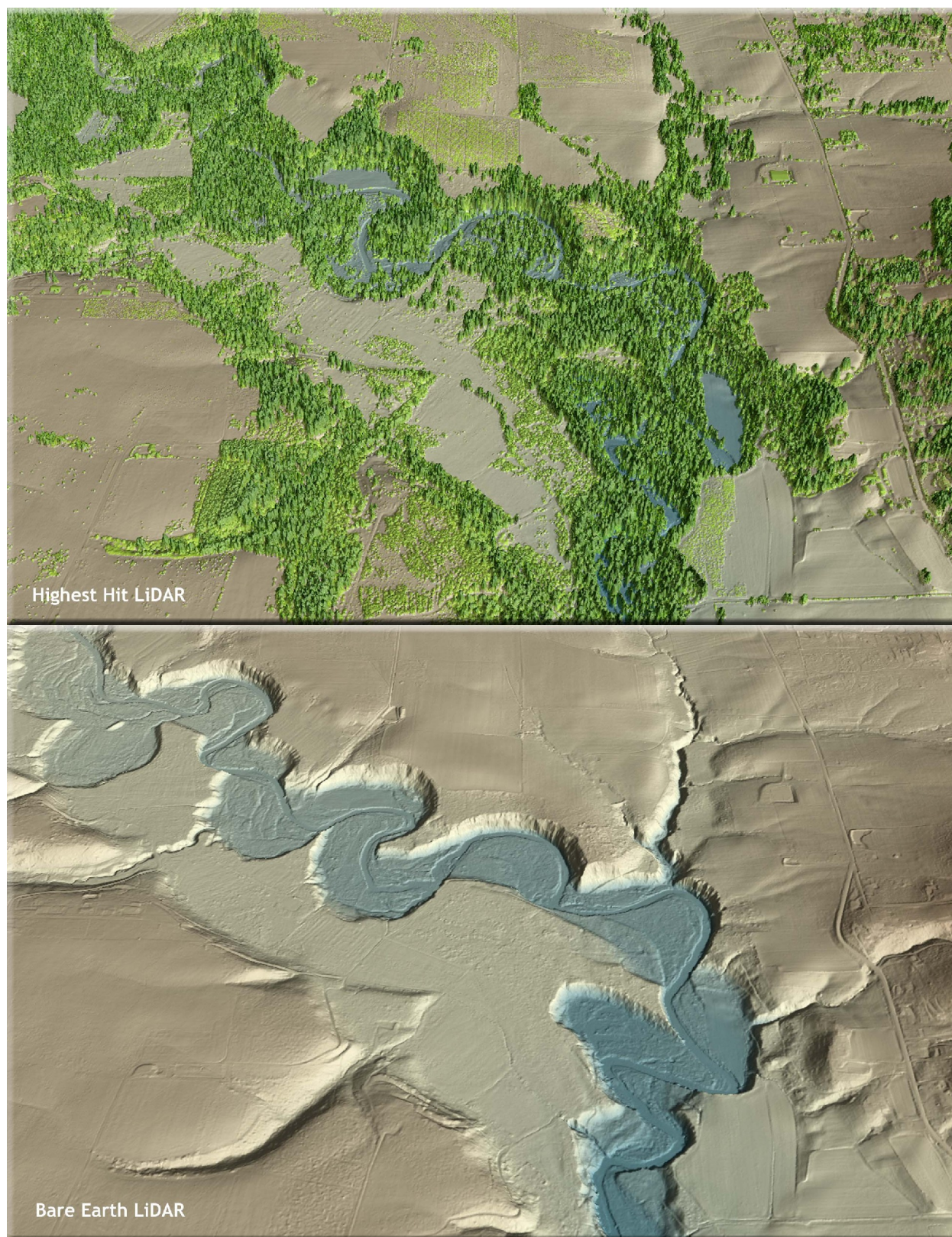


Figure 7.29. 3-d oblique view of the Clackamas River (looking upstream) near Foster Creek (entering from lower right of image) and Deep Creek (entering from upper left of image).

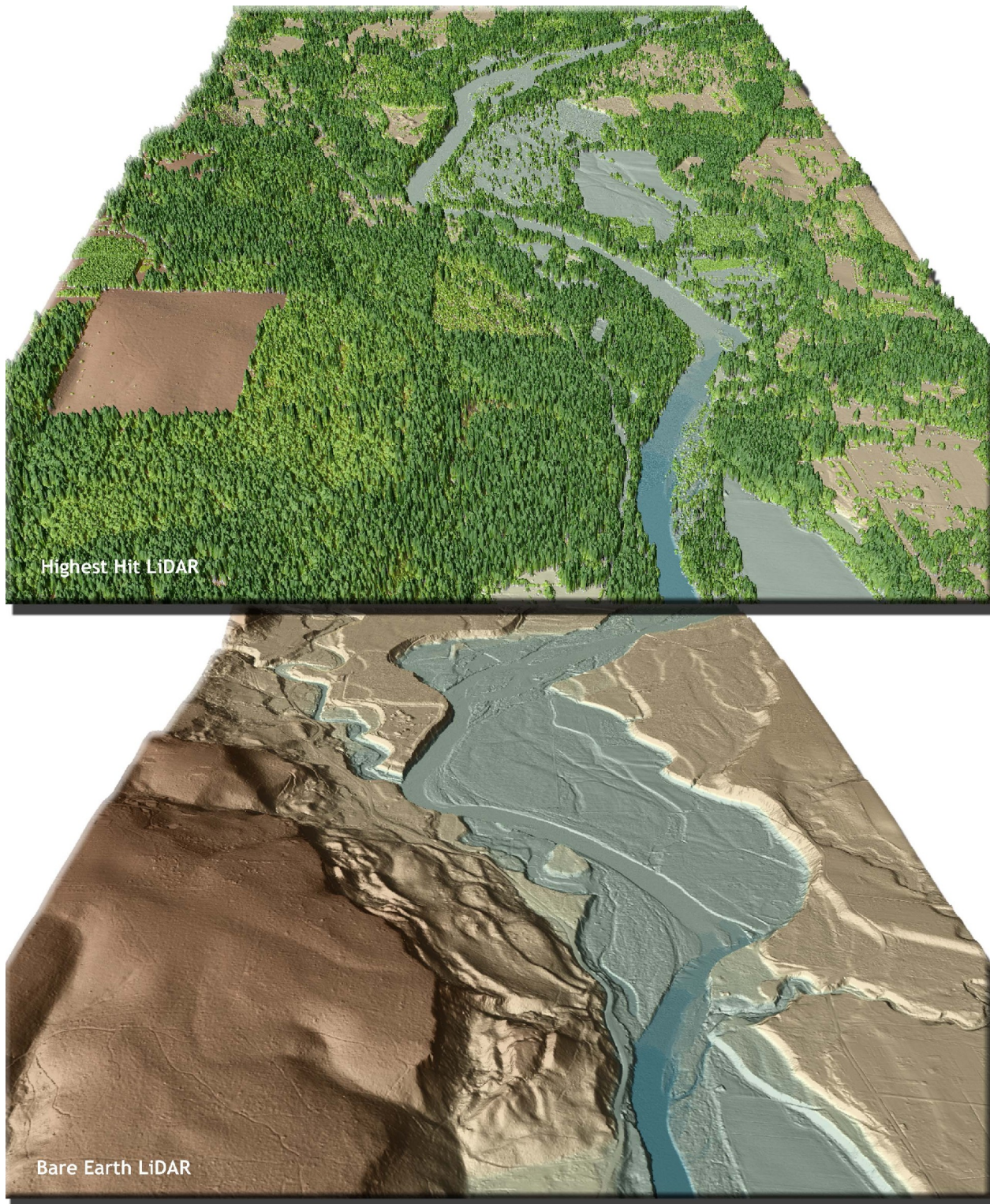


Figure 7.30. 3-d oblique view looking northward at Clackamas River at the Deep Creek confluence.



Figure 7.31. 3-d oblique view looking northward of Martin Creek (flows from bottom of image to upper left) and Mosier Creek (flows from bottom of image to upper right). The ridge between the creeks is The Hogback.



Figure 7.32. 3-d oblique view of the residential development in Northern Clackamas County near Borges Road.



Figure 7.33. 3-d oblique view looking northward at the ridge between Noyer Creek (left) and North Fork Deep Creek (right), near Barton.

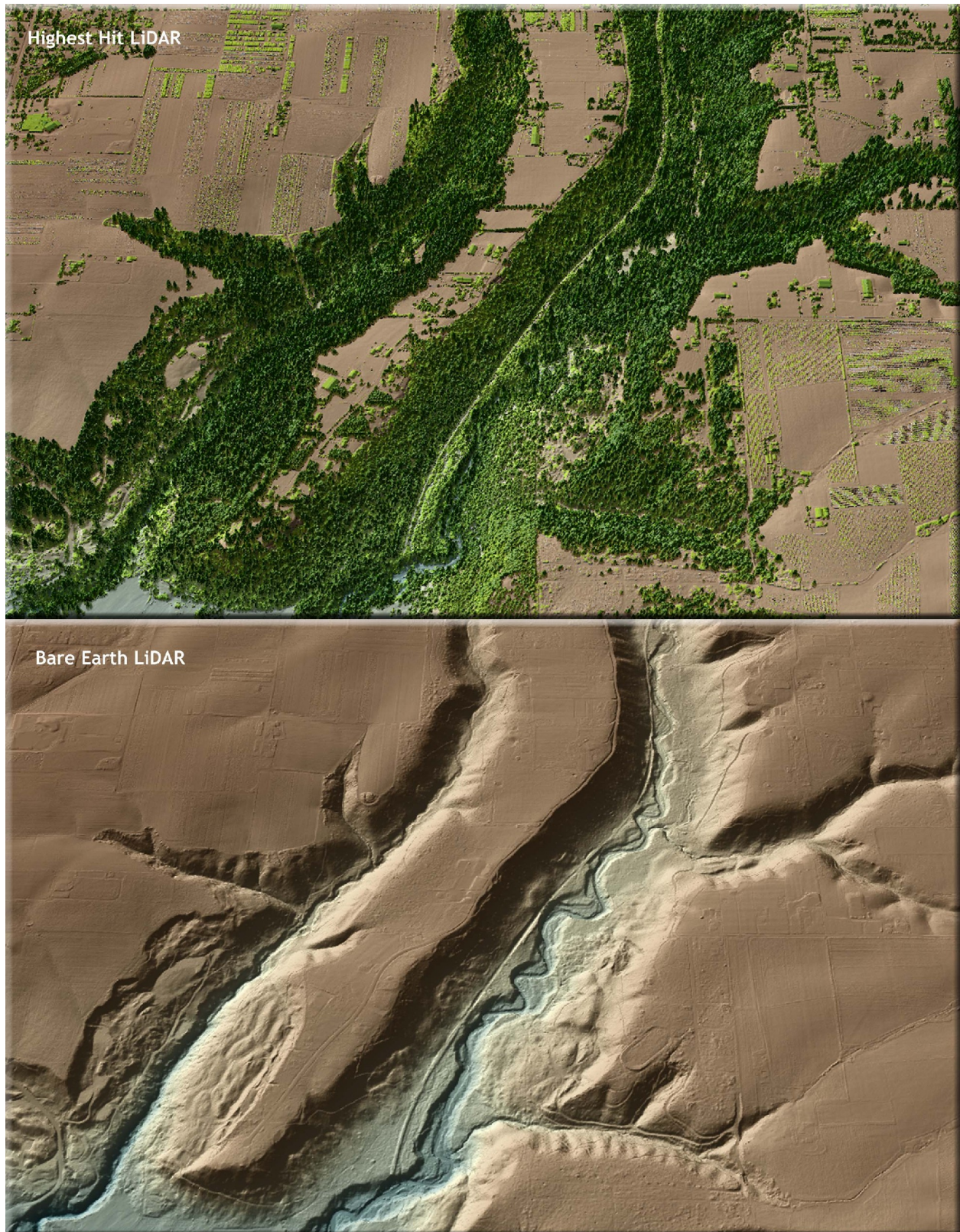


Figure 7.34. 3-d oblique view looking northward at the dam and powerhouse on the Clackamas River in Estacada.



Figure 7.35. 3-d oblique view looking northward at the confluence of Eagle Creek and North Fork Eagle Creek.



Figure 7.36. 3-d oblique view of the headwaters of Muddy Fork, just downhill from the Sandy Glacier on the northwestern side of Mount Hood.

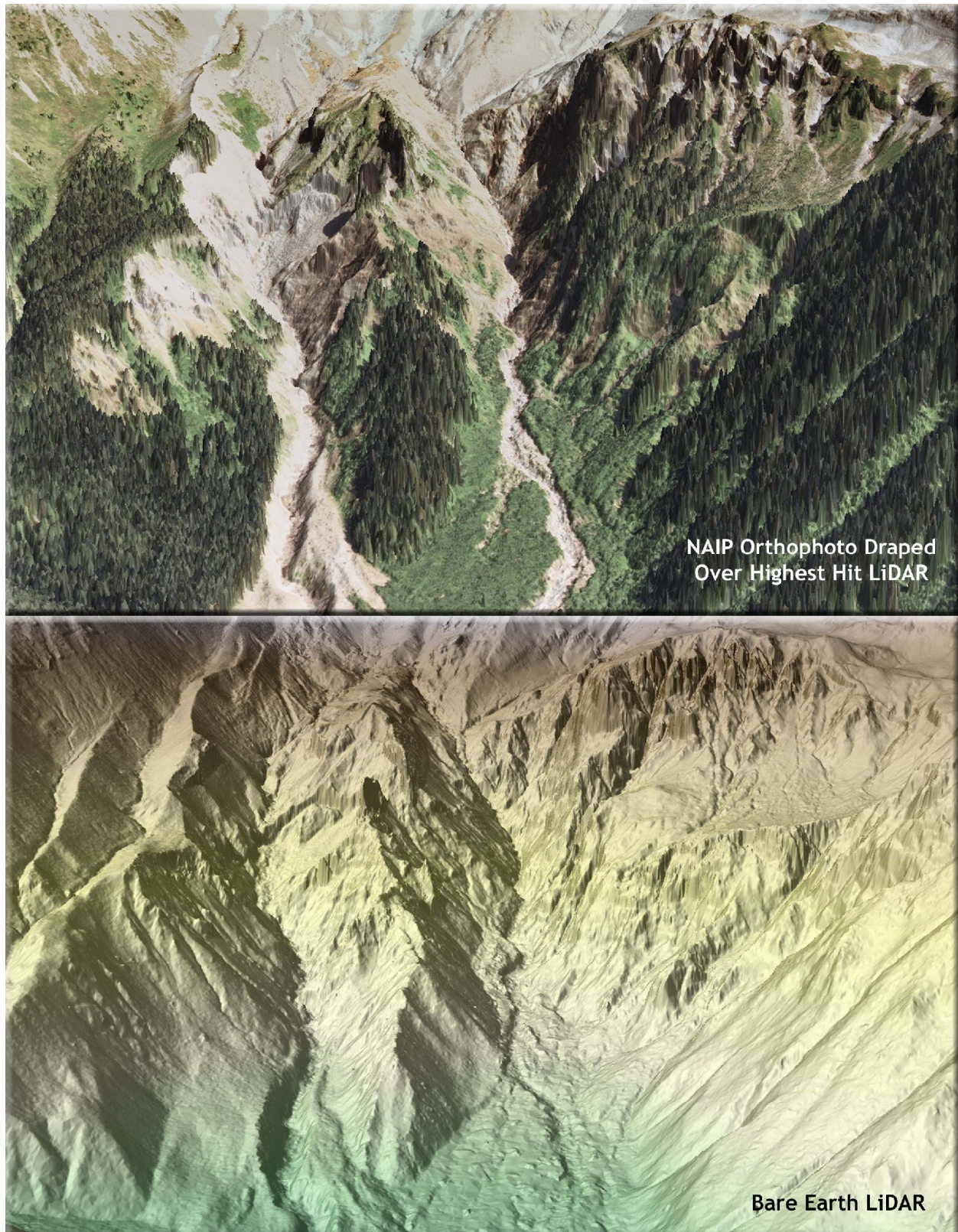


Figure 7.37. 3-d oblique view of the headwaters of Newton Creek on the east side of Mount Hood.

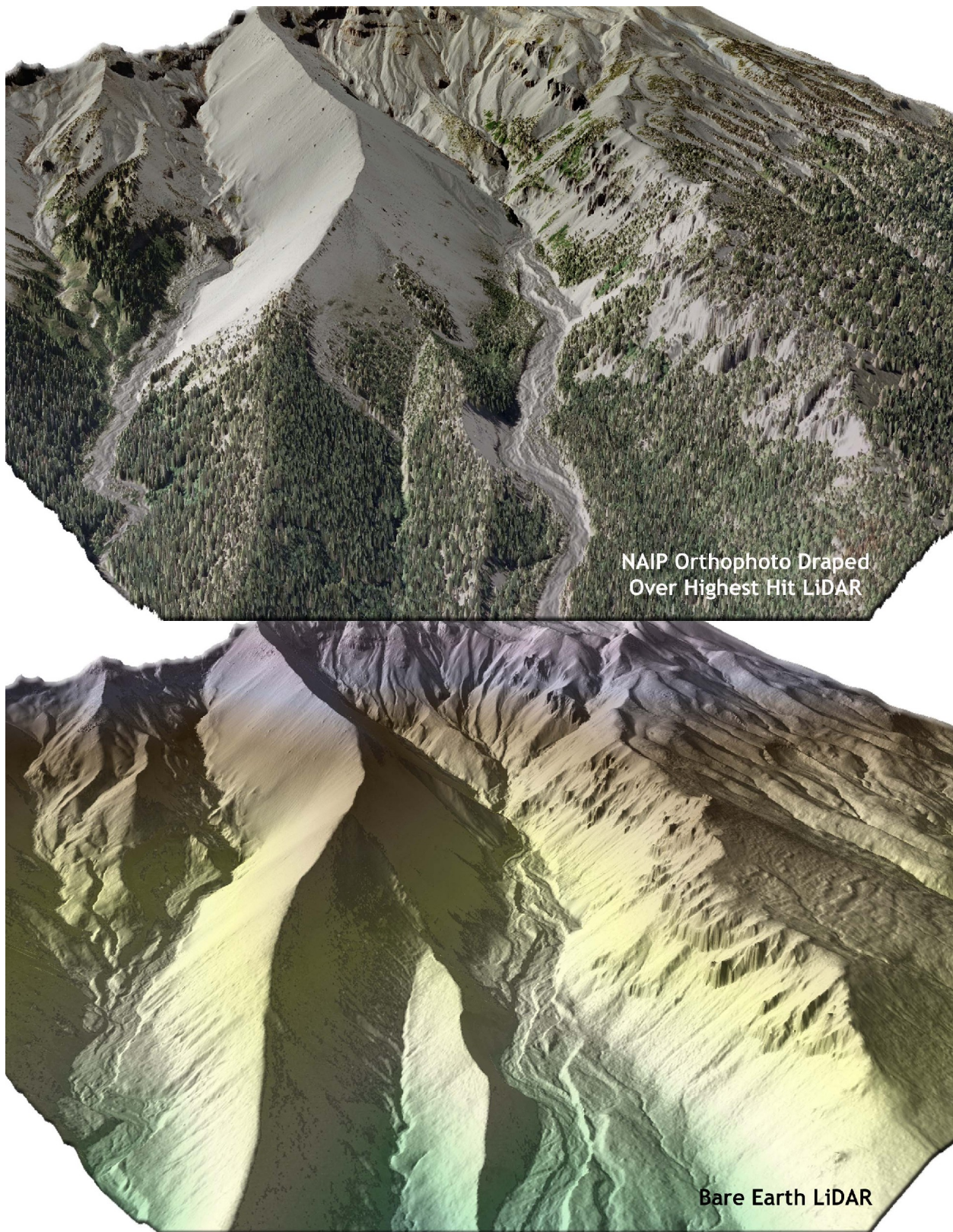


Figure 7.38. 3-d oblique view of Mount Hood Meadows ski area east of Timberline Lodge.

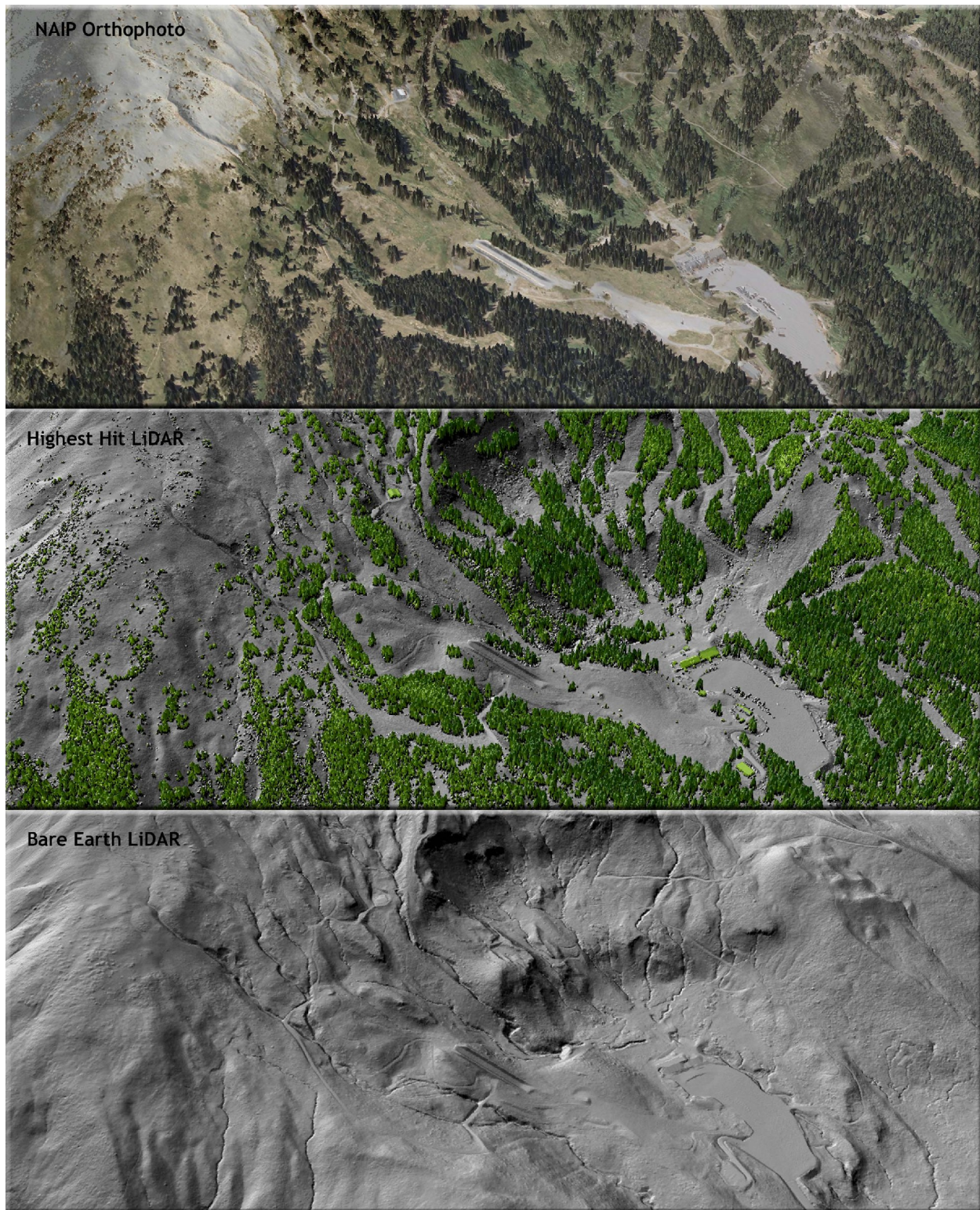


Figure 7.39. View of Timberline Lodge area on Mount Hood.

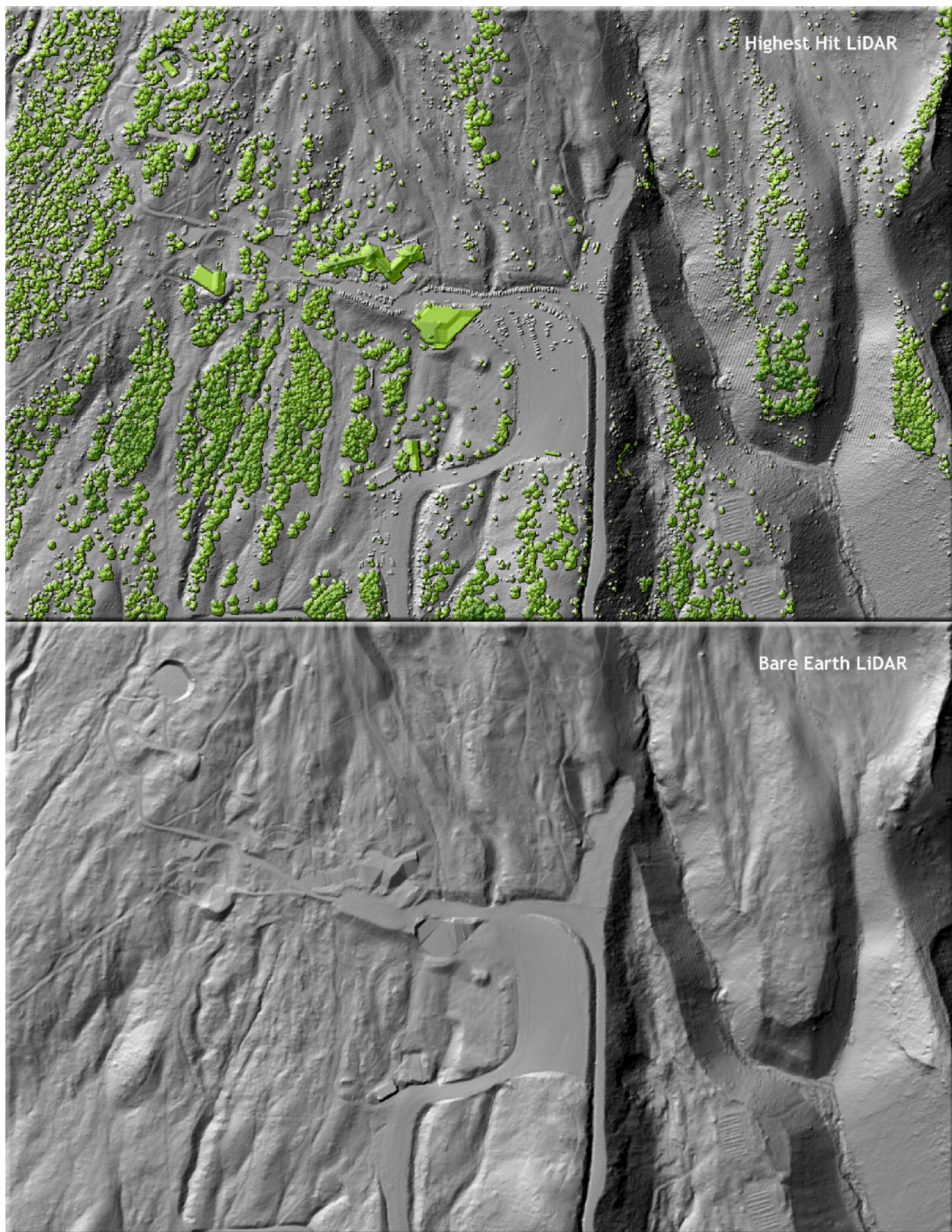


Figure 7.40. 3-d oblique view of the north face of Mount Hood.

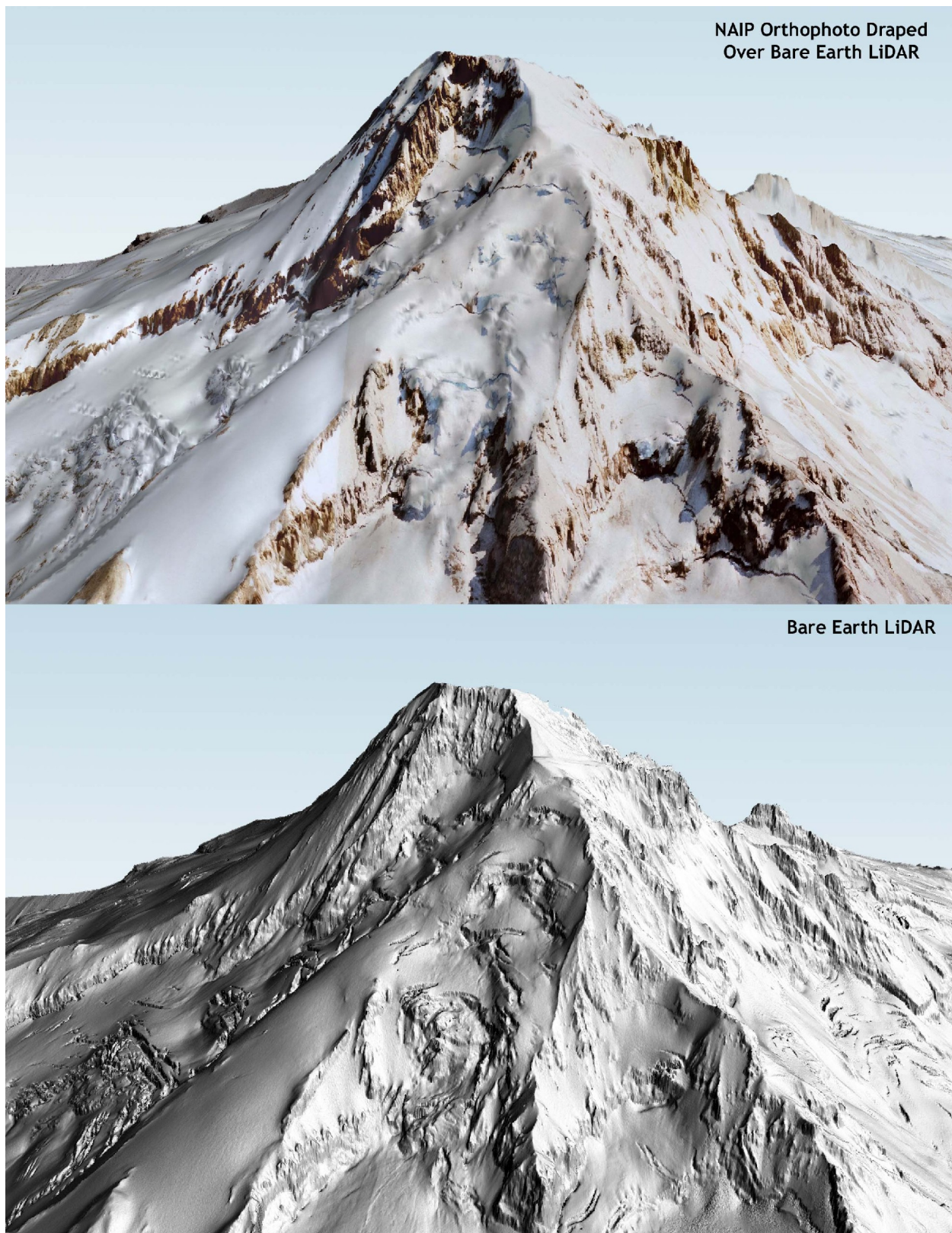


Figure 7.41. 3-d oblique view of the east-northeast face of Mount Hood.

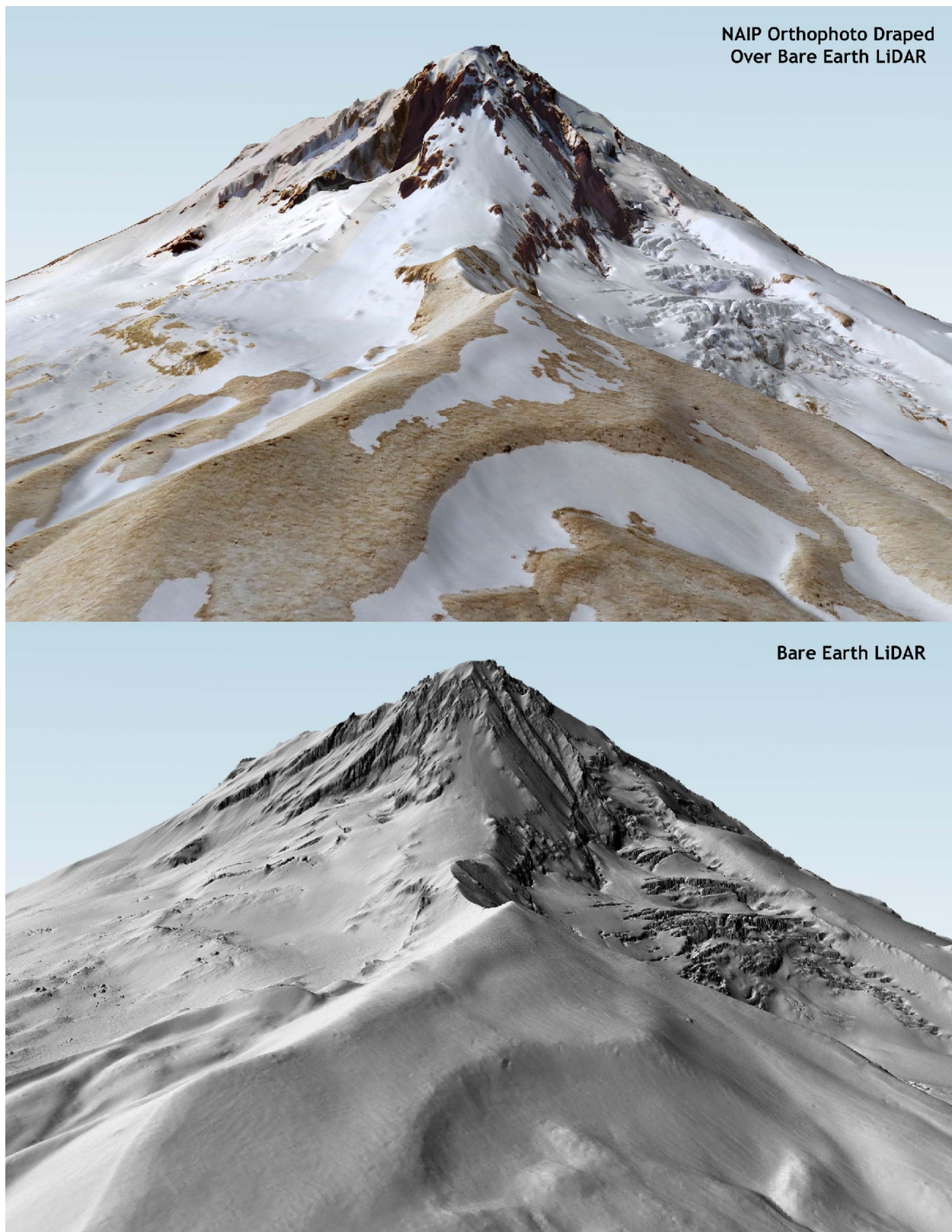


Figure 7.42. 3-d oblique view of the south face of Mount Hood.

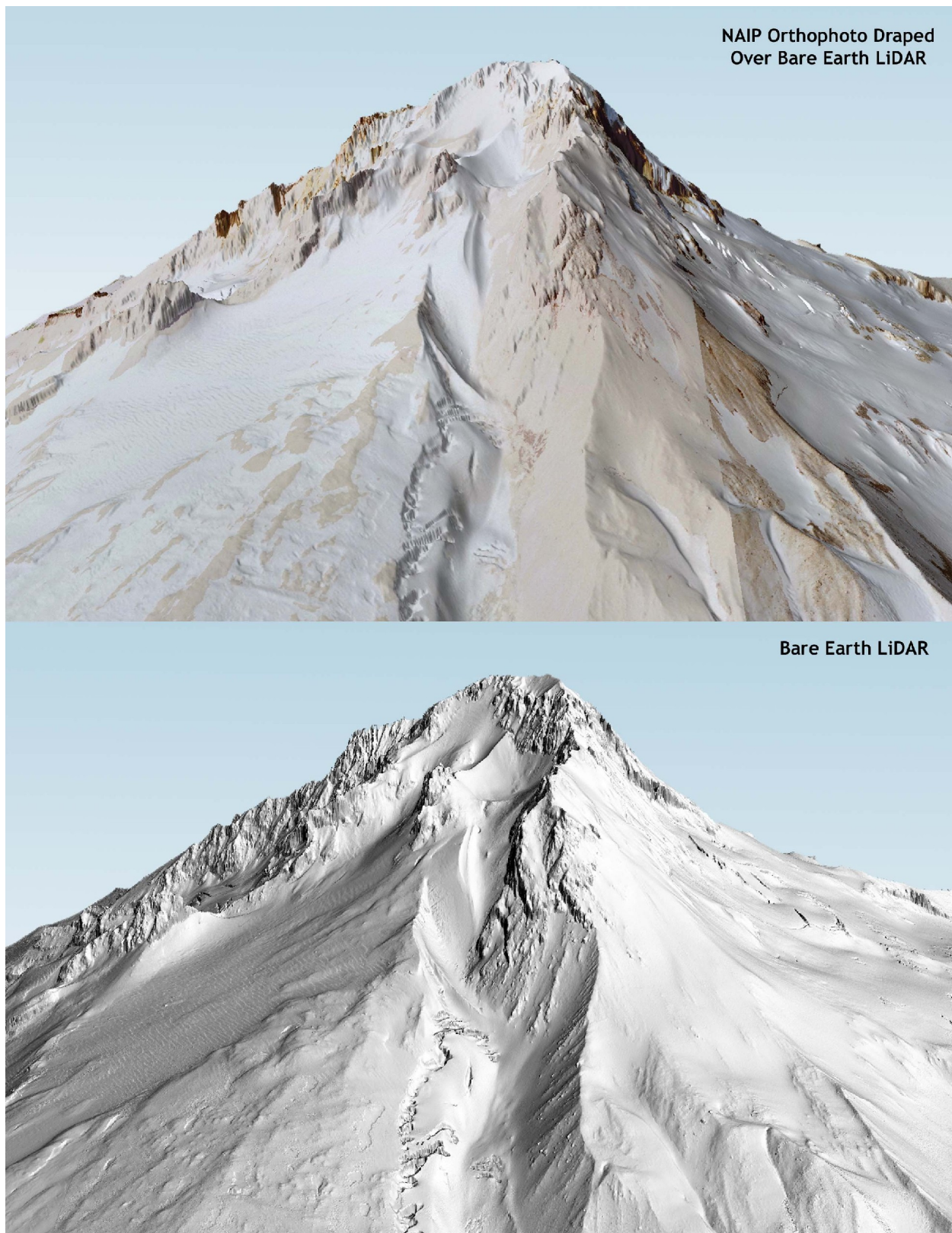


Figure 7.43. 3-d oblique view of the west face of Mount Hood.

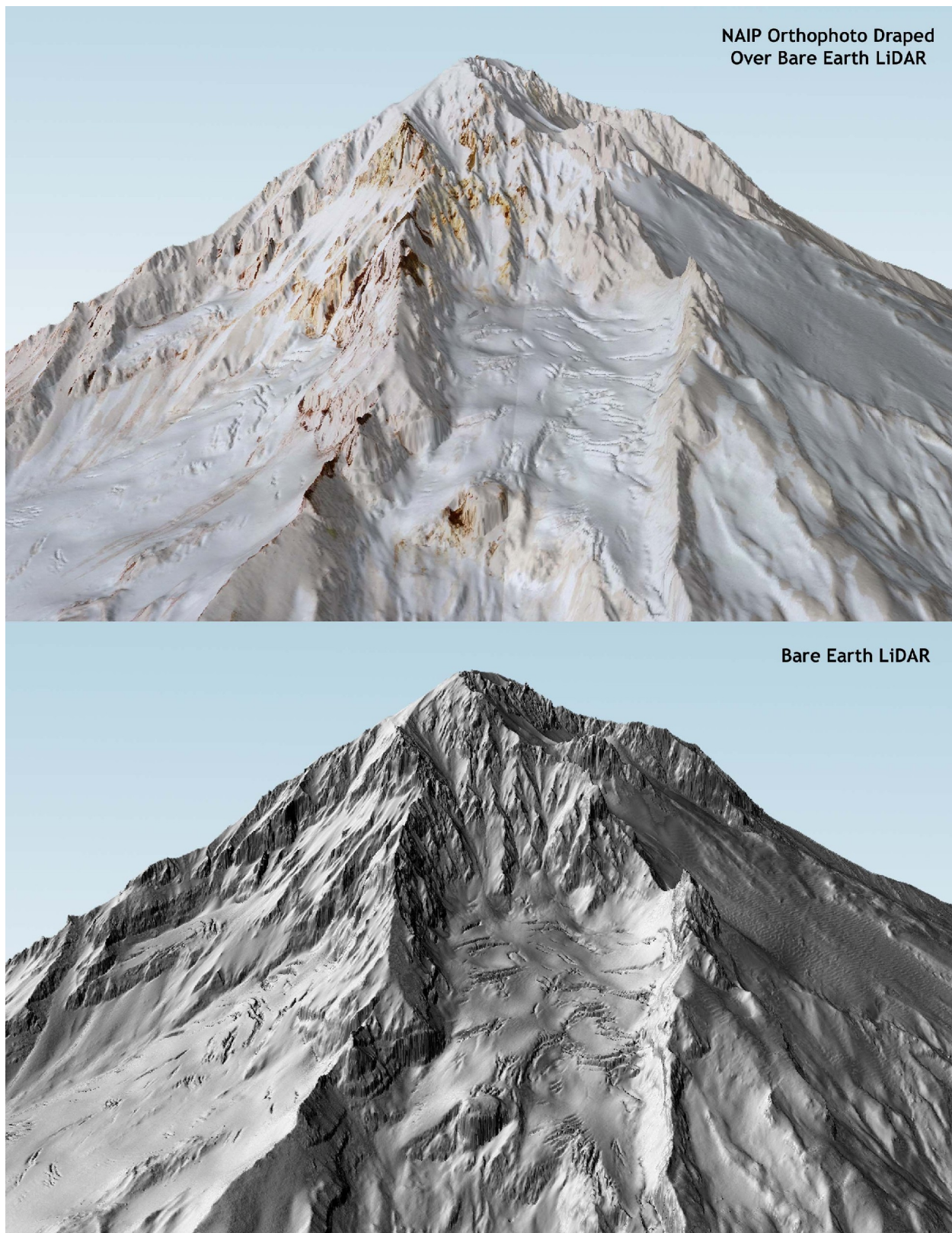


Figure 7.44. Image set illustrating the Sandy River, east of Springdale in Multnomah County, Oregon.



Figure 7.45. Image pair showing the Clackamas River slightly east of it's junction with Collawash.



Figure 7.46. Image pair showing the Sandy River upstream of the confluence with Cedar Creek.



Figure 7.47. Images showing the Bull Run reservoir and the confluence with Cougar and Bear Creeks.

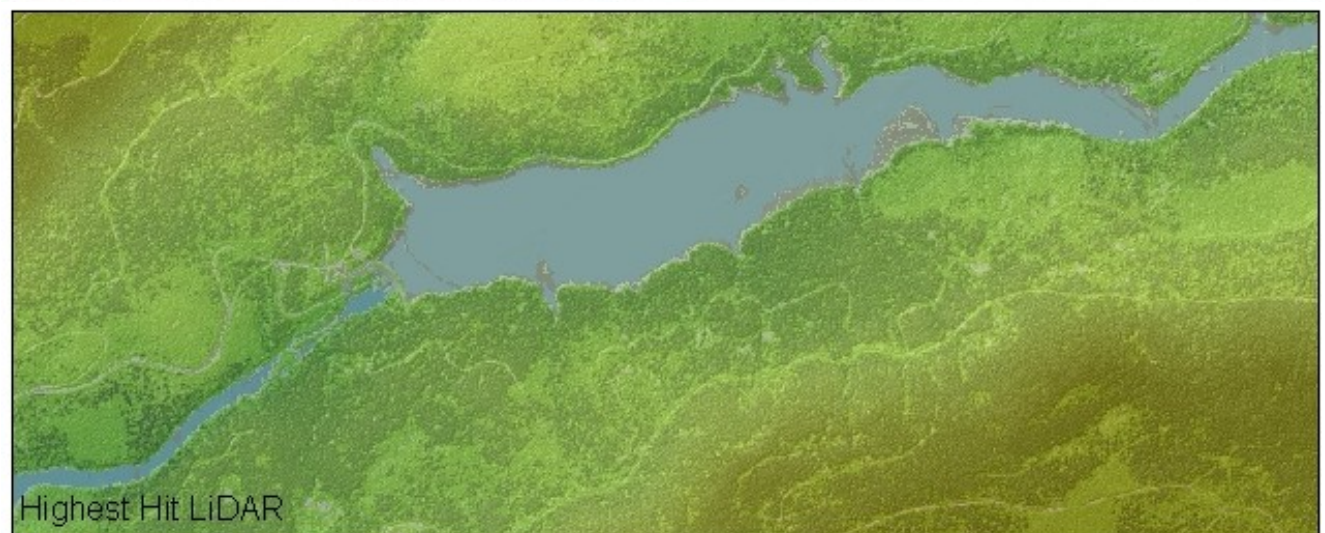
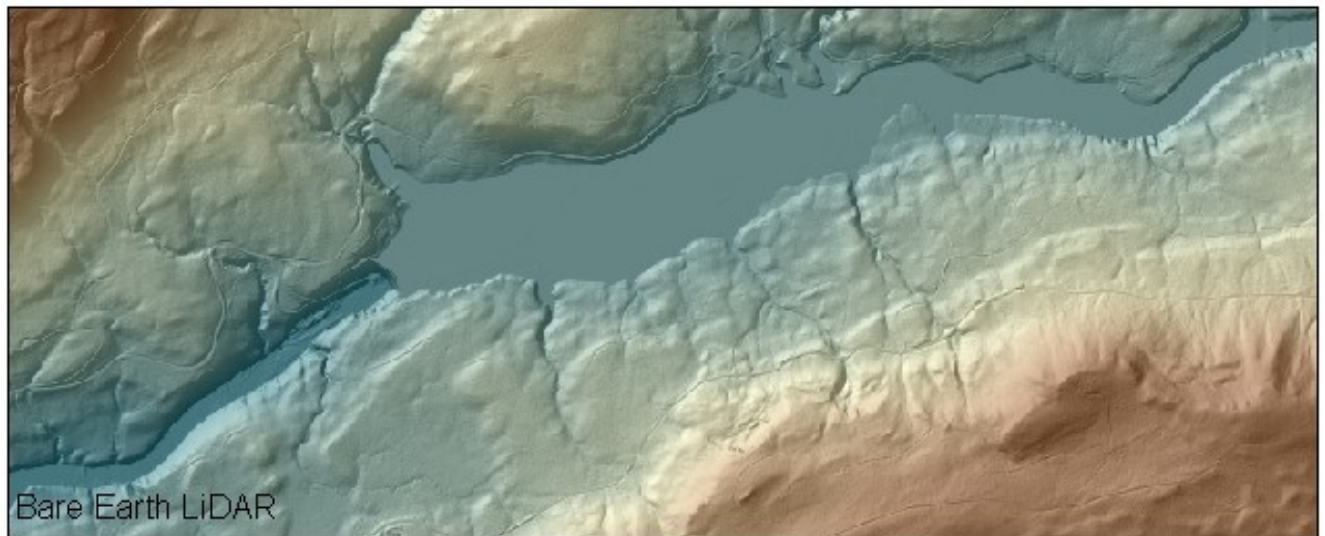
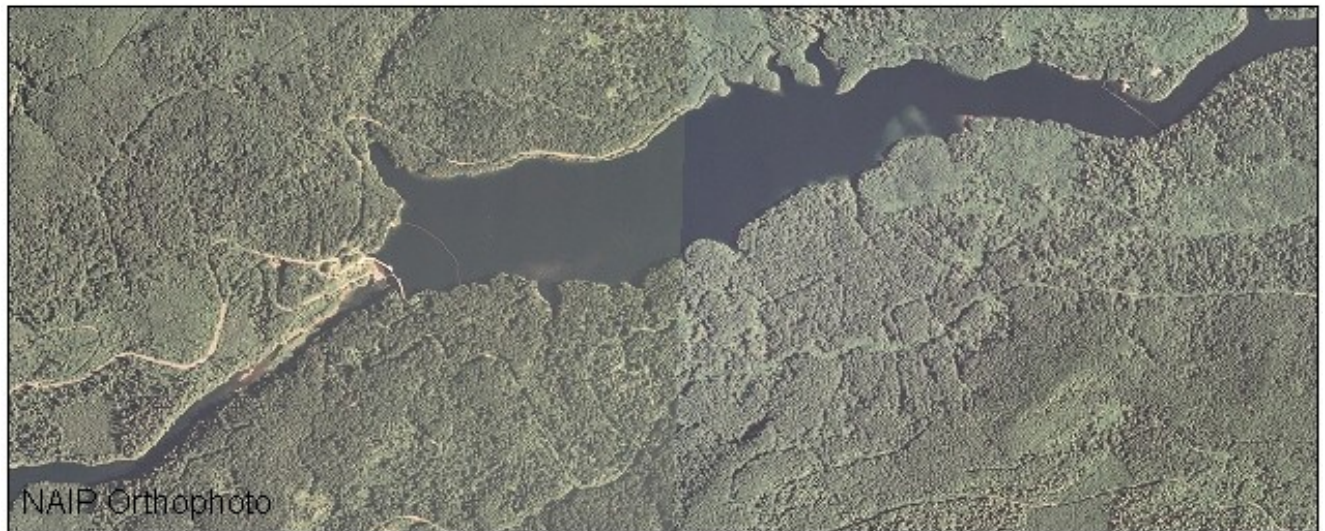


Figure 7.48. Images showing the Bull Run confluence with Camp Creek.

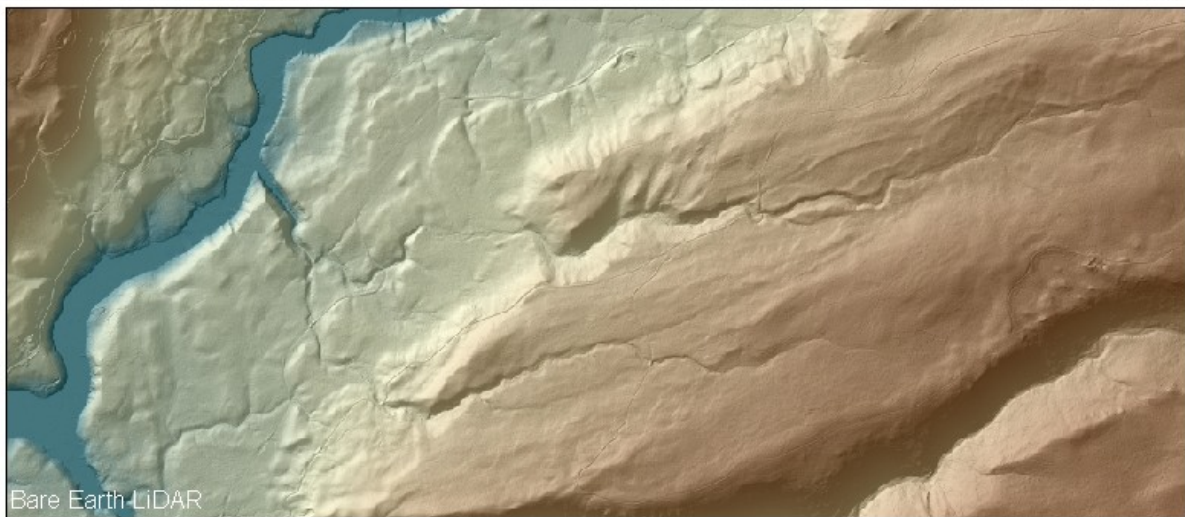


Figure 7.49. Images showing crossing of Highway 35 over White River.



Figure 7.50. Images showing crossing of Highway 35 over White River.



Figure 7.51. Images showing crossing of Highway 35 over White River.

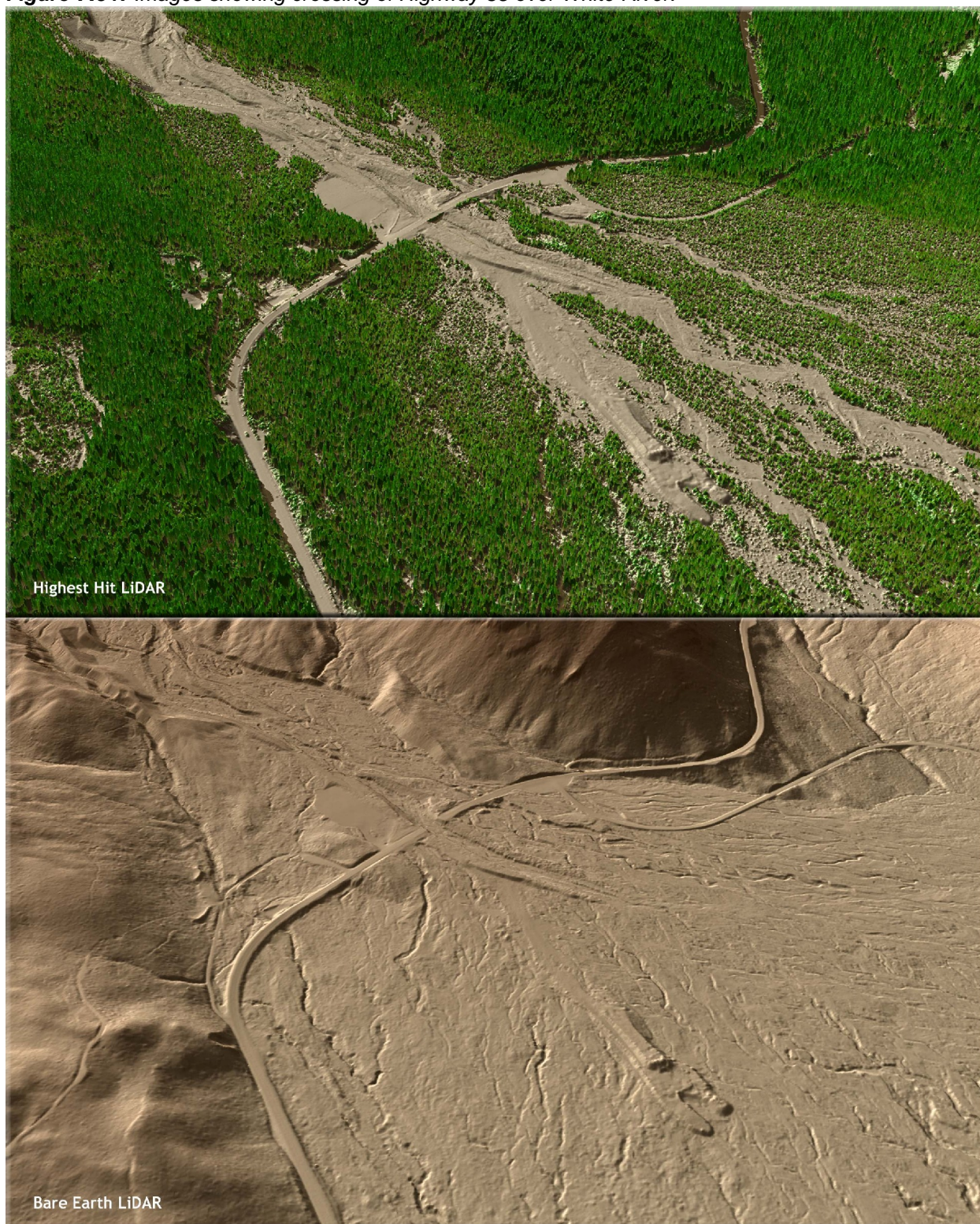


Figure 7.52. Images showing the view to the south over McCord Creek, illustrating Elowah Falls. Top image is derived from NAIP Orthophoto draped over highest hits LiDAR data. Middle image represents highest hits LiDAR data, and lower image is of bare earth LiDAR data.

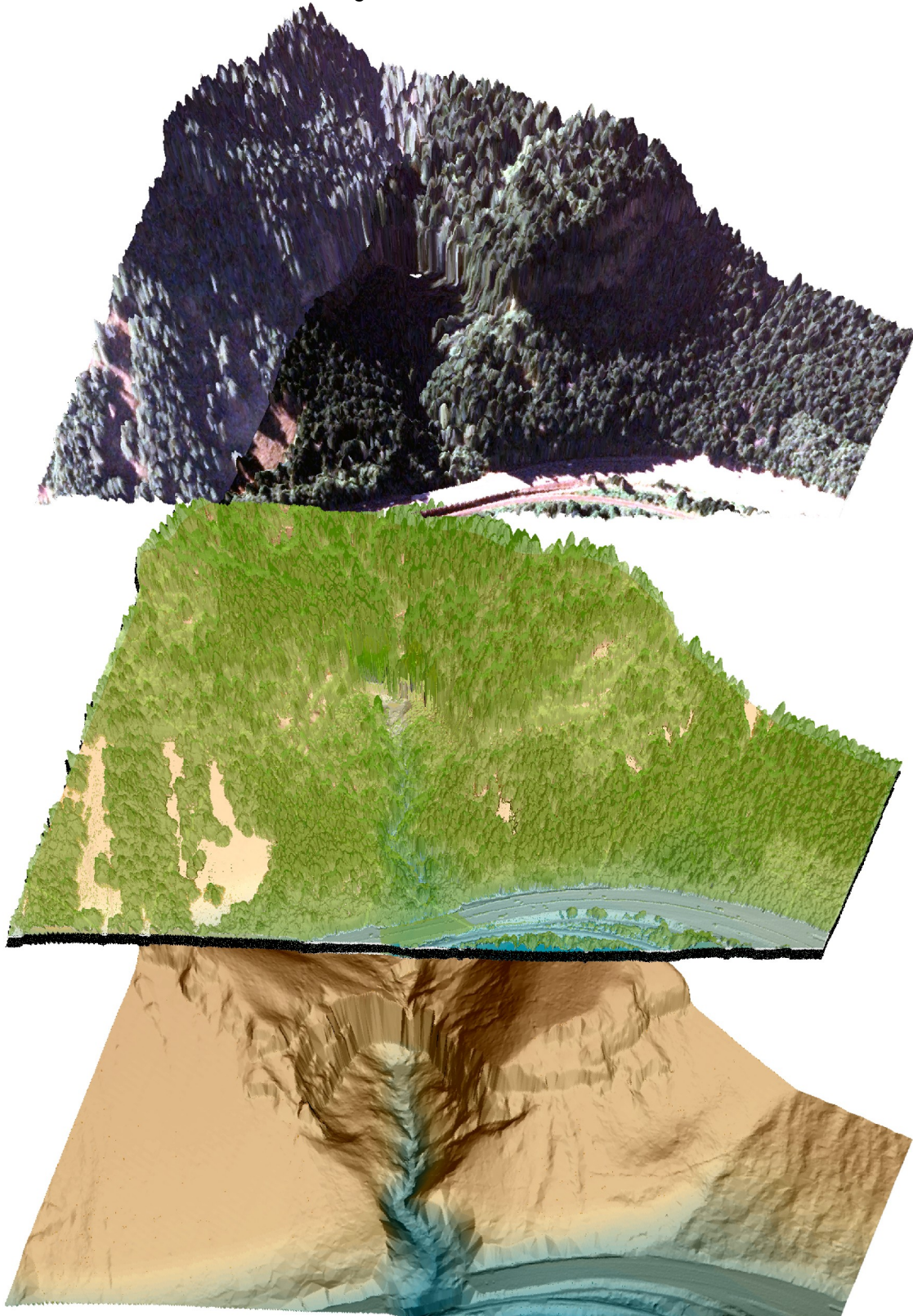


Figure 7.53. Images showing the alluvial debris fan from an unnamed creek entering the Columbia River just downstream of McCord Creek. Top image represents highest hits LiDAR data, and lower image is of bare earth LiDAR data.

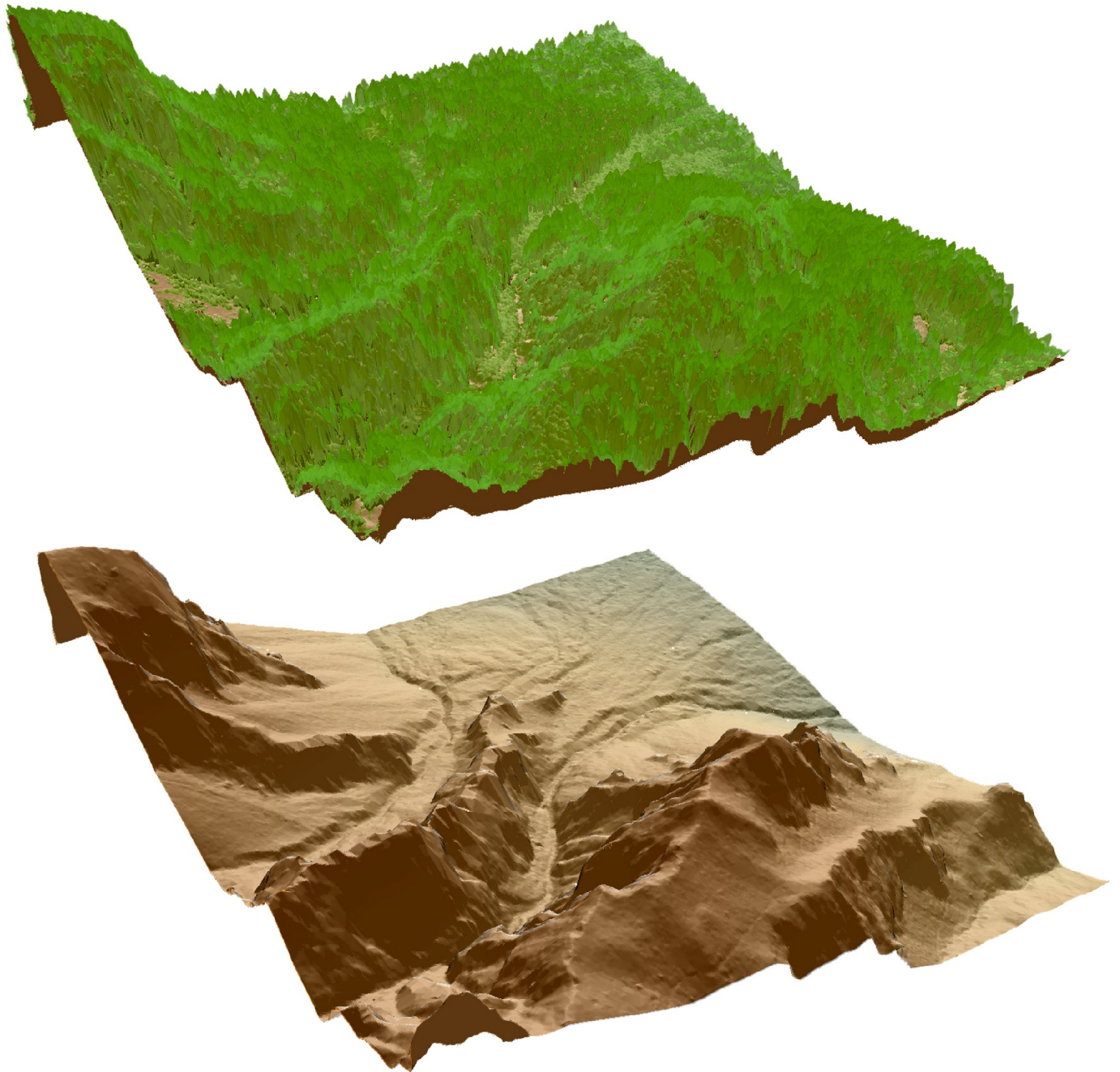


Figure 7.54. Elowah Falls, Columbia River Gorge (Quad 45121E8). Top image derived from LiDAR highest hits, bottom from bare earth LiDAR.

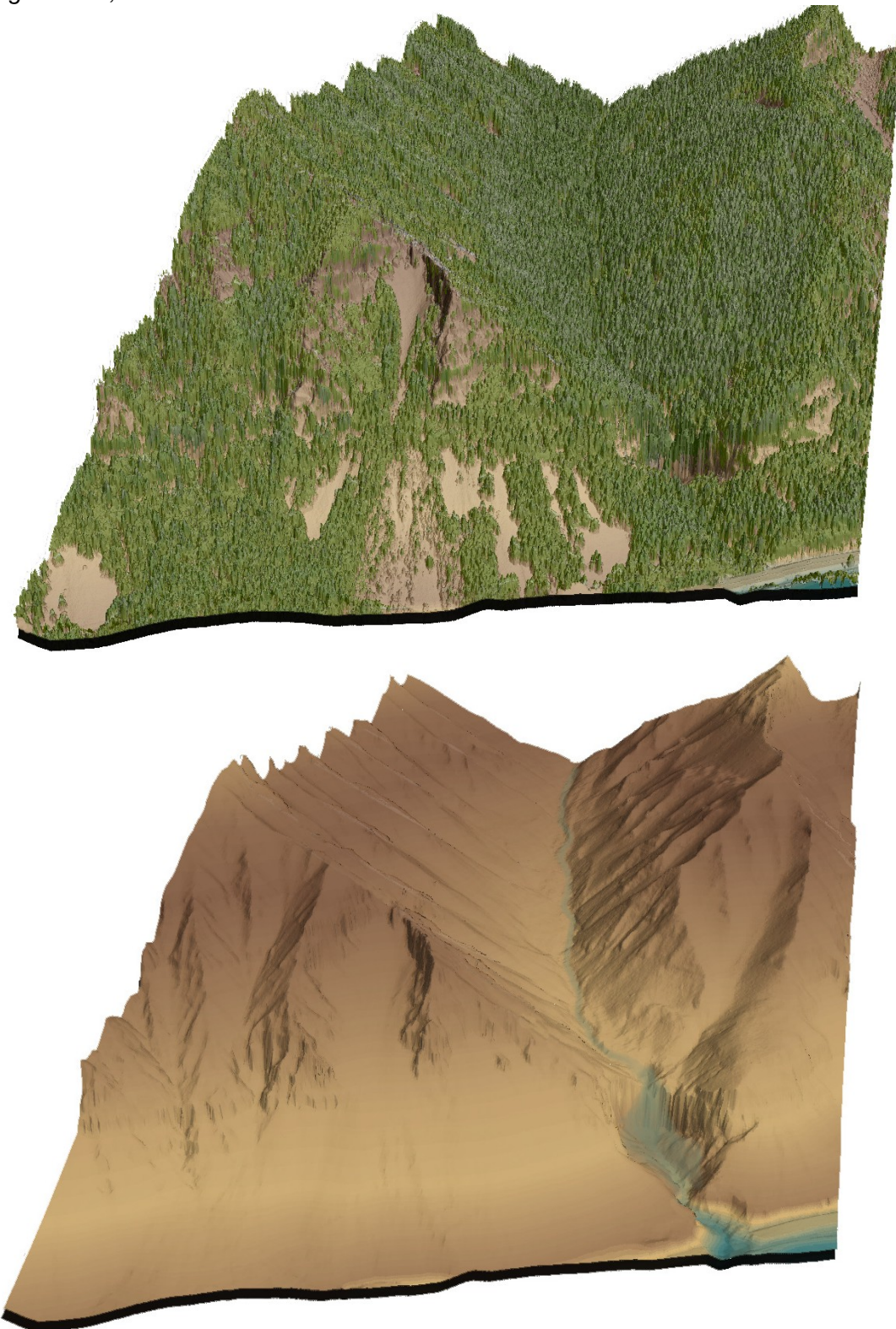


Figure 7.55. Oneonta Falls, Columbia River Gorge (Quad 45122E1). Top image derived from LiDAR highest hits, bottom from bare earth LiDAR.

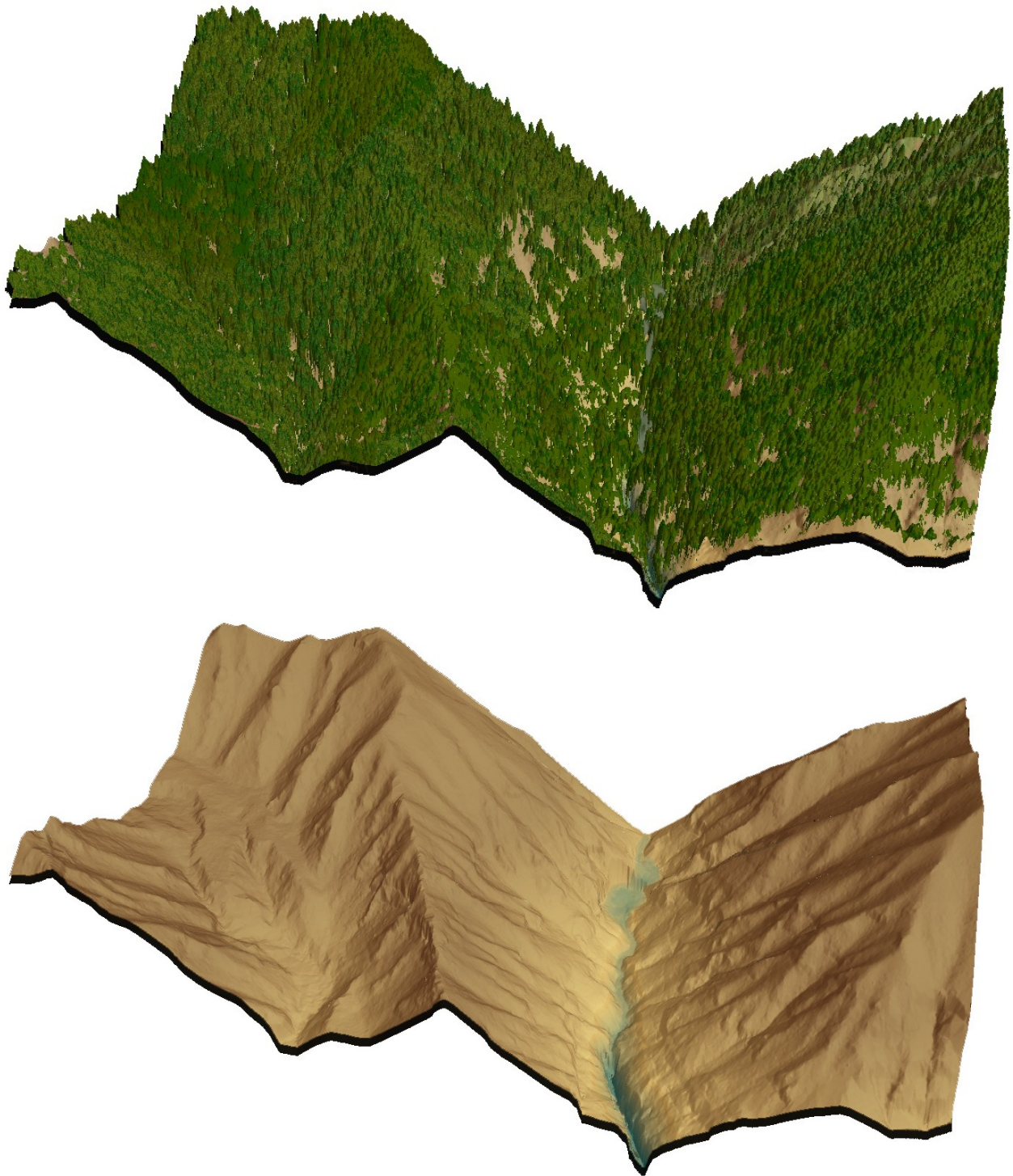


Figure 7.56. Larch Mountain (Quad 45122E1). Top image derived from LiDAR highest hits, bottom from bare earth LiDAR, lower image derived from NAIP orthophoto.

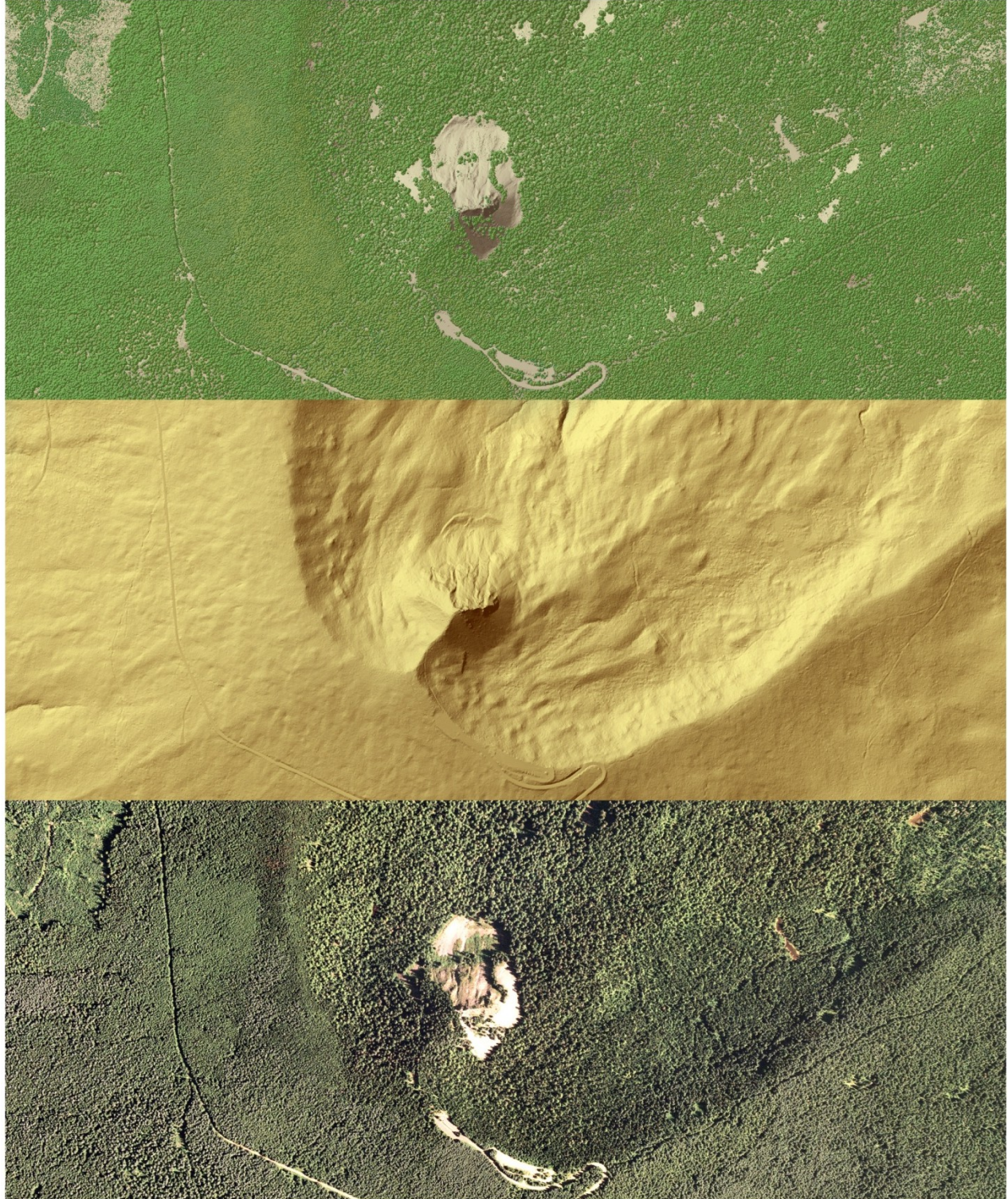


Figure 7.57. Warren Creek Falls, South rim of Columbia River Gorge near Hood River, Oregon. Quad 45121f6.

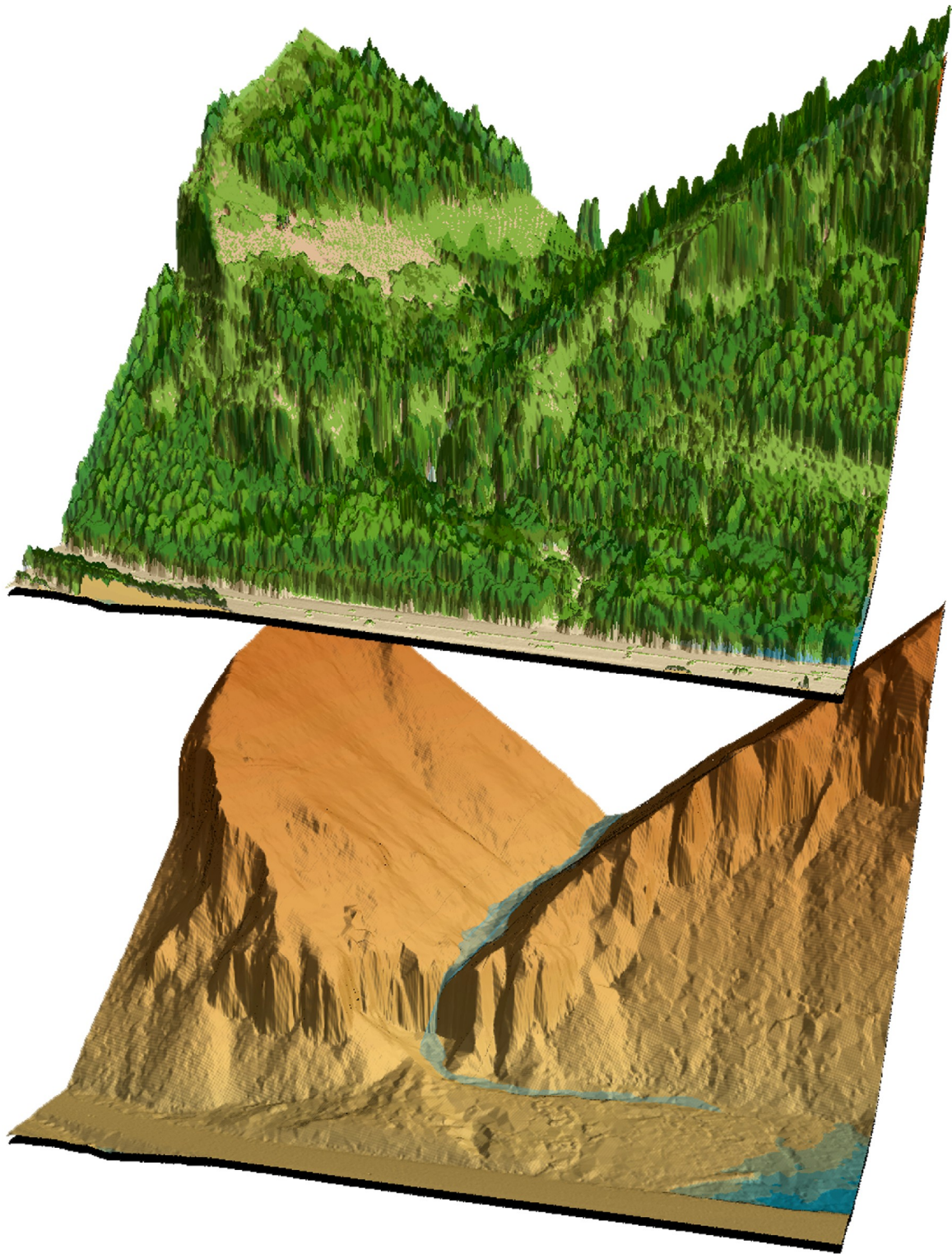


Figure 7.58. View upstream on Hood River, about one mile south of town of Hood River. Quad 45121f5.

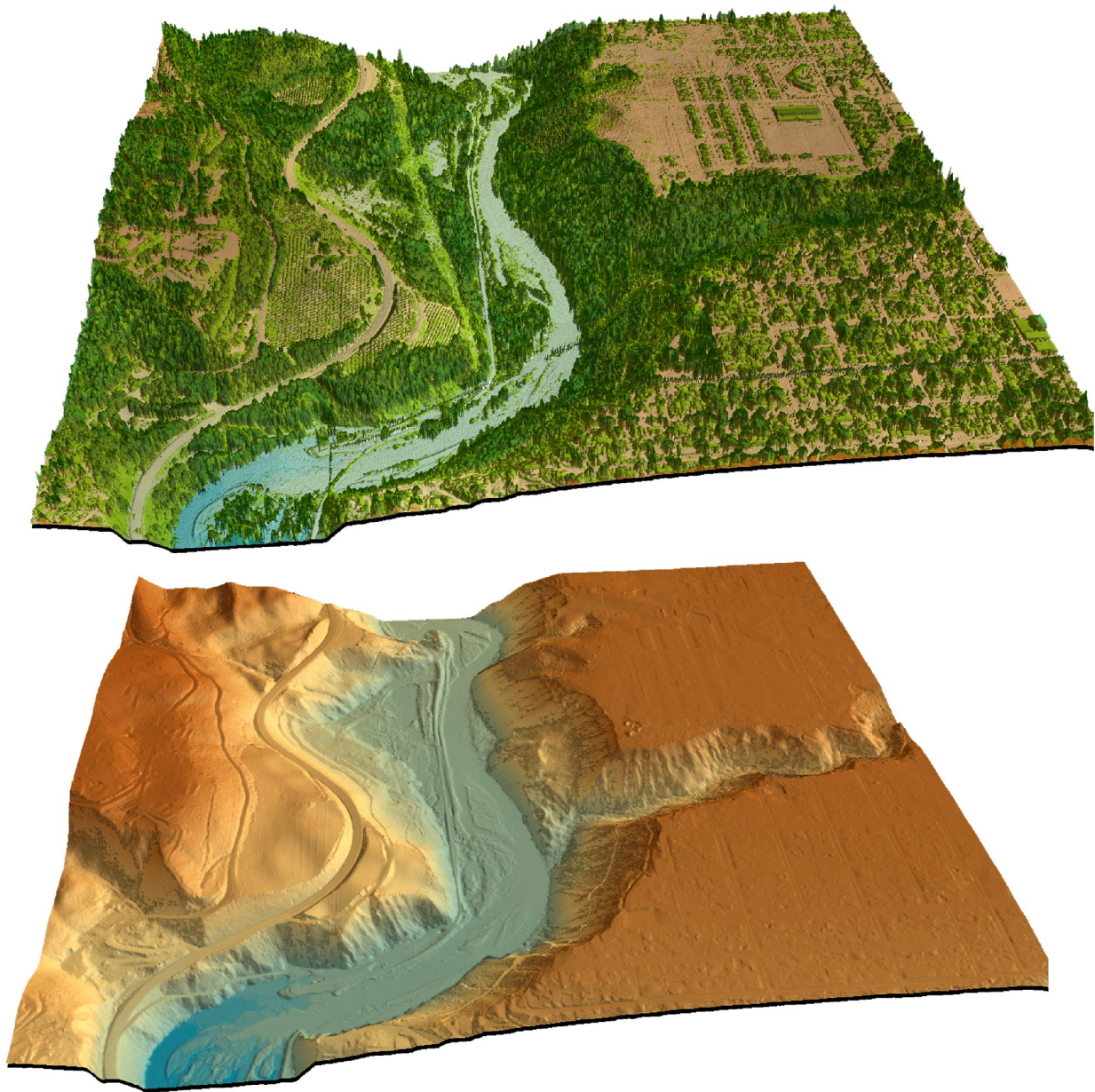


Figure 7.59. Dam on Hood River, upstream of town of Hood River, Oregon. Quad 45121f5.

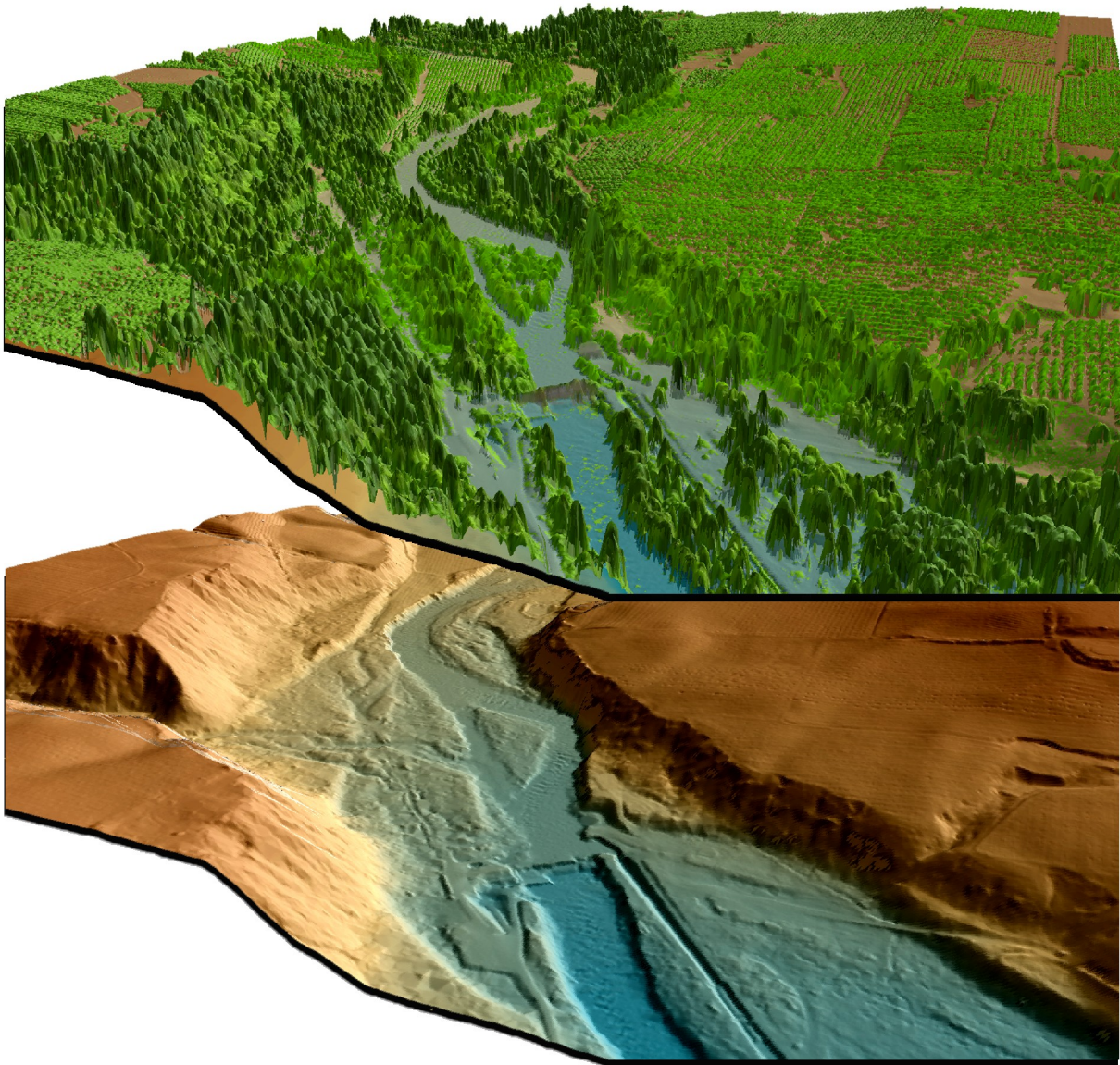
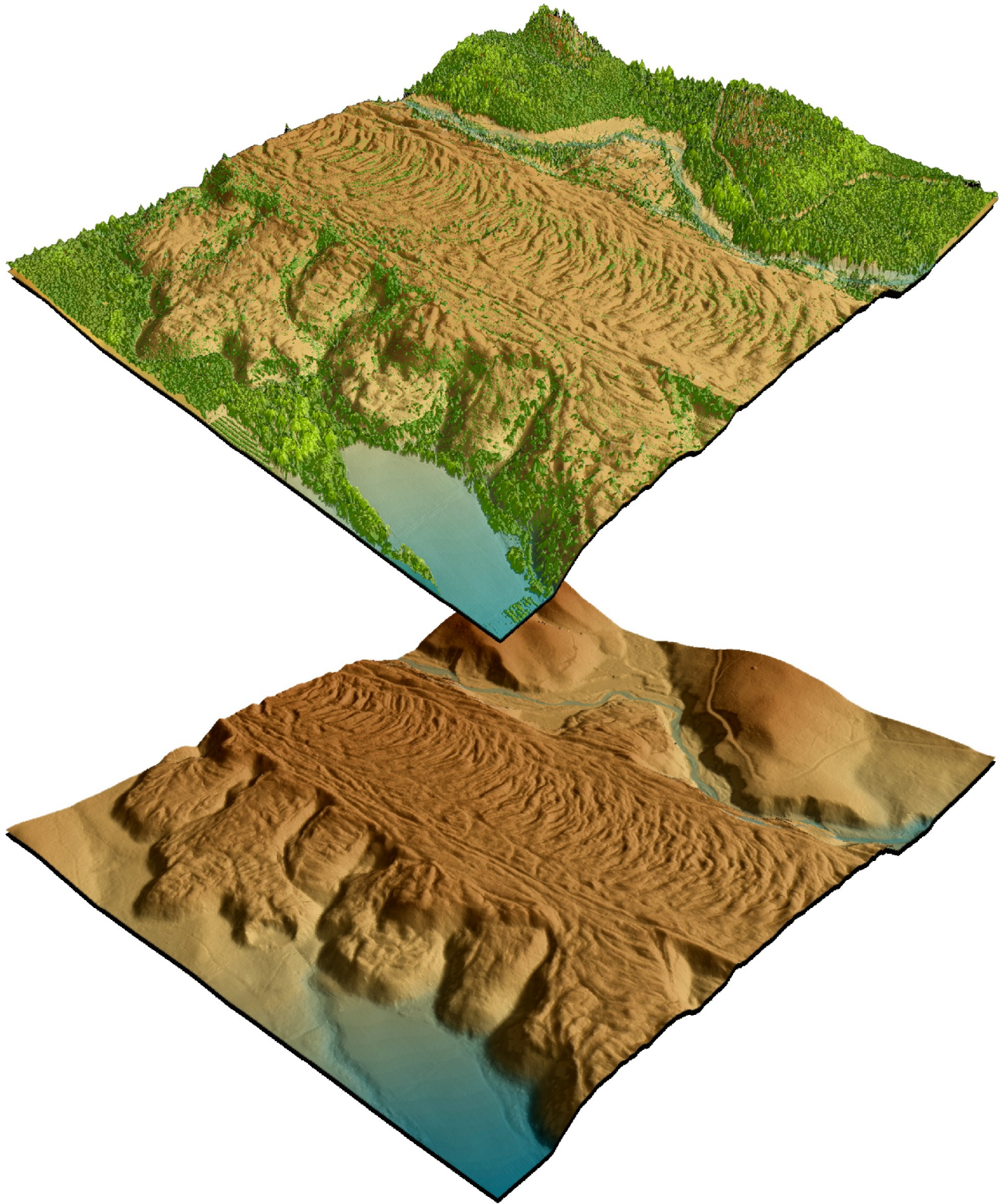


Figure 7.60. *Lava Flow on Mount Hood near White River, Oregon. Quad 45121d6.*



8. Glossary

1-sigma (s) Absolute Deviation: Value for which the data are within one standard deviation (approximately 68th percentile) of a normally distributed data set.

2-sigma (s) Absolute Deviation: Value for which the data are within two standard deviations (approximately 95th percentile) of a normally distributed data set.

Root Mean Square Error (RMSE): A statistic used to approximate the difference between real-world points and the LiDAR points. It is calculated by squaring all the values, then taking the average of the squares and taking the square root of the average.

Pulse Rate (PR): The rate at which laser pulses are emitted from the sensor; typically measured as thousands of pulses per second (kHz).

Pulse Returns: For every laser emitted, the Leica ALS 50 Phase II system can record *up to four* wave forms reflected back to the sensor. Portions of the wave form that return earliest are the highest element in multi-tiered surfaces such as vegetation. Portions of the wave form that return last are the lowest element in multi-tiered surfaces.

Accuracy: The statistical comparison between known (surveyed) points and laser points. Typically measured as the standard deviation (sigma, σ) and root mean square error (RMSE).

Intensity Values: The peak power ratio of the laser return to the emitted laser. It is a function of surface reflectivity.

Data Density: A common measure of LiDAR resolution, measured as points per square meter.

Spot Spacing: Also a measure of LiDAR resolution, measured as the average distance between laser points.

Nadir: A single point or locus of points on the surface of the earth directly below a sensor as it progresses along its flight line.

Scan Angle: The angle from nadir to the edge of the scan, measured in degrees. Laser point accuracy typically decreases as scan angles increase.

Overlap: The area shared between flight lines, typically measured in percents; 100% overlap is essential to ensure complete coverage and reduce laser shadows.

DTM / DEM: These often-interchanged terms refer to models made from laser points. The digital elevation model (DEM) refers to all surfaces, including bare ground and vegetation, while the digital terrain model (DTM) refers only to those points classified as ground.

Real-Time Kinematic (RTK) Survey: GPS surveying is conducted with a GPS base station deployed over a known monument with a radio connection to a GPS rover. Both the base station and rover receive differential GPS data and the baseline correction is solved between the two. This type of ground survey is accurate to 1.5 cm or less.

9. Citations

Soininen, A. 2004. TerraScan User's Guide. Terrasolid.